Analysis of pathogenic alterations in the *Cln3*$^{\Delta ex7/8}$ mouse model (*mus musculus*)

Dissertation

zur Erlangung des akademischen Grades

doctor rerum naturalium

im Fachbereich Biologie,

an der Fakultät für Mathematik, Informatik und Naturwissenschaften

der Universität Hamburg

vorgelegt von

Carolin Schmidtke

Hamburg 2014

Day of oral defense: 6.3.2015

1. Gutachter: Prof. Dr. rer. nat. Thomas Braulke

2. Gutachter: PD Dr. rer. nat. Edgar Kramer

Für meine Familie

Table of Contents

List of Figures

Abbreviations

ANCL	Adult neuronal ceroid lipofuscinosis
AP	Adaptor protein
APS	Ammonium peroxydisulfate
ASB	Arylsulfatase B
bp	Base pairs
BSA	Bovine serum albumin
CD	Cluster of differentiation
cDNA	Complementary DNA
CTB	Cholera toxin subunit B
CtsB	Cathepsin B
CtsD	Cathepsin D
CtsL	Cathepsin L
CtsZ	Cathepsin Z
DAPI	4’,6-Diamidino-2-phenylindole
DMEM	Dulbecco’s modified Eagle medium
DMSO	Dimethylsulphoxide
DNA	Deoxyribonucleic acid
DTT	Dithiothreitol
ECL	Enhanced chemiluminescence
EDTA	Ethylenediaminetetraacetic acid
ER	Endoplasmic reticulum
FACS	Fluorescence activated cell sorting
FBS	Fetal bovine serum
FCS	Fetal calf serum
FSC	Forward scatter
g	Gravity
h	Hours
HEPES	(4-(2-hydroxyethyl)-1-piperazineethanesulfonic acid
HRP	Horseradish peroxidase
IF	Immunofluorescence
IFNγ	Interferon gamma

INCL	Infantile neuronal ceroid lipofuscinosis
JNCL	Juvenile neuronal ceroid lipofuscinosis
kb	Kilobase
kDa	Kilodalton
Lamp	Lysosomal-associated membrane protein
Limp	Lysosomal integral membrane protein
LINCL	Late-infantile neuronal ceroid lipofuscinosis
LRO	Lysosome-related organelle
Lrp	Low density lipoprotein receptor-related protein
LSD	Lysosomal storage disorders
Lyaat1	Lysosomal amino acid transporter 1
MEF	Mouse embryonic fibroblasts
min	Minute
Mpr300	Mannose 6-phosphate receptor of 300 kDa
Mpr46	Mannose 6-phosphate receptor of 46 kDa
mRNA	Messenger ribonucleic acid
NCL	Neuronal ceroid lipofuscinosis
ns	Not significant
PBS	Phosphate buffered saline
PCR	Polymerase chain reaction
PMA	Phorbol 12-myristate 13-acetate
Ppt1	Palmitoyl-protein-thioesterase 1
qRT-PCR	Quantitative real time polymerase chain reaction
s	Seconds
SDS	Sodium dodecyl sulphate
SDS-PAGE	Sodium dodecyl sulphate polyacrylamide gel electrophoresis
SILAC	Stable isotope labelling in cell culture
SSC	Side scatter
TAE	Tris-acetate-EDTA buffer
TBS	Tris buffered saline
TBS-T	Tris buffered saline containing 0.05 % Tween
TEMED	NNN'N'-Tetramethylethylenediamine
TFEB	Transcription factor EB

TfR	Transferrin receptor
TGN	*Trans*-Golgi-Network
TNFα	Tumor necrosis factor alpha
Tris	Tris(hydroxymethyl)aminomethane
v/v	Volume per volume
WB	Western blotting
w/v	Weight per volume
x g	Times gravity

1 Introduction

1.1 Lysosomes

Lysosomes are acidic organelles in eukaryotic cells and were first described by Christian de Duve (De Duve *et al.* 1955). The primary function of lysosomes is the degradation and recycling of macromolecules. Degradation is performed by the concerted action of more than 60 different hydrolases, achieving a complete decomposition of simple and complex macromolecules, including proteins, polysaccharides, lipids and nucleic acids, as well as extracellular material, being delivered to lysosomes by the biosynthetic pathway, endocytosis and autophagy. Depending on the substrate, lysosomal hydrolases are classified as proteases, lipases, nucleases, glycosidases, sulfatases, thioesterases and phosphatases (Lübke *et al.* 2009; Luzio *et al.* 2014). The acidic interior of the lysosome is crucial for the proteolytic activation of several lysosomal hydrolases. The lysosomal pH ranges from pH 4.5 to 5 and is maintained by the V-type ATPase, a transmembrane multi-protein complex that uses the energy of ATP hydrolysis to pump protons across the lysosomal membrane (Forgac 2007). Besides the V-type ATPase, the lysosome harbours 140 - 300 integral and peripheral highly glycosylated proteins (Schröder *et al.* 2007; Chapel *et al.* 2013). They are responsible to maintain the integrity of the lysosomal membrane and are involved in processes such as membrane fusion, transport and sequestration of lysosomal hydrolases and transport of molecules across the lysosomal membrane (Saftig *et al.* 2010; Schwake *et al.* 2013). Most of the properties of lysosomes are shared with a group of cell type-specific compartments referred to as lysosome-related organelles (LRO), including melanosomes, lytic granules and major histocompatibility complex (MHC) class II compartments. In particular cells types, such as osteoclasts, melanocytes and lymphocytes, lysosomes and LRO can also secrete their contents, a process that is known as lysosomal exocytosis. In addition to degradation and secretion, lysosomes and LRO exert complex functions in various physiological processes, such as cholesterol homeostasis, plasma membrane repair, pathogen defence, antigen processing and presentation, secretion of molecules, bone and tissue remodelling, cell death and cell signalling (Saftig and Klumperman 2009; Settembre *et al.* 2013). Moreover, the classical view of the lysosome as the primary degradative compartment of the cell has

been expended in recent years with the identification of lysosomes as signalling organelles (Figure 1), being involved in nutrient sensing, with a central role of TFEB in the regulation of lysosomal biogenesis, lysosome-to-nucleus signalling and lipid catabolism.

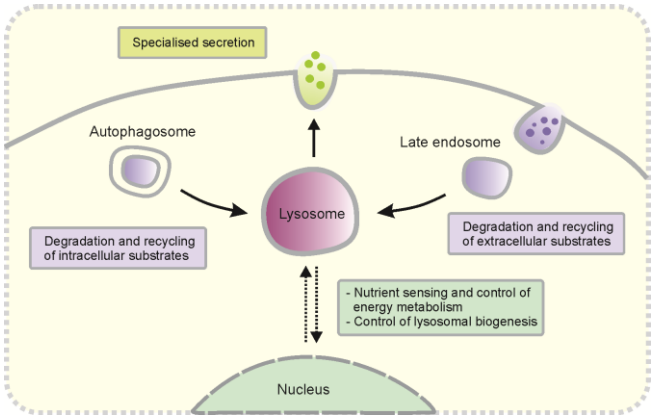

Figure 1: Main functions of the lysosome
Lysosomes are involved in the degradation and recycling of intracellular (via autophagy) and extracellular material (via endocytosis). Lysosomes may undergo exocytosis for membrane repair and to release their content into the extracellular space. Their function in nutrient sensing involves lysosome-to-nucleus signalling that regulates lysosomal biogenesis and energy metabolism (adapted from Settembre *et al*. 2013).

1.1.1 Mannose 6-phosphate-dependent transport of lysosomal enzymes

Newly synthesised lysosomal enzymes are synthesised as inactive precursor proteins and translocated into the lumen of the endoplasmatic reticulum (ER) via their N-terminal signal peptide of 20 – 25 amino acids. After removal of the signal peptide, $Glc_3Man_9GlcNAc_2$-oligosaccharides are transferred to asparagine residues within the NX[S/T] sequence, with X being any amino acid except proline or aspartic acid. The oligosaccharides play a crucial role in protein folding and quality control. Proper folding is ensured by the removal of all glucose and some of the mannose residues, yielding high-mannose type oligosaccharides, allowing lysosomal enzymes to exit the ER via COPII-coated vesicles and to be transported to the Golgi. In the Golgi, high-mannose type oligosaccharides are further modified, either by the addition of complex monosaccharides, such as galactose, fucose, *N*-acetylglucosamine or *N*-acetylneuraminic acid or by the addition of mannose 6-phosphate (M6P) residues (Kornfeld and Kornfeld 1985). The formation of M6P residues is catalysed in a two-step reaction by two enzymes. In the first step, *N*-acetylglucosaminyl-1-phosphate (GlcNAc-

1-phosphate) from uridine diphosphate (UDP)-GlcNAc is transferred to a C6-hydroxyl group of α1,6-branched mannose residues by the GlcNAc-1-phosphotransferase (Reitman and Kornfeld 1981). In a second step, *N*-acetylglucosamine-1-phosphodiester α *N*-acetylglucosaminidase (uncovering enzyme) hydrolyses the GlcNAc-1-phosphodiester, thereby exposing the M6P residue (Kornfeld *et al.* 1999). M6P-moieties on lysosomal enzymes are recognised by two types of M6P-specific receptors, the 46 kDa cation-dependent mannose 6-phosphate receptor (Mpr46) and the 300 kDa cation-independent mannose 6-phosphate receptor (Mpr300). Complexes of the Mpr and their specific M6P-containing ligands exit the TGN in clathrin-coated vesicles, subsequently fusing with endosomal structures. The acidic pH of the endosomal lumen triggers the dissociation of the Mpr-ligand complex, allowing the Mpr to return to the TGN for additional rounds of sorting (Braulke and Bonifacino 2009), while the enzymes are further transported to the lysosome (Dahms *et al.* 1989), undergoing additional post-translational modifications (Braulke and Bonifacino 2009; Makrypidi *et al.* 2012). Minor amounts of newly synthesised lysosomal enzymes escape binding to the Mpr in the TGN and enter the secretory route to be secreted into the extracellular space. The Mpr mainly localise to the TGN and endosomes, whereas approximately 3 to 10 % of the total cellular amount is found at the plasma membrane (Braulke *et al.* 1987). However, only the Mpr300 but not the Mpr46, is involved in endocytosis of M6P-containing ligands (Hickman and Neufeld 1972; Stein *et al.* 1987).

1.1.2 Mannose 6-phosphate-independent transport of lysosomal enzymes

In fibroblast of mucolipidosis type II patients, who lack M6P-containing lysosomal enzymes due to defective GlcNAc-1-phosphotranferase, normal levels of lysosomal enzymes have been detected (Waheed *et al.* 1982). This and various other studies have proposed the existence of alternative, M6P-independent transport pathway for distinct lysosomal enzymes. For instance, the lysosomal enzyme *β*-glucocerebrosidase utilises the lysosomal integral membrane protein Limp2 to be transported to the lysosome M6P-independently. Binding of *β*-glucocerebrosidase to Limp2 already occurs in the ER (Reczek *et al.* 2007). Furthermore, lysosomal sorting of prosaposin and acid sphingomyelinase has been described to be mediated by sortilin, a type 1 transmembrane protein, belonging to the Vps10p super family (Lefrancois *et al.* 2002; Ni and Morales 2006). In addition, it has been shown that a major proportion of newly

synthesised M6P-containing prosaposin is secreted and then re-internalised by the low density lipoprotein receptor-related protein 1 (Lrp1) at the plasma membrane (Hiesberger *et al.* 1998). Lrp1 is a member of the LDL receptor family, which is primarily involved in cholesterol homeostasis (May *et al.* 2007). Lrp2, another member of the LDL receptor family, has been shown to mediate the internalisation of filtered cathepsin B in kidney proximal convoluted tubules, ensuring the supply of enzymatically active cathepin B to these cells (Nielsen *et al.* 2007).

1.1.3 Transport of lysosomal membrane proteins

Lysosomal membrane proteins contain sorting signals of the tyrosine YXXØ or the acid-cluster-dileucine [DE]XXXL[LI] type (X = any amino acid, Ø = hydrophobic amino acid). These consensus sequences are localised in the cytoplasmic tail and mediate lysosomal targeting and endocytosis from the plasma membrane via the interaction with adaptor protein (AP) complexes. Lysosomal membrane proteins reach the lysosomal compartment either directly or indirectly. The direct pathway includes the intracellular pathway from the TGN to early or late endosomes, followed by targeting to the lysosome. In the indirect pathway lysosomal membrane proteins traffic from the TGN to the plasma membrane to be subsequently internalised via clathrin-dependent endocytosis into early endosomes and delivered via late endosomes to the lysosome (Braulke and Bonifacino 2009). Most lysosomal membrane proteins travel through both pathways, while some have been described to use preferentially the direct or indirect way. For instance, mucolipin-1 preferentially use the direct pathway (Miedel *et al.* 2006), while acid phosphatase is transported to the lysosome indirectly via the plasma membrane (Braun *et al.* 1989).

1.2 Lysosomal storage disorders

Lysosomal storage disorders (LSDs) constitute a group of approximately 60 genetic diseases, which are caused by mutations in lysosomal and non-lysosomal proteins, occurring with a total incidence of 1:5,000 live births (Fuller *et al.* 2006). The accumulation of specific macromolecules or monomeric compounds inside the lysosomes is common to all LSDs. Lysosomal diseases are preferentially classified according to the major storage compound and include lipidoses, mucopolysaccharidoses, glycogenosis, neuronal ceroid lipofuscinoses, mucolipidoses

and glycoproteinoses. The clinical spectrum of LSDs is very heterogeneous. While most of the LSDs classically present severe neurological impairment, broad systemic involvement of bone, muscle, liver, kidney and spleen are also observed (Mehta and Winchester 2013). The majority of LSDs is caused by lysosomal hydrolase deficiencies (Ballabio and Gieselmann 2009), while a minor number results from defects in lysosomal membrane proteins (Saftig and Klumperman 2009), including some forms of the neuronal ceroid lipofuscinoses (Kollmann *et al*. 2013).

1.3 Neuronal Ceroid Lipofuscinosis

The Neuronal Ceroid Lipofuscinoses (NCLs) are a group of inherited lysosomal storage disorders. They constitute the most commonly occurring progressive neurodegenerative disorders of childhood with an incidence of 1:12,500 live births worldwide and an estimated carrier frequency of 1 % (Santavuori 1988). The NCLs have been historically classified based on the age of clinical onset, but nowadays depending on the underlying gene mutation (Table 1).

Table 1: Neuronal Ceroid Lipofuscinoses, underlying gene defects and encoded proteins

NCL	***Gene***	***Protein***	***Localisation***	***Phenotype***
CLN1	*PPT1/CLN1*	Protein-palmitoly-thioesterase	Lysosomal matrix	INCL, LINCL, JNCL, ANCL
CLN2	*TPP1/CLN2*	Tripeptidyl-petidase	Lysosomal matrix	INCL, LINCL, JNCL
CLN3	*CLN3*	CLN3	Lysosomal membrane	JNCL
CLN4	*DNAJC5/CLN4*	Cysteine string protein α	Cytoplasm, associated to vesicular membranes	Autosomal dominant ANCL
CLN5	*CLN5*	CLN5	Lysosomal matrix	INCL, LINCL, JNCL, ANCL
CLN6	*CLN6*	CLN6	ER membrane	LINCL, ANCL
CLN7	*MFSD8/CLN7*	CLN7/MFSD8	Lysosomal membrane	LINCL, JNCL
CLN8	*CLN8*	CLN8	ER membrane	LINCL
CLN10	*CTSD/CLN10*	Cathepsin D	Lysosomal membrane	Congenital NCL, JNCL
CLN11	*CLN11/GRN*	Progranulin	Extracellular	ANCL

CLN12	*CLN12/ATP13A2*	ATP13A2	Lysosomal membrane	JNCL
CLN13	*CLN13*	Cathepsin F	Lysosomal matrix	ANCL
CLN14	*CLN14/KCTD7*	potassium channel tetramerisation domain-containing 7	Cytosolic, associated to membranes	INCL

INCL: infantile NCL; LINCL: late infantile NCL; JNCL: juvenile NCL; ANCL: adult NCL

The clinical onset of NCLs is variable and ranges from prenatal/perinatal, infantile, late infantile and juvenile to adult forms. To date thirteen genetically distinct NCL variants including over 365 mutations have been identified (www.ucl.ac.uk/ncl/). The NCL genes code for M6P-containing lysosomal soluble proteins, polytopic membrane proteins localised in lysosomes or the ER, cytosolic proteins and synaptic vesicle associated proteins. Although they are genetically distinct, clinical and pathological hallmarks are similar. Clinically the NCLs share common symptoms, including loss of vision, progressive mental and motor deterioration, myoclonus and epilepsy, leading to premature death (Schulz *et al.* 2013). Disease pathology is characterised by progressive neuronal loss resulting in atrophy of the central nervous system, most pronounced in the retina, the cerebral cortex and the cerebellum. Moreover, NCL pathology is also hallmarked by the accumulation of autofluorescent ceroid lipopigments and proteins in lysosomes of several tissues (Staropoli *et al.* 2012). The storage material in the different genetic forms of NCL is heterogeneous, consisting of proteins, carbohydrates, phospholipids, glycosphingolipids, the anionic lipid bis(monoacetylglycero)phosphate (BMP), dolichols and metals (Cotman and Staropoli 2012). In most NCL forms, the predominantly accumulating protein is the subunit c of the mitochondrial ATP synthase. Subunit c is a 7.5 kDa hydrophobic proteolipid, which constitutes over 50 % of the accumulating storage material (Palmer *et al.* 1989) most likely due to its impaired degradation in the lysosomal compartment (Ezaki *et al.* 1996). The storage material that is predominantly accumulating in CLN1, CLN4 and CLN10 consists of the sphingolipid activator proteins A and D, hydrophobic glycoproteins necessary for the degradation of sphingolipids in lysosomes (Tyynelä *et al.* 1993; Tyynelä and Suopanki 2000; Nijssen *et al.* 2002).

To date, all forms of NCL are incurable. At present there are no curative therapies for any of these disorders and current treatment options are limited to alleviation of the disease symptoms. For three of the four forms of NCL caused by a deficiency in a soluble lysosomal enzyme (CLN1, CLN2, and CLN10), significant progress has been made recently in preclinical studies in mouse models and a naturally occurring affected dog, using a variety of approaches to deliver the missing enzyme, all of which depend on the principle of 'cross-correction'. If the missing enzyme can be successfully delivered to the extracellular space, it will be taken up by receptors at the cell surface, internalised and trafficked to the lysosome (Griffey *et al.* 2006; Chang *et al.* 2008; Tamaki *et al.* 2009; Shevtsova *et al.* 2010; Katz *et al.* 2014). Experimental treatments of CLN1 and CLN2 patients, including gene therapy, neural stem cell therapy, intraventricular enzyme replacement therapy, are currently in clinical trials. The therapeutic outlook is still bleak for those NCL forms caused by mutations in transmembrane proteins. This is because these proteins will not be released to cross-correct neighbouring affected cells, and experimental therapeutic strategies have been limited to blocking selected events, such as neuro-inflammation and deposition of immunoglobulin G in the brain (Seehafer *et al.* 2011).

1.3.1 Juvenile Neuronal Ceroid Lipofuscinosis - CLN3 disease

The classical Juvenile Neuronal Ceroid Lipofuscinosis (JNCL) is caused by mutations in the *CLN3* gene. First symptom in most cases is visual impairment starting at the age of 5 – 7 years and leading to blindness within 2 – 4 years of onset. This is followed by seizures of variable subtypes, advancing motor and cognitive decline, and neuropsychiatric disturbances. Premature death occurs at the end of the first or within the second decade, but rarely beyond the third decade (Cotman and Staropoli 2012). Even though the NCLs are seen as primarily neurodegenerative diseases, recent reports have shown that they affect the human body beyond the brain, as shown by progressive cardiac involvement (Ostergaard *et al.* 2011). Other disease manifestations outside the CNS may involve the vegetative nervous system as well as the immune system.

The first mutations in the *CLN3* gene were identified in JNCL patients in 1995 (The International Batten Consortium (1995)). The *CLN3* gene is located on chromosome 16p11.2 and codes for a 438 amino acid polytopic transmembrane protein. It consists of

15 exons, being highly conserved between species down to yeast. Notably, even exon size and the position of splice site sequences are conserved between species (Mole *et al.* 2011). The majority of the patients (~74 %) are homozygous for a 1.02 kb genomic deletion mutation, which presents the most common mutation and appears to be a founder mutation that arose in a common European ancestor (Mole *et al.* 2011). The 1.02 kb deletion is localised between intron 6 and 8, which results in the deletion of exon 7 and 8, giving rise to the formation of two mutant mRNA transcripts. The major transcript contains exon 1 - 6 spliced to exon 9. The loss of exon 7 and 8 leads to a frameshift in exon 9 and the formation of a premature stop codon, encoding a truncated protein of the first 153 amino acids and 28 additional novel amino acids. The second transcript consists of exon 1 - 6 spliced to exon 10 - 15, encoding a protein that is missing amino acids 154 – 263 as a consequence of exon skipping and formation of a novel splice site (Kitzmüller *et al.* 2008). In addition to the common 1.02 kb deletion, 39 rare mutations have been reported, including insertions, deletions, missense, nonsense and splice site mutations. Approximately 22 % of the patients are compound heterozygous for the 1.02 kb deletion and one of the other rare mutations, while only a small number of patients (~4 %) carry two of the rare mutations (Munroe *et al.* 1997). Most of the rare mutations were mapped to the luminal side of the transmembrane structure, implying that they are crucial sites for CLN3 function.

1.3.2 CLN3 protein

The CLN3 protein is synthesised in the ER and *N*-glycosylated at the positions N71 and N84 in the Golgi compartment. From the Golgi, CLN3 travels to early and late endosomes to be finally delivered to the lysosome. The efficient sorting and transport of CLN3 requires several sorting signals, including the dileucine motif $EEEX_8LI$ in the large cytoplasmic loop and a targeting motif consisting of a stretch of methionine and glycine, separated by 9 amino acids, MX_9G (Kyttälä *et al.* 2004; Storch *et al.* 2004). Controversial data were published, whether CLN3 binds the adaptor proteins AP1 and AP3, which mediate sorting and lysosomal targeting of CLN3 (Storch *et al.* 2004; Kyttälä *et al.* 2005). A small fraction of CLN3 may be transported to the plasma membrane, from where it is subsequently internalised into the endocytic system. In addition to TGN sorting motifs, C-terminal prenylation, presumably in the form of

farnesylation, is required for the efficient endosomal sorting processes of CLN3 (Storch *et al.* 2007).

The exact function of CLN3 is unknown, although CLN3 has been associated with various processes mainly in the endo-lysosomal system. JNCL fibroblasts and *Δbtn1*-yeast, representing a deletion of the *CLN3* orthologue, have been shown to harbor defects in lysosomal/vacuolar acidification (Pearce and Sherman 1998; Holopainen *et al.* 2001; Gachet *et al.* 2005). Moreover, defective arginine transport into the vacuole of *Δbtn1*-yeast has been described (Kim *et al.* 2003). In $Cln3^{ki}$ cerebellar cells, JNCL fibroblasts and the *Δbtn1*-yeast model, deficiencies in bulk endocytosis were observed (Fossale *et al.* 2004; Luiro *et al.* 2004; Codlin *et al.* 2008). $Cln3^{ki}$ cerebellar cells additionally presented defects in maturation of autophagosomes, a process that requires fusion with lysosomes (Cao *et al.* 2006). In neurons endogenous CLN3 has been reported to be enriched in synaptosomal fractions isolated from nerve terminals (Luiro *et al.* 2001). In line with these findings, alterations in neurotransmitter and receptor levels at synapses of Cln3 genetic mouse models were described (Kovacs *et al.* 2006; Herrmann *et al.* 2008; Finn *et al.* 2011). CLN3 function in vesicular compartments close to the plasma membrane may involve interaction with components of the actin cytoskeleton (Uusi-Rauva *et al.* 2008; Getty *et al.* 2011), with lipid rafts enriched in cholesterol and sphingolipids (Persaud-Sawin *et al.* 2004; Rakheja *et al.* 2004) or with ion channels and their accessory proteins (Chang *et al.* 2007; Uusi-Rauva *et al.* 2008).

1.3.3 Cln3 animal models

Currently four JNCL mouse models have been generated and characterised. Two different Cln3 knock-out models were created by disrupting the *Cln3* gene in either exon 1-6 (Mitchison *et al.* 1999) or exon 7-8 (Katz *et al.* 1999). In addition, a Cln3 reporter mouse was established by replacing exon 1 – 8 with a *lacZ* reporter gene (Eliason *et al.* 2007). The Cln3 knock-in mouse model ($Cln3^{ki}$) harbours a 1.02 kb deletion mutation, the most common genetic defect in CLN3 patients. By homologous recombination and Cre-*lox* P-mediated technology the deletion was introduced into the murine *Cln3* gene (Cotman *et al.* 2002). With the exception of visual loss (Seigel *et al.* 2002), all Cln3 mouse models display pathological features of CLN3 disease, including accumulation of subunit c of the mitochondrial ATP synthase, astrogliosis, neurological

dysfunction and neurodegeneration (Katz *et al.* 1999; Mitchison *et al.* 1999; Cotman *et al.* 2002; Pontikis *et al.* 2005; Eliason *et al.* 2007; Herrmann *et al.* 2008). Of note, studies in the Cln3 reporter mouse model demonstrated an osmoregulated role for Cln3 protein in control of renal water and potassium balance (Stein *et al.* 2010). However, depending on the genetic background and environment, disease onset (at 10 to 20 months of age) and behavioural abnormalities may vary across the different Cln3 mouse models.

Even so, the *Cln3*^{ki} mouse model represents the only genetically accurate model for CLN3 disease. The pathologic hallmark of CLN3 disease, accumulation of lysosomal storage, is present before birth in neuronal and non-neuronal tissues. *Cln3*^{ki} mice appear normal at birth but at 10 to 12 months of age they develop neurological abnormalities, including clasping and an altered gait, but seizures have not been observed. *Cln3*^{ki} mice die prematurely between 12 and 18 months of age (Cotman *et al.* 2002). Moreover, a delay in axon pruning at the neuromuscular junction and neurodevelopmental delay has been reported (Song *et al.* 2008; Osorio *et al.* 2009). Past 3 months of age, *Cln3*^{ki} mice displayed electroretinographic changes indicating cone function deficits and a progressive decline of retinal post-receptoral function, but no loss of photoreceptors. Moreover, alteration in haematopoiesis were proposed in *Cln3*^{ki} mice, as serum ferritin concentrations, mean corpuscular volume of red blood cells and reticocyte counts were increased and in addition, vacuolated peripheral blood lymphocytes were already observed in neonates (Staropoli *et al.* 2012).

1.3.4 Immunological alteration in CLN3 disease

Lysosomes and lysosome-related organelles constitute the primary degradative compartment of the cell. The catabolic function of these organelles is crucial for several immunological processes, such as removal of pathogens by phagocytosis, cytokine secretion and antigen processing and presentation (Colbert *et al.* 2009). Several lysosomal storage disorders have now been associated with alterations in systemic and neuroimmune responses, which may be directly or indirectly linked to disease pathology. For instance, patients with the lysosomal storage disorders Gaucher disease, mucopolysaccharidosis VII and α-mannosidosis were described to be predisposed towards immune suppression, whereas patients suffering from GM2 gangliosidosis,

globoil cell leukodystrophy and JNCL are predisposed towards immune system hyperactivity (Castaneda *et al.* 2008).

A striking feature of CLN3 disease is the presence of vacuolated lymphocytes in the peripheral blood of CLN3 patients, presenting also a diagnostic hallmark of the disease (Schulz *et al.* 2013). However, it remains unclear, whether lysosomal storage material contributes to lysosomal and cellular dysfunction. Examination of peripheral blood of *Cln3*^{ki} mice revealed an increase in size and frequency of reticulocytes, indicating possible abnormalities in haematopoiesis. Moreover, vacuolated lymphocytes and subtle differences in T cell frequencies were observed in peripheral blood of *Cln3*^{ki} mice (Staropoli *et al.* 2012). The link, however, between lysosomal dysfunction in CLN3 disease and possible alterations in the peripheral immune system needs to be elucidated.

In addition, several studies have pointed towards neuro-inflammation in CLN3 pathology. Activated microglia were observed in the *Cln3*$^{-/-}$ and *Cln3*^{ki} mouse model, predicting areas that will undergo neurodegeneration (Pontikis *et al.* 2004; Pontikis *et al.* 2005). Moreover, microglia of *Cln3*^{ki} mice were shown to exist in a primed state to produce inflammatory mediators (Xiong and Kielian 2013). In the *Cln3*$^{-/-}$ mouse model, infiltration of T lymphocytes and activation of microglia in the optic nerve has been observed from 15 months of age. Interestingly, absence of sialoadhesin, a monocyte restricted adhesion molecule that is important for interactions with lymphocytes, significantly ameliorated disease progression (Janos Groh, NCL Congress 2014).

2 Aim of the study

CLN3 disease is a neurodegenerative lysosomal storage disorder caused by mutations in the *CLN3* gene, coding for a lysosomal transmembrane protein of unknown function.

So far, it is unclear whether the non-functional CLN3 protein directly impairs lysosomal homeostasis. Therefore, the present study is focused on

- the protein composition of lysosomes in *Cln3*^{ki} cerebellar cells, carrying the 1 kb deletion (Δex7/8), using SILAC-based quantitative proteomic analysis, and
- validation of dysregulated proteins and lysosomal targeting pathways in *Cln3*^{ki} cerebellar cells.

Besides profound neurological impairment, recent studies suggested that CLN3 disease also displays alterations in the immune system. Therefore, experiments have been performed to examine the impact of Cln3 deficiency on

- the composition and tissue distribution of immune cells,
- presence of storage material in immune cells of *Cln3*^{ki} mice,
- macrophage-mediated processes, such as antigen-processing and presentation, as well as T cell response *in vitro* and *in vivo*.

3 Materials and Methods

3.1 Materials

3.1.1 Equipment, consumables and chemicals

Table 2: Equipment

Device	*Model*	*Manufacturer*
Autoclave	3850 EL	Systec
Balance (fine)	AC100	Mettler Toledo
Balance	BP2100 S	Sartorius
Block thermostat	Rotilabo H 250	Roth
Centrifuge	5418, 5415R, 5804R	Eppendorf
CO_2 incubator	Innova CO-170	New Brunswick Scientific
Cryogenic freezing unit	Nalgene™ Cyro 1 °C	Nalgene
Douncer	1 ml	Wheaton
Electrophoresis chamber (Agarose gels)	PerfectBlue Maxi M	PeqLab Biotechnologie
Electrophoresis chamber (SDS-PAGE)	PerfectBlue Twin S, M	PeqLab Biotechnologie
Power supply	peqPOWER E300	PeqLab Biotechnologie
Film developer	Curix 60	Agfa
γ-Counter	Wallac 1470	Perkin Elmer
Gel dryer	GelAir Dryer	Bio-Rad
Ice machine	AF10	Scotsman
Immunoblot imager	ChemiDoc XRS	Bio-Rad
Incubation shaker	Innova 4230	New Brunswick Scientific
Laminar flow hood	Herasafe	Thermo Scientific
Liquid nitrogen cryogenic storage container	Arpege 55	Air Liquide
Magnetic stirrer	MR Hei-Mix L	Heidolph
Microscope	CKX31	Olympus
Microscope, confocal	TCS SP5	Leica
Microscope, confocal	Axiovert 200	Zeiss
Microwave	Promicro	Whirlpool

pH meter	MP220	Mettler Toledo
Photometer	BioPhotometer	Eppendorf
Pipettes	Research	Eppendorf
Pipette controller	peqMATE	PeqLab Biotechnologie
Plate reader	MultiscanGo	Thermo Scientific
Real Time PCR Cycler	Mx3000P	Stratagene
Roller mixer	SRT6	Stuart, Staffordshire
Shaker	Rocky	Fröbel Labortechnik
Thermocyler	peqSTAR	PeqLab Biotechnologie
Tranfer chamber	PerfectBlue Web S	PeqLab Biotechnologie
Ultrasonic bath	Elmasonic 15	Elma
UV transluminator and imager	EBox VX2	PeqLab Biotechnologie
Vacuum pump	PC 2004 VARIO	Vacuubrand
Vortex	peqTWIST	PeqLab Biotechnologie
Water bath	C 10	Schütt Labortechnik
FACS unit	Canto II	BD Bioscience

Table 3: Consumables

Consumable	***Company***
Amicon Ultra Centrifugal filters, 0.5 ml	Merck
Coverslips	Glaswarenfabrik Karl Hecht
Cyrovials	Nunc
Cuvettes	Plastibrand
Disposable material for cell culture	BD Bioscience, Sarstedt, Nunc
Disposable cell scraber	Sarstedt
FACS tubes	BD Bioscience
Immersion oil 518 C	Zeiss
Lens paper MN 10 B	Zeiss
Microscope slides	Engelbrecht
Needles	Becton GmbH
Nitrocellulose membrane Protran™	Whatman GmbH
Parafilm	Bemis
Pipette tips	Sarstadt, Eppendorf
Scintillation tubes	Perkin Elmer
Reaction tubes	Sarstadt, Eppendorf

Scalpels	Braun
Sephadex PD-10	GE Healthcare
Sterile syringe filters	VWR
Syringes	Braun
Transparent foil	Pütz Folien
Whatman paper	Whatman GmbH
X-ray films	GE Healthcare

Table 4: Chemicals

Chemical compound	***Company***
Acetic acid	Merck
Acrylamide/Bisacrylamide	Roth
Agar	Roth
Agarose	AppliChem
Ammonium chloride (NH_4Cl)	Sigma-Aldrich
Ammonium peroxydisulfate (APS)	Roth
Aqua-Polymount	Polyscience
Beta-mercaptoethanol	Sigma-Aldrich
Bovine serum albumin (BSA) powder	Serva
Brefeldin A (BFA)	Sigma-Aldrich
Bromophenol blue	Bio-Rad
Bovine serum albumin (BSA) powder	Serva
BSA solution for Bradford (2 mg/ml)	Thermo Scientifc
Calcium chloride ($CaCl_2$)	Merck
4‘,6-Diamidino-2-phenylindole (DAPI)	Roth
Dextran-stabilized magnetite beads (Fe_3O_4)	Liquid Research Limited
Dextran 10,000 MW, AF546-labelled	Invitrogen
Dimethlysulfoxide (DMSO)	Roth
Dithiothreitol (DTT)	Sigma-Aldrich
Ethanol	Merck
Ethidium bromide	Sigma-Aldrich
Ethlendiaminetetraacetate (EDTA)	Roth
Glycerol	Roth
Glycine	Roth
HEPES	Roth

Hydrochloric acid (HCl)	Merck
Hydrogen peroxide (H_2O_2)	Merck
Isopropanol	Roth
Luminol	Roth
Magnesium chloride ($MgCl_2$)	Sigma-Aldrich
Methanol	Merck
Milk powder non-fat dry	Roth
NNN'N'-Tetramethylethylenediamine (TEMED)	Sigma-Aldrich
Paraformaldehyde	Sigma-Aldrich
p-Cumaric acid	Sigma-Aldrich
Peptone/tryptone	Roth
p-Nitrophenyl-N-Acetyl-β-D-glucosamid	Sigma-Aldrich
Potassium chloride (KCl)	Roth
Potassium hydrogen carbonate	Roth
Potassium dihydrogen phosphate	Roth
Potassium iodine (KI)	Roth
Protease inhibitor cocktail	Sigma-Aldrich
Saponin	Sigma-Aldrich
Sodium acetat	Merck
Sodium azid	Sigma-Aldrich
Sodium citrate	Merck
Sodium chloride (NaCl)	Roth
Sodium dodecyl sulphate (SDS)	Sigma-Aldrich
Sodium di-hydrogen phosphate	Merck
Sodium hydrogen carbonate	Roth
Sodium hydroxide (NaOH)	Roth
[^{125}I]-Sodium iodine	Hartmann Analytic GmbH
Sodium pyrovate	Sigma-Aldrich
Thioglycolate medium	BD Bioscience
Triton X-100	Sigma-Aldrich
Trizma base (Tris-Cl)	Sigma-Aldrich
Tween 20	Sigma-Aldrich
Yeast extract	Roth

3.1.2 Kits and assays

Table 5: Kits and assays

Kit	*Company*
Bio-Rad Protein Assay	Bio-Rad
GeneJET™ RNA purification kit	Thermo Scientific
High Capacity cDNA Reverse Transcription	Invitrogen
KAPA2G Fast HS Genotyping Mix	Peqlab Biotechnologie
IODOGEN® Labelling Kit	Thermo Scientific
Taqman® Gene Expression Assay	Invitrogen

3.1.3 Proteins, standards and inhibitors

Table 6: Proteins and standards

Proteins/Standards	*Company*
α_2-macroglobulin	Provided by Prof. Dr. Jörg Heeren ((Ashcom *et al.* 1990; Laatsch *et al.* 2009))
Arylsulfatase B (ASB)	BioMarin
Cholera toxin subunit B, AF546-labelled	Invitrogen
DQ-BSA	Invitrogen
Receptor associated protein (RAP)	Gift from Dr. S. Markmann
PeqGOLD Protein Marker IV	PeqLab Biotechnologie
1 kb DNA ladder	Thermo Scientific

Table 7: Inhibitors

Inhibitors	*Company*
Brefeldin A	Sigma-Aldrich
Protease Inhibitor Cocktail	Roche Diagnostics

3.1.4 Antibodies

Table 8: Primary antibodies

Antibody	*Reactivity*	*Host*	*Dilution*	*Company*
α-Tubulin (T9026)	mouse	mouse	1:2000 (WB)	Sigma-Aldrich
Cathepsin B (GT15047)	mouse	goat	1:2000 (WB)	Neuromics
Cathepsin D (sc6486)	mouse	goat	1:1000 (WB)	Santa-Cruz
Cathepsin L (MAB9521)	mouse	rat	1:1000 (WB)	R&D

Cathepsin S (sc6505)	mouse	goat	1:1000 (WB)	Santa Cruz
Cathepsin Z (AF1033)	mouse	goat	1:1000 (WB)	R&D
CD3 (145-2C11)	mouse	rabbit	1 µg/ml (Cell culture)	Biolegend
Cd74 (ln-1)	mouse	rat	1:5000 (WB)	BD Bioscience
GAPDH (sc25778)	mouse, human	goat	1:1000 (WB)	Santa Cruz
Gm130 (610822)	Mouse	mouse	1:200 (IF)	BD Bioscience
Lamp1	Mouse	rat	1:1000 (WB)	Hybridoma 1D4B
Lamp2	Mouse	rat	1:1000 (WB)	Hybridoma ABL-93
Limp2	Mouse	rabbit	1:2000 (WB)	Gift from Dr. M. Schwake
Lrp1 (ab92544)	Mouse	rabbit	1:3000 (WB)	Abcam
Lyaat1 (N-13)	mouse, human	goat		Santa Cruz
Mpr300	Rat	goat	1:2000 (WB), 1:100 (IF)	own preparation
subunit c, ATP synthase	mouse, human	rabbit	1:100 (IF)	Gift from Prof. S. Cotman
subunit c, ATP synthase	mouse, human	rabbit	1:2000 (WB)	Gift from Prof. Dr. E. Neufeld
Transferrin receptor (H68.4)	Mouse	mouse	1:1000 (WB)	Invitrogen

Table 9: Antibodies for flow cytometry

Antibody	***Reactivity***	***Host***	***Fluorophore***	***Dilution (per 10^6 cells)***	***Clone***	***Company***
CD3	mouse	Human	V450	0.5 µg	eBio500A2	eBioscience
CD4	mouse	rat	PE	0.5 µg	RM4-5	eBioscience
CD4	mouse	rat	V450	0.5 µg	RM4-5	eBioscience
CD4	mouse	rat	PerCP	0.5 µg	RM4-5	BioLegend
CD8a	mouse	rat	PE-Cy7	0.5 µg	53-6.7	eBioscience
CD8a	mouse	rat	V450	0.25 µg	53-6.7	BD Bioscience
CD11b	mouse	rat	PerCP	0.5 µg	M1/70	eBioscience
CD11c	mouse	rat	V450	1 µg	N418	BioLegend
CD19	mouse	rat	PerCP	0.25 µg	eBio1D3	eBioscience
CD44	mouse	rat	APC	0.25 µg	IM7	eBioscience
CD62L	mouse	rat	APC-Cy7	0.5 µg	MEL-14	BioLegend
Gr1	mouse	rat	APC-Cy7	0.25 µg	RB6-8C5	eBioscience
IFNγ	mouse	rat	PE	0.5 µg	XMG1.2	BD Bioscience

IFNγ	mouse	rat	FITC	0.5 µg	XMG1.2	eBioscience
Ly6C	mouse	rat	FITC	1 µg	AL-21	BD Bioscience
MHCII	mouse	rat	PE	0.25 µg	M5/114.15.2	eBioscience
TNFα	mouse	rat	APC	0.5 µg	MP6-XT22	eBioscience

Table 9: Secondary antibodies

Antibody	***Dilution***	***Company***
AF488-coupled anti-rabbit IgG	1:500 (IF)	Invitrogen
AF546-coupled anti-mouse IgG	1:500 (IF)	Invitrogen
AF546-coupled anti-rat IgG	1:500 (IF)	Invitrogen
HRP-coupled anti-goat IgG	1:3000 (WB)	Dianova
HRP-coupled anti-mouse IgG	1:3000 (WB)	Dianova
HRP-coupled anti-rabbit IgG	1:3000 (WB)	Dianova
HRP-coupled anti-rat IgG	1:3000 (WB)	Dianova

3.1.5 Mammalian cells lines and media

Table 10: Mammalian cell lines

Cell line	***Provider***
Cln3^{ki} cerebellar cells	Prof. Dr. S. Cotman (Fossale *et al.* 2004)
Cln3^{ki} mouse embryonic fibroblasts	Own preparation

Table 11: Cell culture media and solutions

Media/solutions	***Company***
Dulbecco's modified eagle's medium (DMEM)	Invitrogen
Pierce SILAC Quantification Kit (89983)	Thermo Scientific
Fetal calf serum (FCS)	GE Healthcare
Geneticin	Invitrogen
GlutaMax™	Invitrogen
IL-2	Novartis
LPS	Sigma-Aldrich
Opti-MEM®-1 + GlutaMax™	Invitrogen
Penicillin/Streptomycin	Invitrogen
Phosphate buffered saline (PBS) 10x	Invitrogen
Roswell Park Memorial Institute 1640 (RPMI 1640)	Invitrogen
Trypsin/EDTA	Invitrogen

3.1.6 Commonly used buffers

Table 12: Commonly used buffers

Buffer	*Components*
PBS	137 mM NaCl, 2.7 mM KCl, 10 mM Na_2HPO_4, 1.76 mM KH_2PO_4; pH 7.4
TBS	10 mM Tris/HCl, 150 mM NaCl; pH 7.4
TAE	40 mM Tris/HCl, pH 8.5, 20 mM acetic acid, 2 mM EDTA
ACK	155 mM NH_4Cl, 10 mM $KHCO_3$, 100 µM EDTA, pH 7.2

3.1.7 Software

Table 13: Software

Software	*Company*
Adobe Photoshop 7.0	Adobe Systems
CorelDraw v11.633	Corel
Endnote X4.0.2	Thomson Reuters
GraphPad PRISM	Graphpad Software Inc.
Image Lab™	Bio-Rad
Leica LAS AF Lite	Leica
Mascot search engine Version 2.4.1	Matrix Science
Meta Fluor	MDS Analytical Technologies
Microsoft Office 2010	Microsoft
MxPro Realime PCR 4.6.1	Stratagene Europe
Proteome Discoverer Version 1.4.0.288	Thermo Scientific
Quantity One v4.6.7	Bio-Rad
TILL vision	TILL Photonics/FEI

3.2 Molecular Biology Methods

3.2.1 Genotyping of *Cln3^{ki}* mice

KAPA Mouse Genotyping Hot Start Kit was used for extraction of genomic DNA from tail biopsies and cell pellets. Genotyping PCR was performed according to the manufacturer's instructions using wild type primers, WtF and WtR, to obtain a ~250 bp band and *Cln3^{ki}* primers, 552F and Ex9RA, to obtain a ~500 bp band. Primer sequences are listed in section 9.1. Following PCR cycling conditions were used:

Table 14: PCR conditions for genotyping of *Cln3*^{ki} mice

Temperature	*Time*	
95 °C	5 min	
95 °C	30 s	34 cycles
58 °C	30 s	
72 °C	35 s	
72 °C	5 min	

3.2.2 Agarose gel electrophoresis

Agarose gel electrophoresis was used to separate nucleic acid molecules by size. Shorter molecules move faster and migrate farther than long molecules. In general, lower concentrations of agarose are more suitable for larger molecules because the separation between bands of similar size is greater. 1 – 3 % (w/v) agarose in TAE buffer was used to pour gels along with ethidium bromide at a final concentration of 0.5 µg/ml. Each sample was mixed with one-sixth volume of 6x concentrated loading dye and run at 120 V until the loading dye reached the last third of the gel. Ethidium bromide bound to nucleic acids was visualized by UV illumination and sizes of the fragments were estimated by comparison with DNA size markers.

3.2.3 RNA isolation from cells

Fermentas RNeasy Kit was used to isolate RNA from cultured cells following the manufacturer's instructions. RNA was eluted with 50 µl HPLC pure water and RNA quality was analysed by agarose gel electrophoresis. RNA samples were quantified by NanoDrop and stored at -80 °C.

3.2.4 cDNA preparation

cDNA synthesis from isolated RNA was performed according to the instructions of the High Capacity cDNA Reverse Transcription Kit. For quantitative real time PCR (qRT PCR) 1 µg RNA was used for cDNA synthesis.

3.2.5 Quantitative real time PCR

qRT PCR is a method to simultaneously amplify and quantify cDNA. Real time technology is based on the detection of a fluorescent signal produced proportionally during the amplification of a DNA target. Real time assays determine the point in time during cycling when amplification of a PCR product is first detected. The cycle number at which the reporter dye emission intensity rises above background noise is called threshold cycle (C_T). The C_T is determined at the exponential phase of the PCR reaction and is inversely proportional to the copy number of the target. Hence, the higher the starting copy number of the nucleic acid target, the sooner a significant increase in fluorescence is observed and the lower the C_T. The TaqMan® Gene Expression Assays are based on 5’ nuclease activity of the Taq-polymerase. The assay of the target gene consists of a pair of unlabelled PCR primers and a TaqMan® probe with a FAM™ dye label on the 5' end, and a non-fluorescent quencher on the 3' end, preventing detection of the fluorescence. Once the Taq-polymerase cleaves the probe via its endogenous nuclease activity, the dye is separated from the quencher and fluorescence can be detected. During the PCR reaction increasing amounts of the dye are released, which leads to an increasing fluorescence signal proportional to the amount of amplicon synthesized.

The samples were prepared as shown in Table 14 and run on Mx3000P cycler (Table 15). The reaction steps were initial denaturation at 95 °C for 10 min, followed by 40 cycles consisting of denaturation at 95 °C for 30 s and a combined annealing and extension step at 60 °C for 1 min.

Table 15: Sample preparation for qRT PCR

Component	***Volume (µl)***
MaximaTM Probe qPCR Master Mix (2x)	10
HPLC H2O	7
Template cDNA	2
TaqMan® Gene Expression Assay	1

Table 16: Cycle protocol for qRT PCR

Step	*Purpose*	*Temperature*	*Time*
1	Initial denaturation	95 °C	10 min
2	Denaturation	95 °C	30 s
3	Annealing and extension	60 °C	1 min

Relative quantification was used to determine the ratio between the quantity of the target gene in the *Cln3*^{ki} and wild-type samples. The housekeeping gene *β-actin* was used to normalise for slight differences in starting cDNA levels. After normalisation of the target gene according to the housekeeping gene levels, the change in C_T between the different samples was calculated, with a lower C_T indicating earlier amplification and therefore higher expression levels. The relevance of C_T changes was inferred by calculating the linear fold change ratio using the $2^{\Delta\Delta CT}$ method. ΔC_T values were calculated as follows:

$\Delta C_T = C_T$ (target gene) – C_T (*β-actin*)

$\Delta\Delta C_T = \Delta C_T$ (*Cln3*^{ki}) – ΔC_T (wild-type)

3.3 Cellular Biology Methods

3.3.1 Mammalian cell culture

For sub-culturing of adherent cells, medium was aspirated, cells were washed with phosphate buffered saline (PBS) and cells were removed from the culture vessel using 1 ml of 1 x trypsin-EDTA to cover the surface and incubated for a few minutes at 37 °C. Trypsin-EDTA was deactivated with medium. Cells were re-seeded at the appropriate densities, for example at 1:10 dilutions for routine passage. When required cell numbers were determined using a Neubauer haemocytometer. Cells were cultured in polystyrene flasks for passaging or in 35 mm and 60 mm petri dishes for experiments.

Cerebellar precursor cell line

Cultured cerebellar cells derived from *Cln3*^{ki} mice were maintained DMEM containing 10 % (v/v) heat-inactivated FCS, 100 IU/ml penicillin, 50 mg/ml streptomycin, 1 x Glutamax, 24 mM KCl, 200 µg/ml geneticin 110 mg/ml sodium pyruvate in humidified air at 33 °C and 5 % CO_2.

Peritoneal macrophages

For preparation of macrophages mice were injected intraperitoneal with 2 ml thioglycollate to activate macrophages causing peritonitis. 6 days after injection mice were sacrificed and peritoneal cavity was rinsed twice with 5 ml medium to collect macrophages. Cells were kept on ice to prevent clumping and centrifuged at 310 x g for 5 min at 4 °C, re-suspended in fresh medium and seeded at appropriate densities. Macrophages were maintained in RPMI-1640 containing 5 % (v/v) FCS, 2 mM L-glutamin, 50 mg/ml gentamycin and 50 µM β-mercaptoethanol (complete RPMI medium) for 3 days until used for experiments.

Primary mouse embryonic fibroblasts

Mouse embryonic fibroblasts (MEF) were isolated from mouse embryos at days E12.5. Red tissue was removed and the embryo was minced and trypsinised for 10 min at 37 °C. Digestion was stopped by adding DMEM containing 10 % (v/v) FCS and isolated cells were centrifuged at 900 x g for 5 min at room temperature, re-suspended in fresh medium and seeded. Primary mouse embryonic fibroblasts were maintained in DMEM containing 10 % (v/v) FCS and 100 IU/ml penicillin, 50 mg/ml streptomycin, 1 x Glutamax in humidified air at 37 °C and 5 % CO_2.

Splenic T and B cell blasts

Immune cells from spleen were isolated as described in 3.3.11. Cells isolated from one spleen were distributed to two flasks and cultured in complete RPMI medium with for 5 days. T and B cells blasts were obtained by stimulation with 1 µg/ml anti-CD3 antibody and 10 U/ml interleukin-2 (IL-2), or 10 µg/ml lipopolysaccharide (LPS), respectively. Complete RPMI medium supplemented with IL-2 or LPS, respectively, was refreshed after 2 days.

3.3.2 Cryopreservation of cerebellar precursor cells

Cells were trypsinised and pelleted at 1000 x g and re-suspended in FCS containing 10 % dimethylsulphoxide (DMSO). Cells were aliquoted to cryovials, transferred to a Cryo Freezing Container and frozen at -80 °C. For rescue of frozen cells, aliquots were thawed quickly at 37 ^{o}C, transferred to 10 ml of medium, pelleted at 1000 x g for 4 min and re-suspended in medium and seeded.

3.3.3 Conditioning of medium

Cerebellar cells were washed with PBS and incubated in OPTIMEM for 24 h at 33 or 37 °C, respectively. Conditioned medium was removed and centrifuged at 1000 x g at 4 °C for 4 min to pellet dead cells and concentrated using centrifugal filters according to the manufacturer's instructions.

3.3.4 Endocytosis of [^{125}I]-labelled proteins

Arylsulfatase B (ASB) and α_2-macroglobulin (α_2-MG) were iodinated with sodium [^{125}I](75 TBq/mmol) and IODO-GEN® as described (Braulke *et al.* 1987) to specific activities. Cells grown in 6 cm dishes were incubated with DMEM/0.1 % (w/v) BSA (DMEM/BSA) for 1 h, followed by incubation with the respective [^{125}I] labeled proteins (~250,000 cpm/ml) in DMEM/BSA in the absence or presence of 10 mM mannose 6-phosphate (M6P) or 30 µM receptor-associated protein (RAP) for the indicated time points. Cells were washed with PBS and either harvested or chased in DMEM/BSA for the indicated time points. Cell lysis was performed in PBS containing 0.2 % (w/v) Triton X-100 and protease inhibitors as described in 3.4.1. Protein concentration was determined by Bradford assay (3.4.2) and samples were separated by SDS-PAGE (3.4.3). The gel was placed between two cellophane foils and dried for 2 h in a gel dryer, subsequently applied to an X-ray film and visualized by autoradiography.

3.3.5 Binding of [^{125}I]-labelled ASB

Cells were cultured on 3.5 cm plates and cooled to 4 °C, followed by the incubation with [^{125}I]-ASB (~600,000 cpm/ml) in DMEM/BSA and 20 mM Hepes, pH 7.4 in the absence or presence of 10 mM M6P. For measuring the binding of [^{125}I]-ASB to total amounts of Mpr300, medium contained 0.1 % (w/v) saponin. Cells were washed with ice-cold PBS and harvested. The cell-associated radioactivity was determined in a γ-Counter and related to protein amount.

3.3.6 Endocytosis of transferrin

Cells were cultured on coverslips in 24-well plates and incubated in serum-free medium containing 25 µg/ml AlexaFluor546-transferrin at 33 °C for 10 min. Subsequently, cells

were washed three times with PBS and fixed in 4 % (w/v) paraformaldehyde for 15 min at room temperature.

3.3.7 Endocytosis of cholera toxin subunit B

Cells were cultured on coverslips in 24-well plates and incubated in serum-free medium containing 1 µg/ml AlexaFluor488-labelled cholera toxin subunit B for the indicated time points at 4 or 33 °C. Subsequently, cells were washed three times with PBS and fixed in 4 % (w/v) paraformaldehyde for 15 min at room temperature or at 4 °C.

3.3.8 Endocytosis of dextran

Cells were cultured on coverslips in 24-well plates and incubated in medium containing 100 µg/ml AlexaFluor546-labelled dextran for 24 h at 33 °C. Subsequently, cells were washed three times with PBS and fixed in 4 % (w/v) paraformaldehyde for 15 min at room temperature.

3.3.9 Endocytosis of DQ-BSA

Peritoneal macrophages grown in 3.5 cm dishes were incubated in RPMI/BSA for 1 h, followed by incubation with 10 µg/ml DQ-BSA in the absence or presence of 50 mM NH_4Cl for 15 min at 37 °C. Cells were washed with PBS and either fixed in 4 % paraformaldehyde for 30 min on ice or chased in RPMI/BSA in the presence or absence of 50 mM NH_4Cl at 37 °C for the indicated time points. After fixation cells were washed with PBS and kept on ice until FACS analysis.

3.3.10 Stable isotope labelling by amino acids in cell culture

Stable isotope labelling by amino acids in cell culture (SILAC) is an approach for *in vivo* incorporation of isotopic labelled amino acids into proteins for mass spectrometry-based quantitative proteomics. The method allows protein quantification through metabolic encoding of whole cell or single organelle proteomes using stable isotope labelled amino acids (‘heavy’ and ‘light’) that are incorporated into all newly synthesised proteins.

Cln3^{ki} and wild-type cerebellar cell line were cultured in DMEM medium for SILAC supplemented with 10 % FBS and either conventional light ($^{12}C_6$-L-lysine/L-arginine)

or heavy labelled ($^{13}C_6$-L-lysine/L-arginine) isotopes. After six passages, cells were incubated for 24 h in medium containing 10 % dextran-stabilised magnetite. After washing with PBS, cells were chased for 36 h chase in magnetite-free heavy or light medium, respectively (Figure 2). Cells were harvested and processed as described in (3.4.6).

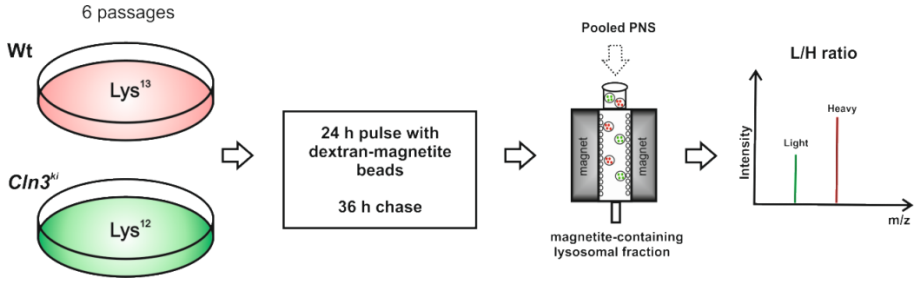

Figure 2: Scheme of SILAC-based proteomic analysis

3.3.11 Isolation of cells from tissue

Bone marrow

Skin and muscles were removed from hind leg with forceps and scissors. A 27G cannula was used to rinse femur and tibia with PBS. Cells were collected and centrifuged at 370 x g for 5 min at 20 °C. For erythrocyte lysis supernatant was discarded and cells re-suspended in 3 ml ACK buffer and incubated for 3 min at room temperature. 10 ml PBS was added to stop the lysis reaction and cells were passed through a ø70 µm cell strainer. Cells were centrifuged as previously described and re-suspended in 1 ml complete RPMI medium for subsequent stimulation or in PBS for FACS staining.

Spleen

Spleen was removed and placed on a ø200 µm metal sieve set in a culture dish filled with 5 ml PBS. The spleen was meshed with the piston of a 2 ml syringe and collected and centrifuged at 370 x g for 5 min at 20 °C. Erythrocyte lysis was performed as described before and cells were re-suspended in 3 ml complete RPMI medium for subsequent stimulation or in PBS for FACS staining.

3.3.12 *In-vitro* stimulation of lymphocytes

Stimulation of T cells to produce cytokines was performed in FACS tubes in a total volume of 1 ml with complete RPMI medium for 4 h at 37 °C. 2 x 10^6 cells isolated from spleen or bone marrow were stimulated with phorbol-12-myristate-3-acetate (PMA) and ionomycin or with the peptides listeriolysin O ($LLO_{189-201}$) and ovalbumin ($OVA_{257-264}$) (Table 17). The combination of PMA and ionomycin is routinely used as a T cell receptor (TCR) independent model to study T cell activation (Truneh *et al.* 1985). PMA activates protein kinase C, while ionomycin is an ionophore that is used to raise intracellular levels of Ca^{2+}. The peptides listeriolysin O ($LLO_{189-201}$) and ovalbumin ($OVA_{257-264}$) were used to specifically stimulate T cells. $LLO_{189-201}$ activates listeriolysin O-specific CD4+ T cells, while $OVA_{257-264}$ activates ovalbumin-specific CD8+ T cells. These peptides present imuno-dominant epitopes from *Lm*OVA, which provoke a strong T cells response in C57BL/6 mice.

After 30 min brefeldin A (10 µg/ml) was added to the cell suspension to prevent the secretion of cytokines. Brefeldin A blocks intracellular protein transport by inducing the fusion of the Golgi stacks with the endoplasmic reticulum. As a consequence, newly synthesized cytokines are retained within the tubular structure and can be stained intracellularly for flow cytometric analyses (Kursar *et al.* 2002).

Table 17: Substances used for stimulation of T cells

Substance	***Concentration***	***Company***
PMA	50 ng/µl	Sigma-Aldrich
Ionomycin	1 µM	Sigma-Aldrich
$LLO_{189-201}$	10 µM	JPA
$OVA_{257-264}$	1 µM	JPA

3.3.13 Flow cytometry measurement and data analysis

Flow cytometry is a technique that was used to count cells regarding size and granularity and to analyse the expression of surface and intracellular proteins.

The fluidics system of a flow cytometer is used to transport the prepared suspension of cells in a stream of carrier fluid and present them as a single line of particles to the excitation source. The illumination of stained and unstained particles and the detection of scatter and fluorescent light signals is a central part in flow cytometry. Emission, in

the form of light scattering, occurs when excitation light is absorbed and then re-radiated by the particles, with no change in wavelength. Fluorescence occurs when a molecule excited by light of one wavelength returns to a lower state by emitting light of a longer wavelength. In flow cytometers light is collected by two lenses termed the forward and side collection lenses, depending on their orientation as viewed from the entering laser beam. The forward collection lens gathers scattered light over a region centred on the laser beam axis. Forward scatter (FSC) can be used to obtain information of particle size. The side scatter (SSC) lens has a high numerical aperture for maximum fluorescence collection efficiency and collects light at 90 degrees to the laser beam axis. Side scatter can be used to differentiate particle populations based on morphology. Once the fluorescence light from a cell has been captured by the collection optics, the spectral component of interest for each stain must be separated spatially for detection. This separation of wavelength is achieved using dichroic (45 degrees) and emission (normal incidence) filters. Detection occurs via photomultiplier tubes that have high gain and sensitivity and are therefore assigned to side scatter and fluorescence detection. The electronically collected data was compensated and corrected for overlapping emission spectra. As described before cell discriminating parameters such as size and granularity are acquired by measuring FSC and SSC light, respectively. Comparison of area and height parameters of FSC and SSC allows differentiation of doublet and single cells. Using fluorochrome-labelled antibodies, cell populations can be identified and distinguished via unique surface proteins and furthermore, intracellular proteins such as cytokines can be detected. All measurements were performed on a FACS Canto II and data was analysed using BD FACSDIVA^{TM} software.

3.3.14 Surface staining for flow cytometry

1-2 x 10^6 spleen or bone marrow cells were re-suspended in 100 µl PBS and blocked with 50 µl PBS containing 1 µl native rat serum (NRS) and 0.5 µl F_c-receptor blocking solution (F_c-block: anti-CD16/CD32 antibody) for 5 min at room temperature. NRS prevents unspecific antibody binding and the F_c-block significantly reduces background staining by specific binding to F_c-receptors. 50 µl of surface antibody mix was added and incubated in the dark for 20 min on ice. Samples were washed with 5 ml cold PBS and centrifuged at 370 x g for 5 min at 20 °C. Cells were re-suspended in 100 µl PBS and analysed by flow cytometry, or stained intracellularly.

3.3.15 Intracellular staining for flow cytometry

After surface staining cells were re-suspended in 200 µl PBS containing 2 % (w/v) paraformaldehyde and incubated in the dark for 15 min at room temperature. Cells were washed with PBS containing 0.2 % (w/v) BSA (PBS/BSA) as previously. Intracellular blocking was performed in 50 µl PBS containing 1 µl NRS, 0.5 µl F_c-block and 0.3 % (w/v) saponin in the dark for 5 min at room temperature. 50 µl of intracellular antibody mix was added and incubated in the dark for 20 min at room temperature. Cells were washed as previously and re-suspended in 100 µl PBS/BSA and analysed by flow cytometry.

3.3.16 Immunofluorescence microscopy

Adherent cells were seeded on 12 mm round glass cover slips at 70 % confluence. After 24 h incubation at 33 or 37 °C, respectively, cells were washed with PBS and fixed in 4 % (w/v) paraformaldehyde for 15 min at room temperature. To mask free aldehyde groups cells were washed with 50 mM NH_4Cl. Subsequently, cells were permeabilised with PBS containing 0.1 % (w/v) saponin for 10 min and non-specific antibody binding was blocked by incubation with PBS containing 5 % (w/v) BSA (PBS/BSA). Cover slips were incubated with primary antibodies in PBS/BSA for 1 h, washed 3 times and incubated with the respective fluorochrome-conjugated secondary antibodies for 30 min at room temperature. Coverslips were incubated for 5 min with DAPI (1:1000 in PBS), washed as previous and sealed in mounting medium. Cells were analysed on a confocal laser scanning microscope and images were merged using Adobe Photoshop.

3.3.17 Lysosomal pH measurements by ratiometric fluorescence imaging

Wild-type and *Cln3*^{ki} cerebellar cells were plated on glass coverslips and grown overnight in the presence of 500 µg/ml of Oregon Green 514–conjugated dextran. Cells were washed and chased for 1 h at 33 °C. Before imaging cells were incubated in at 33 °C serum-free medium for 1 h. Imaging was performed according to (Steinberg *et al.* 2010). Images were acquired at 33 °C using a microscope (Axiovert 200) equipped with a 100x 1.3 NA oil-immersion lens, and with excitation at 440 and 488 nm. pH was measured by fluorescence ratiometric imaging using a filter wheel to rapidly alternate between excitation filters. For each genotype at least 6 different cells with at least 10

single lysosomes each were measured in 150 mM NaCl, 1mM $MgCl_2$, 2 mM $CaCl_2$, 10 mM glucose, and 10 mM HEPES, pH 7.4. At the end of each experiment an *in situ* calibration was performed. Cells were incubated in an isotonic buffer (145 KCl, 1mM $MgCl_2$, 10 mM glucose, 20 mM HEPES) buffered to pH ranging from 4 to 6.5 and containing 10 µg/ml of the ionophore nigericin. Images were acquired after 5 min of incubation to ensure equilibration of pH across compartments. The resulting fluorescence intensity ratio data as a function of pH were fit to a Boltzmann sigmoid and used to interpolate pH values from the experimental ratio data. Filter wheel and camera were controlled by Meta Fluor software. Image acquisition was performed with TILL vision software.

3.3.18 Determination of *Listeria monocytogenes* titers

Age (>8 weeks) and sex-matched mice were infected intravenously with the indicated doses of wild-type *L. monocytogenes* strain EGD (*Lm*EGD) or of a *L. monocytogenes* strain expressing ovalbumin (*Lm*OVA) (Foulds *et al.* 2002). Bacterial inocula were controlled by plating serial dilutions on tryptic soy broth (TSB) agar plates. Mice were sacrificed on day 3 or 8 after infection and spleen and liver were removed. Organs were homogenized in 0.1 % (w/v) Triton X-100 and serial dilutions of homogenates were plated on TSB agar plates. To determine bacterial burdens colonies were counted after 24 h of incubation at 37 °C.

Table 18: Bacteria strains

Bacteria strain	***Provider***
Listeria monocytogenes (*Lm*EGD)	Provided by Prof. H.W. Mittrücker
Listeria monocytogenes (*Lm*OVA)	Provided by Prof. H.W. Mittrücker

3.4 Biochemical methods

3.4.1 Preparation of protein homogenates from cultured cells

Cells grown in culture dishes were washed with ice-cold PBS, harvested by scraping and centrifuged (1000 x g, 5 min, 4 °C). Cells grown in suspension were collected by centrifugation as previously described and washed with ice-cold PBS. Cell pellets were

re-suspended in lysis buffer and incubated on ice for 30 min. Lysates were centrifuged (13000 x g, 10 min, 4 °C) and supernatants were collected. Protein content was quantified by Bradford assay.

3.4.2 Bradford assay

Protein quantification of cell extracts was performed using the Biorad Bradford Protein Assay, a colorimetric method that involves the binding of Coomassie Brilliant Blue G-250 dye to proteins. Under acidic conditions, the dye consists in a protonated red form, which is converted to an unprotonated blue form upon protein binding and can be measured in a photometer at an absorption maximum of 595 nm. A standard series of BSA (0, 2.5, 5, 10, 15 and 20 µg/ml) was prepared and protein concentration was determined according to the manufacturer's instructions.

3.4.3 Sodium dodecylsulfate polyacrylamide gel electrophoresis

Anode buffer:	25 mM Tris/HCl, pH 8.6, 192 mM glycine
Cathode buffer:	25 mM Tris/HCl, pH 8.6, 192 mM glycine, 0.1 % (w/v) SDS
Transfer buffer:	25 mM Tris/HCl, pH 7.4, 192 mM glycine, 20 % (v/v) methanol
Laemmli sample buffer:	125 mM Tris/HCl, pH 6.8, 1 % (w/v) SDS, 10 % (v/v) glycerol, 0.01 % (w/v) bromophenol blue

In sodium dodecylsulfate polyacrylamide gel electrophoresis (SDS-PAGE) proteins are separated according to their electrophoretic mobility. SDS is an anionic detergent that denatures secondary structure and introduces a negative charge to each protein. Since the binding ratio is 1.4 g SDS per 1 g protein, an approximately uniform mass charge ratio is given and the migration through the gel is directly related to only the size of the protein. Gels consisted of 4 % acrylamide stacking and 8 – 15 % resolving gels (Table 19). A layer of isopropanol covers the resolving gel to ensure even setting before the stacking gel is poured. Protein samples were incubated with 4 x SDS sample buffer at 95 °C for 4 min prior to loading. SDS gels were run at 20 mA per mini gel and 50 mA per maxi gel until the sample buffer reached the bottom of the gel. A transfer stack kept

together in a plastic cassette was assembled (fiber pad, 3 whatman paper, nitrocellulose membrane, resolving gel, 3 whatman paper, fiber pad) and the separated proteins were transferred to nitrocellulose membranes in cold transfer buffer for 75 min at 400 mA.

Table 19: SDS-gel solutions

Component	***Stacking gel***	***Resolving gel***
Acrylamide/Bis-Acrylamide	4 % (v/v)	8 – 15 % (v/v)
Tris/HCl, pH 8.8	-	375 mM
Tris/HCl, pH 6.8	100 mM	-
SDS	0.1 % (w/v)	0.1 % (w/v)
APS	0.1 % (w/v)	0.016 % (w/v)
TEMED	0.1 % (v/v)	0.08 (v/v)

3.4.4 Western blotting

Western blotting was used to detect proteins with high specificity and selectivity via a chemiluminescence reaction. Membranes were incubated in TBS containing 5 % (w/v) milk and 0.05 % Tween (milk/TBS-T) to block non-specific antibody binding. Primary antibodies (Table 8) were incubated in milk/TBS-T for 1 h at room temperature or overnight at 4 °C and subsequently washed three times for 5 min with TBS-T. Membranes were then incubated with the appropriate horseradish peroxidise-conjugated secondary antibody in milk/TBS-T for 30 min and washed as previous. Immuno-reactive bands were detected using an enhanced chemiluminescence (ECL) reagent, prepared by mixing solution 1 and 2 (Table 20). The ECL reagent was immediately applied to the membrane and incubated for 30 s. Excess liquid was removed and membranes were imaged on an immunoblot imager (ChemiDoc). Relative proteins amounts were quantified by densitometric analysis of immune-reactive bands using Image Lab™. Molecular masses were estimated by comparison with electrophoretic mobilities of molecular mass marker proteins.

Table 20: ECL solutions

Solution 1	0.1 M Tris/HCl pH 8.5

	2.7 mM luminol 0.44 mM p-coumaric acid
Solution 2	0.1 M Tris/HCl pH 8.5 0.02 % (v/v) H_2O_2

3.4.5 Enzyme activity measurements

The activity of lysosomal hydrolases was determined in cell lysates and conditioned media. 4-nitrophenyl-conjugated monosaccharides served as synthetic substrates to measure enzyme activity. Under acidic conditions the respective sugar residue is cleaved by the hydrolase and 4-nitrophenol is released, which can be measured photometrically after the addition of an alkaline stop buffer. 4-nitrocatecholsulfate served as a substrate for sulfatases, resulting in the release of a sulphate residue and 4-nitrocatechol.

Table 21: Buffers used for enzyme activity measurements

Reaction buffer	0.1 M sodium citrate, pH 4.6 0.2 % Triton-X 100 0.4 % BSA
Stop buffer	0.4 M glycin/NaOH, pH 10.4

Samples (20 µl) containing the respective protein concentration (Table 22) were mixed with 20 µl substrate in reaction buffer and incubated at 37 °C for the indicated time points. The reaction was stopped by the addition of 160 µl stop buffer and released 4-nitrophenol or 4-nitrocatechol was measured at 405 or 515 nm, respectively. All measurements were performed in triplicates.

Activity A was calculated according to the following equation:

$$A = \frac{\Delta E/\min \, x \, V_{Total}}{\varepsilon \text{ x d x } V_{Sample}}$$

A = enzyme activity [U; 1 U = 1 µmol/min]

ΔE/min = difference in extinction per time

ε = molar extinction coefficient
[p-nitrophenol: 18.45/µmol*cm; p-nitrocatechol 12.6/µmol*cm]

V_{Sample} = Sample volume [20 µl]

V_{Total} = Total reaction volume [200 µl]

d = cuvette thickness [1 cm]

Table 22: Substrates and conditions for enzyme activity measurements

Lysosomal enzyme	*Substrate*	*Concentration*	*µg protein*	*Incubation time (h)*
β-hexosaminidase	p-nitrophenyl-N-acetyl-β-D-glucosamid	10 mM	4	1
Arylsulfatase A	Nitrocatecholsulfate	10 mM	20	16

3.4.6 Sample preparation for mass spectrometry

Cerebellar cells were washed with ice-cold PBS, harvested by scraping and re-suspended in buffer A (10 mM HEPES, 250 mM sucrose, 15 mM KCl, 1.5 mM magnesium acetate, 1 mM $CaCl_2$, 1 mM DTT). To obtain the postnuclear supernatant (PNS), cells were homogenised using a tight pestle, and nuclei and unbroken cells were removed by centrifugation at 1000 x g for 10 min at 4 °C. A Miltenyi LS magnetic column was placed into a MACS separator magnet and equilibrated with 0.5 % (w/v) BSA in PBS. The PNS was applied onto the column and allowed to pass by gravity flow. To remove any remaining DNA, 1 ml buffer A containing 10 U DNase I was applied onto the column and incubated for 10 min at room temperature. After washing with 1 ml of buffer A, the column was removed from the magnet and lysosomes were eluted with 2 x 500 µl buffer A (Figure 2). The protein concentration was quantified by Bradford assay as described in 3.4.2. Equal protein amounts of the lysosomal eluates of *Cln3*^{ki} and wild-type cerebellar cells were combined and concentrated in Amicon centrifugal filters at 14000 x g at 4 °C. Concentrated samples were incubated with 4 x SDS sample buffer at 95 °C for 5 min, followed by alkylation in the presence of 1 % acrylamide for 30 min at room temperature. Samples were separated by SDS-PAGE as described previously (3.4.3). The gel was washed with HPLC H_2O, stained with Coomassie Blue for 1 h and was subsequently destained in H_2O. The band profile of the gel was divided into 10 fragments and digested with trypsin as described in (Shevchenko *et al.* 2006). Desalting was performed by StageTipping according to (Rappsilber *et al.* 2007).

3.4.7 Mass spectrometry and data analysis

For mass spectrometric measurement, the samples were loaded directly onto the analytical column (ESI spray tip produced in house with a Sutter P2000 laser puller device from 360 µm OD, 100 µm ID fused silica capillary packed with 5 µm particles [Dr. Maisch, reprosile C-18 AQ]) in 100 % buffer A (water with 0.1 % trifluoracetate) using a Thermo EASY-nLC 1000 at a flow rate of 1 µl/min. The column was washed for 10 min with 100 % A at a flow rate of 1 µl/min. Peptides were eluted with a linear gradient from 100 % A to 65 % A/35 % B (acetonitrile with 0.1 % trifluoracetate) in 60 min. Peptides eluting from the column were ionized in the positive ion mode using a capillary voltage of 1600 V and analysed using a Thermo Orbitrap Velos mass spectrometer. One survey scan at a mass range of m/z 400 to m/z 1200 and a resultion of 30000 was acquired in the Orbitrap mass analyzer followed by fragmentation of the 10 most abundant ions in the ion trap part of the instrument. The repeat count was set to one and the dynamic exclusion window to 60 s.

The raw data files were processed with Proteome Discoverer and searched with the Mascot search engine against Swissprot database swissprot_2013_03.fasta (Version 2.0) containing 539616 sequences, taxonomy: mouse. Propionamide was set as fixed modification, as variable modifications protein N-acetylation, methionine oxidation, $^{13}C_6$-L-lysine isotopic labeling and N-terminal oxidation of glutamic acid and glutamine to pyroglutamic acid were considered. Up to two missed cleavages were accepted. The search was performed with a mass tolerance of 10 p.p.m mass accuracy for the precursor ion and 0.6 Da for the fragment ions. Search results were processed with Proteome Discoverer filtered with a false discovery rate of 0.01, and only proteins with at least two unique peptides were considered. As a quantification method SILAC 2plex was used and results were normalised to mean protein amount.

3.5 Animal experiments

Mice were kept in the animal facility of the University Medical Center Hamburg-Eppendorf under barrier conditions at a constant light-dark-cycle of 12 h. All experiments were performed on *Cln3*^{ki} mice inbred on a C57BL/6N background in comparison to wild-type mice. Tail biopsies were taken in the animal facility and genotyped according to 3.2.1. Peritoneal injections of thioglycollate and infections with

L. monocytogenes were performed as described in 3.3.1 and 3.3.18, respectively. Animals were sacrificed by CO_2 inhalation and subsequent cervical dislocation. All animal experiments were conducted according to the German Animal Protection Law.

4 Results

4.1 Lysosomal protein composition in *Cln3*^{ki} cerebellar cells

CLN3 is a lysosomal membrane protein, whose function in the endosomal-lysosomal compartment is still poorly understood. In previous studies CLN3 deficiency has been associated with defective vesicular trafficking, arginine and lipid transport, pH regulation, and autophagosomal maturation (Kollmann *et al.* 2013). The predominantly accumulating material in CLN3 deficient lysosomes is the highly hydrophobic proteolipid subunit c of the mitochondrial ATP synthase. Various mechanisms of lysosomal dysfunction leading to accumulation of lysosomal storage material are conceivable and have been discussed, such as impaired degradation in the lysosome (Ezaki *et al.* 1996), missing or defective selected lysosomal enzymes, changes in the lysosomal environment such as pH or disrupted trafficking pathways to and from the lysosome (Seehafer and Pearce 2006; Cotman and Staropoli 2012). However, it remains to be elucidated, whether the absence of functional CLN3 protein has an impact on the protein composition in the lysosomal compartment.

To gain insights into possible dysregulation of lysosomal protein composition, SILAC-based quantitative proteomic analysis was performed in lysosomal fractions of the previously established immortalised cerebellar neuronal precursor cell line from *Cln3*^{ki} and wild-type mice (Fossale *et al.* 2004). Wild-type and *Cln3*^{ki} cerebellar cells were cultured in media containing heavy labelled ($^{13}C_6$-L-lysine) or light labelled ($^{12}C_6$-L-lysine) isotopes, respectively. After six passages, cells were incubated for 24 h in medium containing dextran-stabilised magnetite, followed by a 36 h chase period in magnetite-free heavy or light medium. Subsequently, cells were harvested and homogenised, and lysosomal fractions were pooled via a magnetic column and prepared for mass spectrometry analysis.

Processing of the raw data with Proteome Discoverer software and subsequent search of the Swissprot database using Mascot search engine revealed a total number of 2132 proteins in lysosomal fractions of wild-type and *Cln3*^{ki} cerebellar cells. Only proteins with at least two unique peptide pairs were considered and the peptide pairs were required to be identified in two or three replicates of the SILAC experiments, narrowing

down the total number to 1774 proteins. Based on the Gene Ontology annotations, 91 proteins (Supplement) were assigned to the lysosomal compartment, while the remaining proteins belonged to other cellular compartments, such as endosomes and plasma membrane, or were of unknown function and localisation. These results were further filtered by applying a cut off. Proteins were only considered if they exhibited a light/heavy (L/H) ratio of greater than 1.3 or less than 0.7, leading to the identification of a total of 37 lysosomal proteins. The SILAC L/H ratio indicates fold-enrichment of proteins in *Cln3*^{ki} compared to wild-type lysosomal fractions (*Cln3*^{ki}/wt) and was determined in mean of two or three individual SILAC experiments. Among the lysosomal proteins, 29 soluble and 8 membrane proteins were identified to be differentially regulated. In addition, three cargo receptors of the endocytic pathway (mannose 6-phosphate receptor 300 (Mpr300), low density lipoprotein related receptor 1 and 2 (Lrp1 and Lrp2) were found to be differentially expressed.

4.1.1 Identification of lysosomal soluble proteins in *Cln3*^{ki} cerebellar cells

The application of SILAC-based quantitative proteomics was used to quantify changes in protein expression and provided a comprehensive picture of lysosomal alterations between wild-type and *Cln3*^{ki} cerebellar cells. The proteomic analysis revealed that 29 soluble proteins were differentially expressed in lysosomal fractions of *Cln3*^{ki} compared to wild-type cerebellar cells (Figure 3).

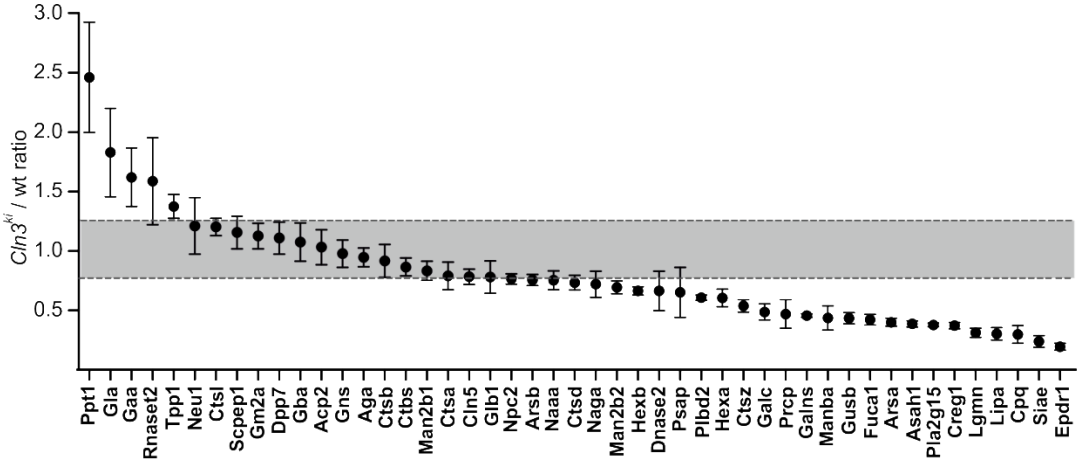

Figure 3: SILAC-based quantitative proteomic analysis of lysosomal soluble proteins in wild-type and *Cln3*^{ki} cerebellar cells

Lysosomal soluble proteins identified by SILAC-based quantitative proteomic analysis from isolated lysosomal fractions were plotted against C*ln3*^{ki}/wt ratio representing the L/H ratio of three individual SILAC experiments (mean, ±SD). The L/H ratio indicates the fold change of lysosomal soluble proteins

in *Cln3*^{ki} compared to wild-type cerebellar cells. Proteins that remained unchanged are shown within the grey-coloured area, indicating the cut off range.

These data show that levels of five lysosomal soluble proteins, palmitoyl-protein thioesterase 1 (Ppt1), *α*-galactosidase A (Gla), lysosomal *α*-glucosidase (Gaa), ribonuclease T2 (Rnaseset2) and tripeptidyl-peptidase 1 (Tpp1) were 1.4- to 2.5-fold increased in lysosomal fractions of *Cln3*^{ki} compared to the wild-type. In contrast, the amount of 24 proteins was predominantly decreased in lysosomes of *Cln3*^{ki} cerebellar cells. Among them, proteins were identified involved in glycan degradation (*N*-acetylgalactosamine-6-sulfate (Galns), *β*-glucoronidase (Gusb), *α*–mannosidase (Man2b2), *α*-L-1-fucosidase (Fuca1) and *β*-mannosidase (Manba)) and in sphingolipid degradation (*β*-hexosaminidase subunit *α* (Hexa), *β*-hexosaminidase subunit *β* (Hexb), *α*-*N*-acetylgalactosaminidase (Naga), galactosylcerebrosidase (Galc), arylsulfatase A (Arsa), acid ceramidase (Asah1)). These proteins, as well as lysosomal Pro-X carboxypeptidase (Prpc), deoxyribonuclease-2-alpha (Dnase2), prosaposin (Psap), putative phospholipase B-like 2 (Pldb2), group XV phospholipase A2 (Pla2g15), Creg1, legumain (Lgmn), lysosomal acid lipase (Lipa), carboxypeptidase (Cpq), sialiate O-acetylesterase (Siae), mammalian ependymin-related protein 1 (Epdr1), cathepsin D (Ctsd) and cathepsin Z (Catz) were observed to be decreased by 27 to 81 % in *Cln3*^{ki} lysosomal fractions compared to the wild-type.

In order to validate the proteomics data, the expression of selected lysosomal proteins was verified by western blot analysis of total cell extracts, enzyme activity measurements and determination of relative mRNA expression levels using qRT PCR.

Western blot analysis of cathepsin B, followed by densitometric analysis revealed that the amounts of the precursor (38 kDa) and mature (35 kDa) forms were significantly reduced by 30 % in total cell extracts of *Cln3*^{ki} compared to wild-type cerebellar cells (Figure 4 A). These results stand in contrast with those from the SILAC-based proteomic analysis. Displaying an L/H ratio of 0.9, cathepsin B did not reach the cut off value to be considered as significantly changed. However, by western blot analysis differences in cathepsin B protein expression could be detected between the two genotypes. Similarly, reduced protein levels of the 38 kDa precursor form of cathepsin B were detected in conditioned media of *Cln3*^{ki} cerebellar cells. Additionally,

decreased cathepsin B protein levels were accompanied by a 35 % reduction in mRNA expression level (Figure 4 C).

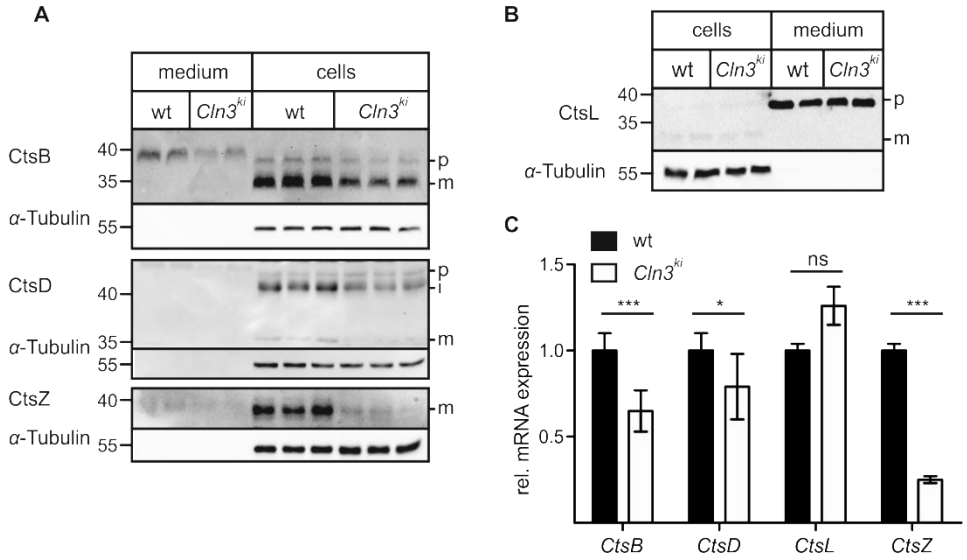

Figure 4: Protein and mRNA expression of cathepsins in wild-type and *Cln3*^{ki} cerebellar cells
(A-B) Total cell extracts (10-15 µg protein) and 10 % of concentrated conditioned media of three and two individual samples of wild-type and *Cln3*^{ki} cerebellar cells, respectively, were separated by SDS-PAGE under reducing conditions and analysed by western blotting using antibodies against cathepsin B (CtsB), cathepsin D (CtsD), cathepsin L (CtsL) and Cathepsin Z (CtsZ). The positions of molecular mass marker proteins are indicated in kDa. α-Tubulin was used as loading control. Precursor (p), intermediate (i), mature (m). **(C)** Relative mRNA expression levels of *Cln3*, *CtsB*, *CtsD*, *CtsL* and *CtsZ* in *Cln3*^{ki} (white columns) compared to wild-type (black columns) cerebellar cells (mean, ±SD, n=3, **P*≤0.05, ****P*≤0.001).

For comparison, cathepsin L, displaying a SILAC L/H ratio of 1.2 in *Cln3*^{ki} lysosomal fractions, appeared to be unchanged in protein and mRNA levels (Figure 4 B and C). In both genotypes, the majority of newly synthesised cathepsin L is secreted as a 40 kDa precursor form (Dong *et al.* 1989), whereas only small amounts of the precursor and the 29 kDa mature form were detectable intracellularly.

Cathepsin D protein levels were reduced in *Cln3*^{ki} cerebellar cells according to SILAC-based proteomic analysis, presenting an L/H ratio of 0.7. Cathepsin D is synthesised as a 53 kDa precursor form and then proteolytically cleaved to an intermediate form of 43 kDa and two mature forms of 31 and 14 kDa (Gieselmann *et al.* 1985). Western blot analysis revealed that the precursor form is present in both genotypes, whereas the intermediate and mature forms were decreased by 30 % in *Cln3*^{ki} cerebellar cells (Figure 4 A) according to densitometric analysis. The second 14 kDa mature form was not detected due to the absence of antigen epitopes. Conditioned media of *Cln3*^{ki}

cerebellar cells contained slightly reduced amounts of the cathepsin D precursor form. A significant decrease of 21 % in *cathepsin D* mRNA levels was also observed in *Cln3*^{ki} compared to wild-type cerebellar cells (Figure 4 C).

According to SILAC-based proteomic analysis the lysosomal cathepsin Z concentration was reduced by 46 %. Cathepsin Z is synthesised as a 40 kDa precursor protein and then proteolytically processed to a mature 37 kDa form. The mature form of cathepsin Z was detectable in wild-type cerebellar cells, while, strikingly, in *Cln3*^{ki} cerebellar cells cathepsin Z was almost absent, accompanied by a 75 % reduction in *cathepsin Z* mRNA levels (Figure 4 A and C). Similarly, cathepsin Z was present as a precursor form in conditioned media of wild-type but not of *Cln3*^{ki} cerebellar cells.

To investigate whether the absence of Cln3 protein also affects the amount of cathepsins in a different cell type other than cerebellar cells, primary mouse embryonic fibroblast (MEF) cells were analysed by western blotting (Figure 5). Similar to *Cln3*^{ki} cerebellar cells, protein levels of the 38 kDa precursor and 35 kDa mature form of cathepsin B were significantly reduced in total cell extracts of *Cln3*^{ki} compared to wild-type MEF cells. The cathepsin D 43 kDa intermediate form, however, was not decreased, in marked contrast to the 31 kDa mature form, which was barely detectable in *Cln3*^{ki} MEF cells. The 37 kDa mature form of Cathepsin Z was also strongly reduced in *Cln3*^{ki} compared to wild-type MEF cells.

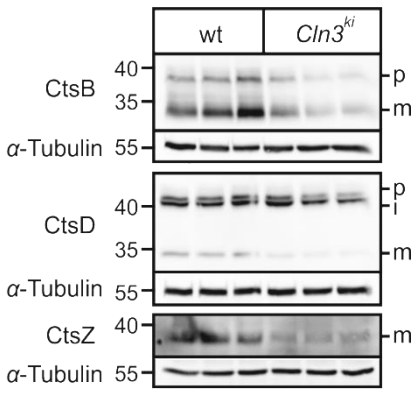

Figure 5: Protein expression of cathepsins in wild-type and *Cln3*^{ki} MEF cells
Total cell extracts (20 µg protein) of three individual samples of wild-type and *Cln3*^{ki} MEF cells were separated by SDS-PAGE under reducing conditions and analysed by western blotting using antibodies against cathepsin B (CtsB), cathepsin D (CtsD) and cathepsin Z (CtsZ). The positions of molecular mass marker proteins are indicated in kDa. α-Tubulin was used as loading control. Precursor (p), intermediate (i), mature (m).

Furthermore, intracellular activities of selected lysosomal enzymes in wild-type and *Cln3*^{ki} cerebellar cells were determined photometrically (Figure 6 A). In *Cln3*^{ki} cerebellar cells β-hexosaminidase and arylsulfatase A activities were significantly

reduced by 26 % and 36 %, respectively. Moreover, decreased activity of *β*-hexosaminidase was accompanied by a 29 % reduction of mRNA expression levels. Similarly, *α-L-1-fucosidase* mRNA expression levels were decreased by 36 % in *Cln3*^{ki} cerebellar cells. *Palmitoyl-protein thioesterase 1* mRNA expression levels were increased by 25 %, whereas *tripeptidyl-peptidase* mRNA levels remained unchanged (Figure 6 B).

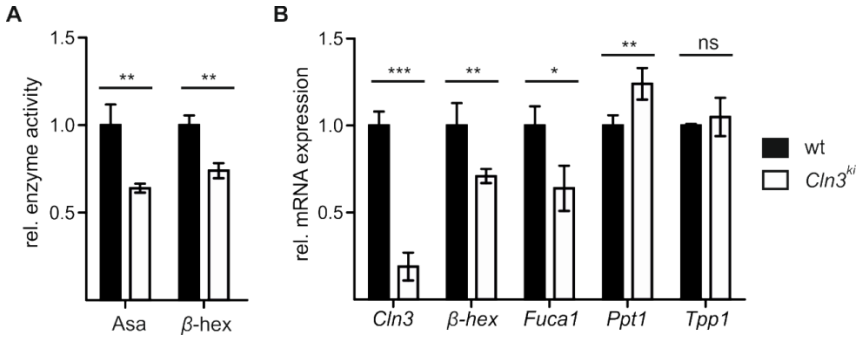

Figure 6: Relative enzyme activity and mRNA expression of lysosomal soluble proteins in wild-type and *Cln3*^{ki} cerebellar cells

(A) Relative enzyme activity of arylsulfatase A (Asa) and *β*-hexosaminidase (*β*-hex) in total cell extracts of wild-type (black columns) and *Cln3*^{ki} (white columns) cerebellar cells **(B)** Relative mRNA expression levels of *Cln3*, *β-hex*, *α-L-1-fucosidase* (*Fuca1*), *palmitoyl-protein thioesterase 1* (*Ppt1*) and *tripeptidyl-peptidase 1* (*Tpp1*) in *Cln3*^{ki} compared to wild-type cerebellar cells (mean, ±SD, n=3, **P*≤0.05, ***P*≤0.01, ****P*≤0.001).

Taken together, SILAC-based proteomic quantification of lysosomal soluble proteins and experimental validation of selected soluble proteins by western blot analysis and enzyme activity measurements showed that absence of functional Cln3 protein affects the amount of cathepsin B, D and Z and of *β*-hexosaminidase and arylsulfatase A. Furthermore, respective reduction of cathepsin B, D and Z in conditioned media and decrease of mRNA levels of *cathepsin B, D* and *Z*, and *β-hexosaminidase* and *α-L-1-fucosidase* suggest that enzyme secretion was not affected in *Cln3*^{ki} cerebellar cells.

4.1.2 Identification of lysosomal membrane proteins in *Cln3*^{ki} cerebellar cells

Lysosomal membrane proteins identified by SILAC-based proteomic analysis were plotted against the L/H ratio indicating the increase or decrease in protein amount in *Cln3*^{ki} compared to wild-type cerebellar cells (Figure 7). Four membrane-associated proteins, lysosomal amino acid transporter 1 (Lyaat1), V-type proton ATPase subunit d

(Va0d1), V-type proton ATPase subunit s (Vas1) and H^+/Cl^- exchange transporter 7 (Clc7) were 1.4- to 1.7-fold increased. In contrast, four proteins, lysosomal integral membrane protein 2 (Limp2), lysosome-associated membrane protein 1 (Lamp1), nicastrin (Nica) and lysosomal-associated transmembrane protein 4A (Lap4A) and were decreased by 32 to 55 %.

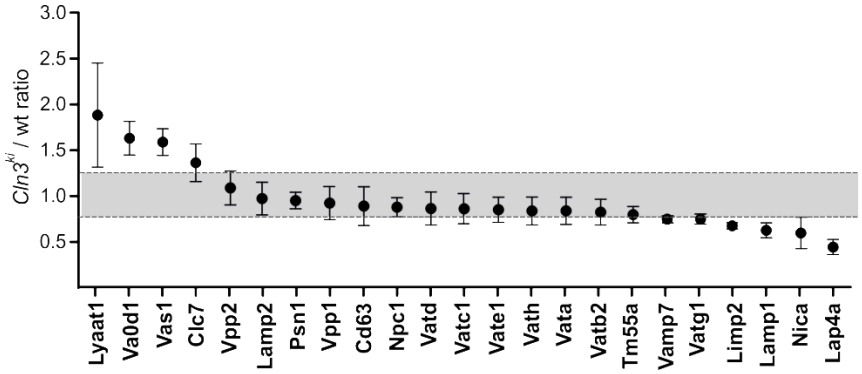

Figure 7: SILAC-based quantitative proteomic analysis of lysosomal membrane proteins in wild-type and *Cln3*^{ki} cerebellar cells

Lysosomal membrane proteins identified by SILAC-based quantitative proteomic analysis from isolated lysosomal fractions were plotted against C*ln3*^{ki}/wt ratio representing the L/H ratio of three individual SILAC experiments (mean, ±SD). The L/H ratio indicates the fold change of lysosomal membrane proteins in *Cln3*^{ki} compared to wild-type cerebellar cells. Proteins that remained unchanged are shown within the grey-coloured area, indicating the cut off range.

The V-type proton ATPase is an ATP-driven enzyme. It transforms the energy of ATP hydrolysis to electrochemical potential differences across the lysosomal membrane via the primary active transport of protons. Loss of functional Cln3 protein had an impact on the composition of several subunits of the V-type proton ATPase in *Cln3*^{ki} cerebellar cells. Only small changes in protein abundance, but not reaching the cut off values, were observed for V-type proton ATPase subunit a1 (Vpp1), subunit a2 (Vpp2), subunit D (Vatd), subunit C (Vatc1), subunit E (Vate1), subunit H (Vath), subunit A (Vata), subunit B (Vtb2) and subunit G (Vatg1). In contrast, protein levels of subunit s (Vas1) and subunit d (Va0d1) were 1.6-fold increased in *Cln3*^{ki} cerebellar cells.

Several genetic models of JNCL have been described to harbour defects in lysosomal acidification (Pearce and Sherman 1998; Holopainen *et al.* 2001; Gachet *et al.* 2005). In order to evaluate possible dysregulation of pH homeostasis, lysosomal pH measurements were performed. Wild-type and *Cln3*^{ki} cerebellar cells were loaded with pH-sensitive Oregon green dextran that is targeted to lysosomes, followed by

ratiometric fluorescence imaging (Figure 8). The steady-state lysosomal pH of wild-type cells and *Cln3*^{ki} cerebellar cells was 4.54 ± 0.09 and 4.49 ± 0.10 (mean, ±SEM), respectively, being virtually identical, ruling out dysregulation of pH homeostasis in *Cln3*^{ki} cerebellar cells.

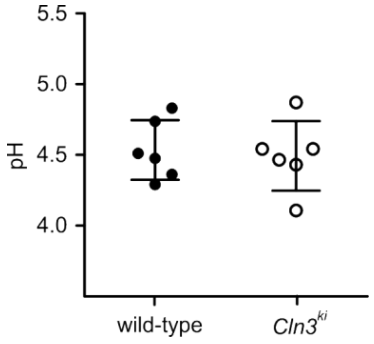

Figure 8: Steady-state lysosomal pH in wild-type and *Cln3*^{ki} cerebellar cells
The lysosomes of wild-type and *Cln3*^{ki} cerebellar cells were loaded with pH-sensitive Oregon green dextran and their pH was measured by ratiometric imaging (mean ±SEM, n = 6). At the end of each experiment an *in situ* calibration was performed to generate a curve relating the 490 nm / 440 nm excitation ratio to pH.

To further validate the proteomic data, expression of selected proteins was analysed by western blotting and the respective mRNA expression was determined by qRT PCR.

The expression of the lysosomal amino acid transporter 1 (Lyaat1) was increased according to SILAC-based proteomic analysis, displaying an L/H ratio of 1.9. Being in line with the proteomic data, western blot analysis of total cell extracts and subsequent densitometric analysis showed that the amount of Lyaat1, related to the expression of *α*-tubulin, was increased by 1.5-fold in *Cln3*^{ki} in respect to wild-type cerebellar cells (Figure 9).

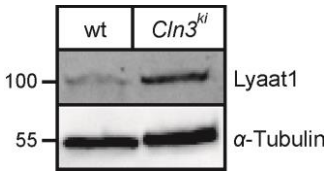

Figure 9: Protein expression of Lyaat1 in wild-type and *Cln3*^{ki} cerebellar cells
Total cell extracts (30 µg protein) of wild-type and *Cln3*^{ki} cerebellar cells were separated by SDS-PAGE under reducing conditions and analysed by Lyaat1 western blotting. The positions of molecular mass marker proteins are indicated in kDa. *α*-Tubulin was used as loading control.

The proteomic analysis revealed that protein levels of the lysosome-associated membrane protein 1 (Lamp1) were decreased by 40 %. In contrast, western blot analysis and subsequent densitometric analysis showed that the amount of Lamp1 was elevated by 2-fold in *Cln3*^{ki} compared to wild-type cerebellar cells (Figure 10 A). These observations were further confirmed by confocal immunofluorescence microscopy (Figure 10 B), indicating an increase in size and number of lysosomes in *Cln3*^{ki}

cerebellar cells. Protein levels of the lysosome-associated membrane protein 2 (Lamp2) in *Cln3*^{ki} cerebellar cells were comparable to wild-type cells, which was initially also evaluated by SILAC-based proteomic analysis. Moreover, the lysosomal integral membrane protein 2 (Limp2), was decreased by 32 % in *Cln3*^{ki} cerebellar cells according to the proteomics data. In contrast, western blot analysis could not confirm a reduction of Limp2 protein amounts, as wild-type and *Cln3*^{ki} cerebellar cells display similar Limp2 protein levels. Strikingly, mRNA levels of all three lysosomal membrane proteins, *Lamp1*, *Lamp2* and *Limp2* were significantly reduced by 30 %, 25 % and 35 %, respectively (Figure 10 C).

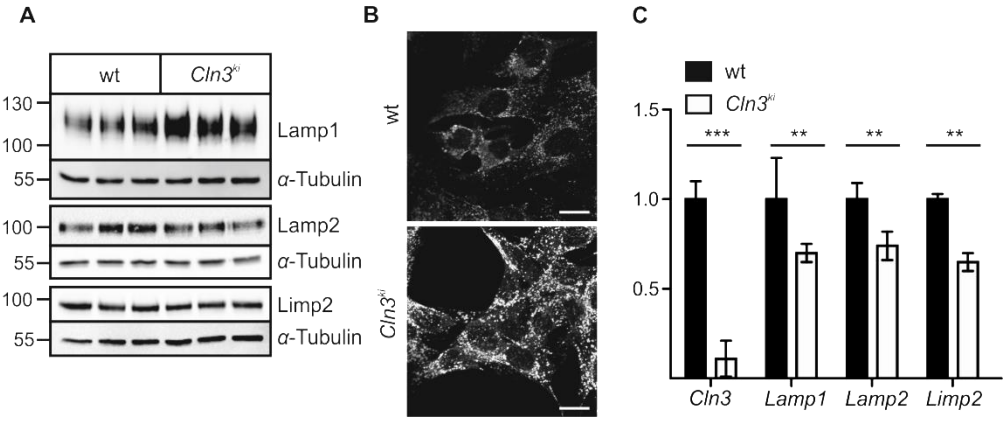

Figure 10: Protein and mRNA expression of Lamp1, Lamp2 and Limp2 in wild-type and *Cln3*^{ki} cerebellar cells

(A) Total cell extracts (10 µg protein) of three individual samples of wild-type and *Cln3*^{ki} cerebellar cells were separated by SDS-PAGE under reducing conditions and analysed by western blotting using antibodies against Lamp1, Lamp2 or Limp2. The positions of molecular mass marker proteins are indicated in kDa. α-Tubulin was used as loading control. **(B)** Wild-type and *Cln3*^{ki} cerebellar cells were analysed for the presence of endogenous Lamp1 by confocal immunofluorescence microscopy. Scale bar = 20 µm. **(C)** Relative mRNA expression levels of *Cln3*, *Lamp1*, *Lamp2* and *Limp2* in *Cln3*^{ki} (white columns) compared to wild-type (black columns) cerebellar cells (mean ±SD, n=3, $^{**}P \leq 0.01$, $^{***}P \leq 0.001$).

4.1.3 Expression of cargo receptors *in Cln3*^{ki} cerebellar cells

In addition to lysosomal proteins, SILAC-based proteomic quantification also revealed dysregulation of the three cargo receptors mannose 6-phosphate receptor 300 (Mpr300), low density lipoprotein related receptor 1 (Lrp1) and low density lipoprotein related receptor 2 (Lrp2) in *Cln3*^{ki} lysosomal fractions (Figure 11 A).

The Mpr300 belongs to the type 1 transmembrane glycoproteins. The main function of the Mpr300, which is shared with the 46 kDa cation-independent mannose 6-phosphate

receptor (Mpr46), is the delivery of newly synthesised lysosomal enzymes from the TGN to endosomes for their final transfer to lysosomes. In addition, Mpr300, but not Mpr46, is involved in ligand internalisation and their delivery to lysosomes from the cell surface (Ghosh *et al.* 2003).

The proteomic analysis revealed a 1.8-fold increase in Mpr300 protein levels (Figure 11 A). These results were verified by western blot and subsequent densitometric analysis showing a 1.5-fold higher amount of Mpr300 in total cell extracts of *Cln3*^{ki} in respect to wild-type cerebellar cells (Figure 11 B). Similarly, relative mRNA expression of *Mpr300* was significantly increased by 1.5-fold in *Cln3*^{ki} cerebellar cells, whereas *Mpr46* transcript levels remained unchanged (Figure 11 D).

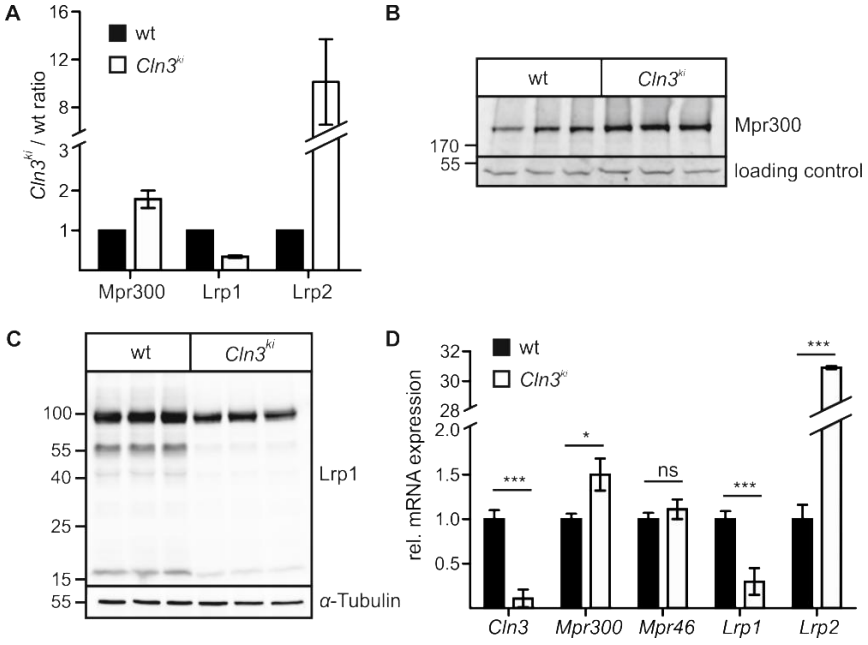

Figure 11: Expression of cargo receptors in wild-type and *Cln3*^{ki} cerebellar cells
(A) Cargo receptors identified by SILAC-based quantitative proteomic analysis from isolated lysosomal fractions were plotted against C*ln3*^{ki}/wt ratio representing the L/H ratio of three individual SILAC experiments (mean, ±SD). The L/H ratio indicates the fold change of cargo receptors in *Cln3*^{ki} (white column) compared to wild-type cerebellar cells (black column). **(B)** Total cell extracts (15 µg protein) of three individual samples of wild-type and *Cln3*^{ki} cerebellar cells were separated by SDS-PAGE under non-reducing conditions and analysed by Mpr300 western blotting. The positions of molecular mass marker proteins are indicated in kDa. Under non-reducing conditions an unspecific band of the Mpr300 at 53 kDa was used as loading control. **(C)** Total cell extracts (15 µg protein) of three individual samples of wild-type and *Cln3*^{ki} cerebellar cells were analysed by Lrp1 western blotting under reducing conditions. The positions of molecular mass marker proteins are indicated in kDa. α-Tubulin was used as loading control. **(D)** Relative mRNA expression levels of *Cln3*, *Mpr300*, *Mpr46*, *Lrp1* and *Lrp2* in *Cln3*^{ki} compared to wild-type cerebellar cells (mean, ±SD, n=3, **P*≤0.05, ****P*≤0.001).

Lrp1 and Lrp2 are cell surface receptors and belong to the LDL receptor family. The members of this family mediate diverse biological functions in endocytic recycling pathways, including their predominant role in cholesterol homeostasis (May *et al.* 2007).

SILAC-based proteomic analysis revealed a 65 % decrease in Lrp1 protein levels in *Cln3*^{ki} compared to wild-type cerebellar cells (Figure 11 A). These results were confirmed by a 70 % reduction of *Lrp1* transcripts and decreased Lrp1 protein amounts as revealed by western blotting (Figure 11 C and D). In addition to the major 100 kDa band of Lrp1, detected in total cell extract of both genotypes, further bands were visible at 55, 40 and 15 kDa.

Moreover, reduction in Lrp1 protein levels could be further confirmed in primary MEF cells from *Cln3*^{ki} mice (Figure 12), indicating that loss of Cln3 protein affects the amount of Lrp1 protein levels also in other cell types.

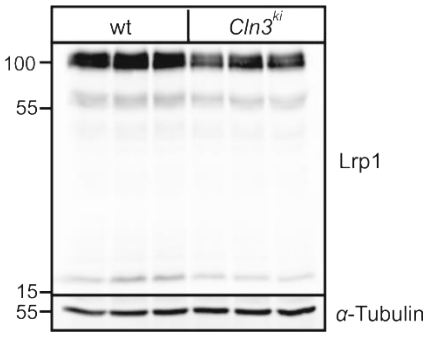

Figure 12: Lrp1 protein levels in primary MEF cells
Total cell extracts (20 µg protein) of three individual samples of primary wild-type and *Cln3*^{ki} MEF cells were separated by SDS-PAGE under reducing conditions and analysed by Lrp1 western blotting. The positions of molecular mass marker proteins are indicated in kDa. *α*-Tubulin was used as loading control.

In contrast, Lrp2 protein levels were strongly increased by 10-fold according to proteomic analysis (Figure 11 A). In line with these results, *Lrp2* mRNA expression was found to be 31-fold up-regulated in *Cln3*^{ki} compared to wild-type cerebellar cells (Figure 11 D).

4.2 Clathrin-dependent endocytosis of ligands in *Cln3*^{ki} cerebellar cells

4.2.1 Mpr300-mediated endocytosis of the lysosomal enzyme arylsulfatase B

Lysosomal enzymes are either directly transported from the TGN to the endosomal-lysosomal compartment, or reach the lysosome indirectly via secretion and re-capture mechanism (Braulke and Bonifacino 2009). The Mpr300 allows re-internalisation and

delivery to the lysosome of secreted lysosomal enzymes containing mannose 6-phosphate (M6P) residues.

To determine whether an increase in the Mpr300 protein levels in *Cln3*^{ki} cerebellar cells has an impact on clathrin-dependent endocytosis of lysosomal enzymes, internalisation assays of human recombinant M6P-containing arylsulfatase B (ASB) were performed. Wild-type and *Cln3*^{ki} cerebellar cells were incubated with [^{125}I]-labelled ASB ([^{125}I]-ASB) in the presence or absence of 10 mM M6P for 20, 40, 60, 80 and 100 min (Figure 13 A). The specific uptake of [^{125}I]-ASB by the Mpr300 is demonstrated by complete inhibition of [^{125}I]-ASB endocytosis in the presence of M6P (Figure 13 A, lane 6, 12). In both, wild-type and *Cln3*^{ki} cerebellar cells, 68 kDa [^{125}I]-ASB precursor bands were detected intracellularly after a pulse time of 20 min, indicating binding by the Mpr300 at the plasma membrane and subsequent internalisation of the ligand-receptor complexes (Figure 13 A, lane 1, 7). After a pulse time of 60 min, a 47 kDa intermediate and a 15 kDa mature form of [^{125}I]-ASB could be detected (Figure 13 A, lane 2, 8) demonstrating the processing of [^{125}I]-ASB in the lysosome (Peters *et al.* 1991). Measurements of specific cell-associated radioactivity (cpm/µg protein) revealed an exponential increase in [^{125}I]-ASB endocytosis during a time course of 100 min (Figure 13 B). Subsequent quantification of the specific cell-associated radioactivity demonstrated a 1.5-fold increase in [^{125}I]-ASB endocytosis in *Cln3*^{ki} compared to wild-type cerebellar cells.

To evaluate whether increased endocytosis of [^{125}I]-ASB in *Cln3*^{ki} cerebellar cells is due to elevated levels of Mpr300 on the cell surface, binding studies were conducted. Wild-type and *Cln3*^{ki} cerebellar cells were incubated with [^{125}I]-ASB at 4 °C in the presence or absence of M6P. As previously shown, an excess of M6P could specifically inhibit binding of [^{125}I]-ASB. In parallel, the total amount of Mpr300 was determined by binding of [^{125}I]-ASB in the presence of 0.1 % saponin. Measurements of cell-associated radioactivity revealed that Mpr300 levels on the cell surface of *Cln3*^{ki} cerebellar cells were increased compared to the wild-type, albeit level of statistical significance were not reached (Figure 13 C). In contrast, the total amount of Mpr300 was significantly increased by 2.2-fold in *Cln3*^{ki} cerebellar cells.

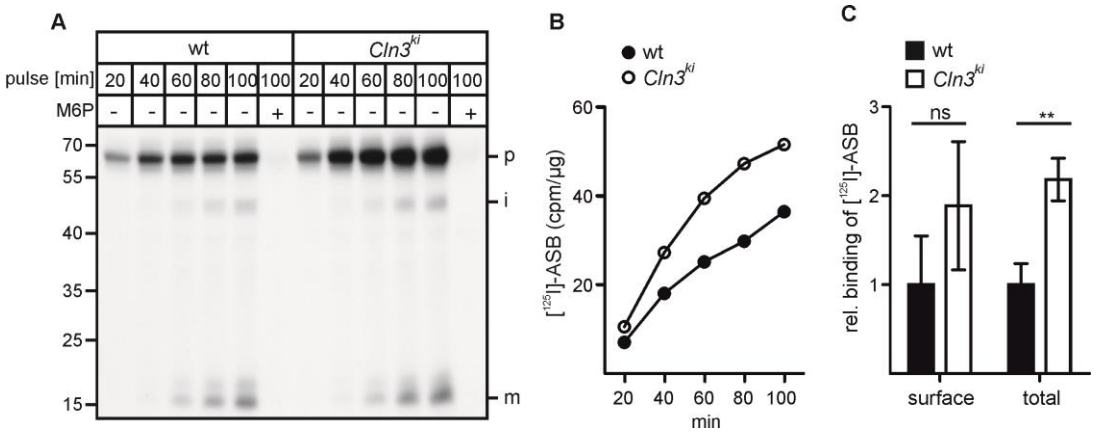

Figure 13: Endocytosis of [^{125}I]-ASB in wild-type and *Cln3^{ki}* cerebellar cells

(A) Wild-type and *Cln3^{ki}* cerebellar cells were incubated with [^{125}I]-ASB (250,000 cpm/ml) for the indicated pulse times at 33 °C in the presence (+) or absence (-) of 10 mM M6P. Total cell extracts (220 µg protein) were separated by SDS-PAGE and internalised [^{125}I]-ASB forms were visualised by autoradiography (p: precursor, i: intermediate, m: mature). **(B)** Absolute radioactivity values of [^{125}I]-ASB (in cpm/µg protein) were determined by γ-counting, corrected by the radioactivity in the presence of M6P and plotted against incubation time (min). **(C)** Wild-type (black column) and *Cln3^{ki}* cerebellar cells (white column) were incubated with [^{125}I]-ASB (600,000 cpm/ml) for 2 h at 4 °C in presence or absence of 10 mM M6P. For measuring the binding of [^{125}I]-ASB to total amounts of Mpr300, medium contained 0.1 % saponin. Cells were harvested and radioactivity was measured and normalised to protein content (mean ±SD, n=3, $^{**}P \leq 0.01$).

Taken together, the thorough expression analysis of Mpr300 revealed a significant increase in both protein and mRNA levels in *Cln3^{ki}* cerebellar cells in respect to wild-type cells. The increase in the total Mpr300 protein amount led to elevated uptake of the lysosomal enzyme ASB.

In addition to [^{125}I]-ASB endocytosis, the processing and degradation of the enzyme was analysed. Wild-type and *Cln3^{ki}* cerebellar cells were incubated with [^{125}I]-ASB in the presence or absence of M6P for 20 or 40 min. To follow lysosomal processing and degradation of [^{125}I]-ASB, cells were subsequently incubated in non-radioactive medium and chased for further 1, 2 and 3 h. After a pulse time of 20 min, and even more strikingly after 40 min, the [^{125}I]-ASB precursor band was detected intracellularly in both genotypes. Intermediate and mature forms of [^{125}I]-ASB were slightly visible after 40 min pulse time (Figure 14 A, lane 1, 2, 7, 8). Measurements of specific cell-associated radioactivity and subsequent quantification revealed that *Cln3^{ki}* cerebellar cells endocytosed 1.8-fold more [^{125}I]-ASB than wild-type cells (Figure 14 B). The binding of [^{125}I]-ASB was specifically blocked by the addition of M6P (Figure 14 A, lane 3, 9).

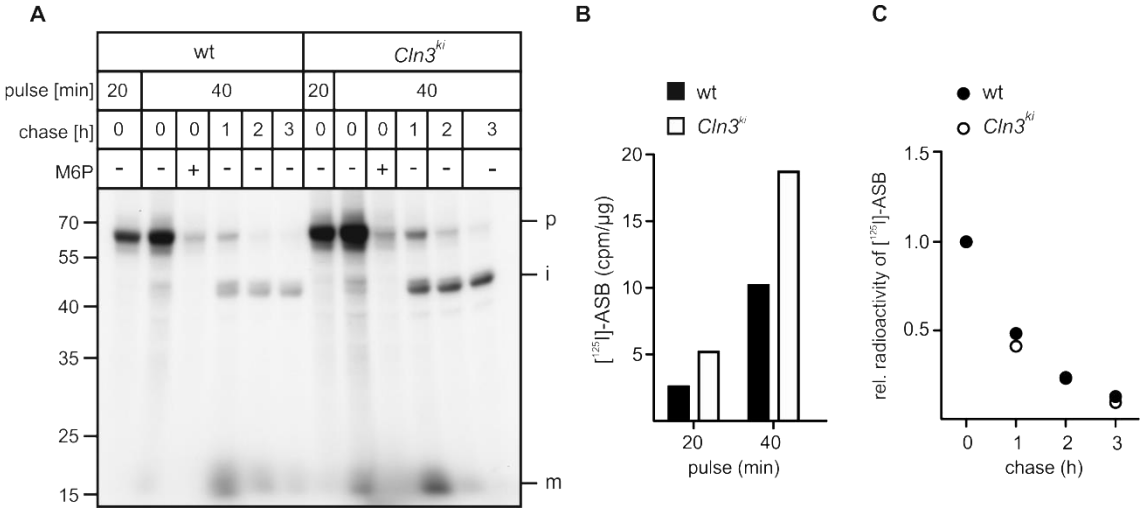

Figure 14: Endocytosis, processing and degradation of [^{125}I]-ASB in wild-type and *Cln3^{ki}* cerebellar cells

(A) Wild-type and *Cln3^{ki}* cerebellar cells were incubated with [^{125}I]-ASB (250,000 cpm/ml) for the indicated pulse times at 33 °C in the presence (+) or absence (-) of 10 mM M6P. Cells were either harvested (lanes 1, 2, 3, 7, 8, 9) or chased for 1, 2 and 3 h (lanes 4 – 6, 10 – 12). Total cell extracts (150 µg protein) were separated by SDS-PAGE and internalised [^{125}I]-ASB forms were visualised by autoradiography (p: precursor, i: intermediate, m: mature). **(B)** Absolute radioactivity values of [^{125}I]-ASB (in cpm/µg protein) were determined by γ-counting, corrected by the radioactivity in the presence of M6P and plotted against pulse time or **(C)** plotted as relative radioactivity of [^{125}I]-ASB against chase time. The 40 min pulse value was set to 1 in both genotypes. The experiment was repeated three times with consistent results.

During the 1 h chase, the precursor form decreased in both genotypes, whereas the intermediate and the mature form increased, indicating processing of [^{125}I]-ASB in the endosomal-lysosomal compartment (Figure 14 A, lane 4, 10). Within 2 and 3 h of chase time, the precursor, as well as the mature form continuously decreased, displaying degradation of these forms. In contrast, the intermediate form remained stable even after 3 h of chase (Figure 14 A, lane 5, 6, 11, 12). Furthermore, specific cell-associated radioactivity was determined by γ-counting and quantification revealed that the kinetics of processing and degradation of [^{125}I]-ASB was similar in both genotypes (Figure 14 B).

4.2.2 Lrp1-mediated endocytosis of α_2-macroglobulin

Cln3^{ki} cerebellar cells displayed significantly reduced levels of Lrp1, as revealed by SILAC-based quantitative proteomic analysis, western blotting and pRT PCR. To determine whether decreased levels of Lrp1 have an impact on the binding and

internalisation of Lrp1-specific ligands, endocytosis of recombinant α_2-macroglobulin (α_2-MG) was examined (Figure 15).

Wild-type and *Cln3*^{ki} cerebellar cells were incubated with [^{125}I]-α_2-MG for 40 min, in the presence or absence of 30 µg/ml receptor associated protein (RAP), a competitive inhibitor of ligand binding to receptors of the LDL receptor family (Mokuno *et al.* 1994; Willnow *et al.* 1995). After 40 min pulse with [^{125}I]-α_2-MG, cells were chased in non-radioactive medium for 1, 2 and 3 h to analyse the proteolytic processing of [^{125}I]-α_2-MG in lysosomes. Endocytosis of [^{125}I]-α_2-MG was completely blocked in the presence of the inhibitor RAP, demonstrating the specific uptake of [^{125}I]-α_2-MG by LDL receptor family members (Figure 15 A, lane 2, 7). Within a pulse time of 40 min, the 130 kDa band of α_2-MG was detected in both genotypes (Figure 15 A, lane 1, 6). However, additional bands at 100, 70 and 50 kDa were detected, presumably presenting degradation products of α_2-MG. The Lrp1-mediated uptake of [^{125}I]-α_2-MG during 40 min pulse time was reduced by 43 % in *Cln3*^{ki} compared to wild-type cerebellar cells (Figure 15 B), corresponding to decreased steady-state protein levels of Lrp1. In both genotypes, within 1 hour of chase the 130 kDa band of [^{125}I]-α_2-MG decreased, whereas the 70 kDa increased and new bands at 40 and 15 kDa appeared, displaying degradation of [^{125}I]-α_2-MG (Figure 15 A, lane 3, 8). Within a chase time of 2 and 3 hours, the 70 kDa did not further increase but decreased, as well as all the additional [^{125}I]-α_2-MG degradation fragments (Figure 15 A, lane 4, 5, 9, 10). However, quantification of cell-associated radioactivity showed that the kinetics of the degradation process was similar in wild-type and *Cln3*^{ki} cerebellar cells (Figure 15 C). Thus, endocytosis of [^{125}I]-α_2-MG was reduced in *Cln3*^{ki} cerebellar cells due to decreased protein expression levels of Lrp1 but transport to lysosomes and subsequent degradation was not affected.

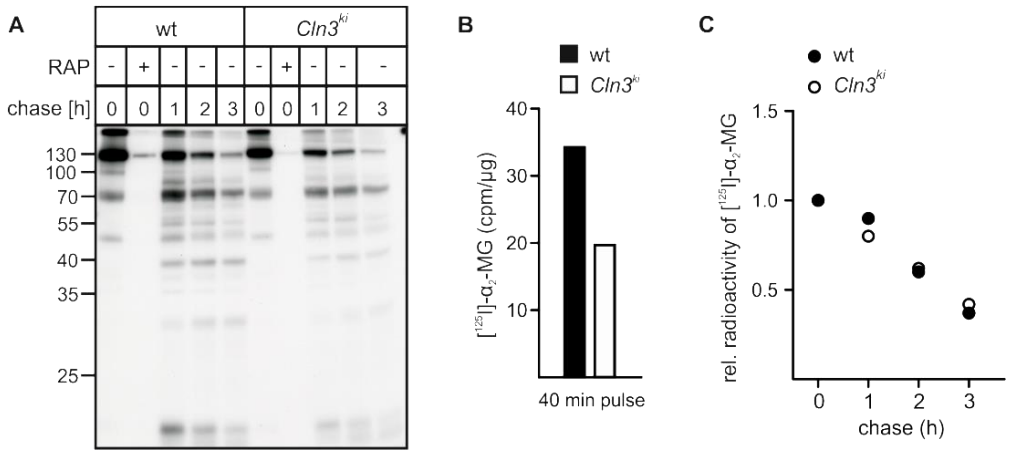

Figure 15: Endocytosis of [^{125}I]-α_2-MG in wild-type and *Cln3^{ki}* cerebellar cells
(A) Wild-type and *Cln3^{ki}* cerebellar cells were incubated with [^{125}I]-α_2-MG (330,000 cpm/ml) for 40 min at 33 °C in the presence (+) or absence (-) of 30 µM RAP. Cells were either harvested (lanes 1, 2, 6, 7) or chased for 1, 2 and 3 h (lanes 3 – 5, 8 – 10). Total cell extracts (150 µg protein) were separated by SDS-PAGE and internalised [^{125}I]-α_2-MG forms were visualised by autoradiography. **(B)** Absolute radioactivity values of [^{125}I]-α_2-MG (in cpm/µg protein) were determined after 40 min pulse by γ-counting and corrected by the radioactivity in the presence of RAP. **(C)** Corrected values were plotted as relative radioactivity of [^{125}I]-α_2-MG against chase time. Pulse values at 40 min were set to 1 in both genotypes.

4.2.3 Transferrin receptor-mediated endocytosis in *Cln3^{ki}* cerebellar cells

Loss of Cln3 protein has an impact on the process of clathrin-mediated endocytosis via Mpr300 and Lrp1, most likely due to altered protein expression of these receptors. The receptor for iron-bound transferrin is another classical example of a cargo receptor in clathrin-mediated endocytosis. Transferrin is an iron-binding protein that facilitates the iron-uptake (Fe^{3+}) into the cell. First, oxidized iron-loaded transferrin (holo-transferrin) binds to the transferrin receptor (TfR). After internalisation, TfR-transferrin complexes are transported to early endosomes, where bound iron will dissociate from transferrin due to low pH. Subsequently, iron-free transferrin (apo-transferrin) is directed to recycling endosomes to travel back to the cell surface, where it will be released from the TfR at neutral extracellular pH (Mayle *et al.* 2012).

To elucidate the effect of Cln3 loss in TfR-mediated internalisation of transferrin, wild-type and *Cln3^{ki}* cerebellar cells were incubated with serum-free medium containing 25 µg/ml AlexaFluor546-transferrin (AF546-transferrin) at 33 °C for 10 min, followed by fixation and analysis by confocal fluorescence microscopy. In both genotypes, internalised AF546-transferrin was localised in vesicular structures, which were

distributed throughout the cell. Even so, *Cln3*^{ki} cerebellar cells significantly internalised more transferrin than wild-type cells (Figure 16 A). Increased endocytosis of transferrin may be due to increased TfR expression, which was analysed by western blotting. The TfR was detectable as a 100 kDa band in both wild-type and *Cln3*^{ki} cerebellar cells. However, no differences in expression levels between the two genotypes were observed (Figure 16 B), which was in accordance to mRNA expression levels (Figure 16 C).

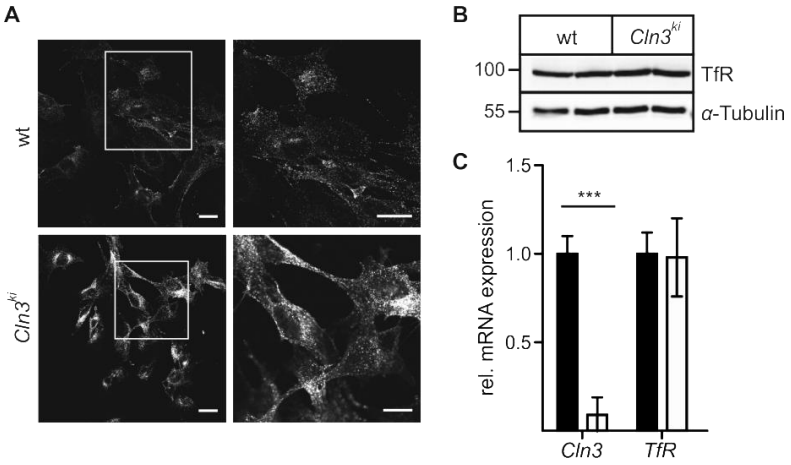

Figure 16: Endocytosis of AF546-transferrin and expression of TfR in wild-type and *Cln3*^{ki} cerebellar cells

(A) Wild-type and *Cln3*^{ki} cerebellar cells were incubated in serum-free medium containing 25 µg/ml AF546-transferrin at 33 °C for 10 min and fixed. Confocal fluorescence microscopy images were captured with identical exposure settings. Regions marked by the white rectangles are shown in the right panel in 2-fold higher magnification. Scale bars = 20 µm. **(B)** Total cell extracts (20 µg protein) of two individual samples of wild-type and *Cln3*^{ki} cerebellar cells were analysed by TfR western blotting. The positions of molecular mass marker proteins are indicated in kDa. α-Tubulin was used as loading control. **(C)** Relative mRNA expression levels of *Cln3* and *TfR* in *Cln3*^{ki} (white columns) compared to wild-type (black columns) cerebellar cells (mean ±SD, n=3, ***$P \leq 0.001$).

4.3 Clathrin-independent endocytosis in *Cln3*^{ki} cerebellar cells

Clathrin-dependent endocytosis of ligands by Mpr300, Lrp1 and TfR are impaired in *Cln3*^{ki} cerebellar cells. In order to elucidate whether clathrin-independent endocytosis mechanisms are also affected by loss of Cln3 protein, GM1 ganglioside-mediated endocytosis of cholera toxin and fluid-phase endocytosis of dextran were examined.

4.3.1 GM1 ganglioside-mediated endocytosis of cholera toxin subunit B

Cholera toxin produced by *Vibrio Cholera* is an enterotoxin composed of two subunits A and B. Subunit B (CTB) builds a ring-like structure and specifically binds to GM1

gangliosides in the plasma membrane. CTB enters the cell via caveolae/raft-mediated pathways (Montesano *et al.* 1982; Shogomori and Futerman 2001). After having entered the cell, CTB traffics retrograde from the plasma membrane to the TGN and ultimately reaching the ER.

To investigate the GM1 ganglioside-dependent uptake of CTB, wild-type and *Cln3*^{ki} cerebellar cells were incubated with 1 µg/ml AlexaFluor488-CTB (AF488-CTB) for 30 min at 33 °C, subsequently fixed and analysed by confocal immunofluorescence microscopy. In both wild-type and *Cln3*^{ki} cerebellar cells AF488-CTB is visible in vesicular structures forming a punctate pattern, but also a cell-surface associated staining is detectable (Figure 17, middle panel). The images were captured with identical exposure settings. The more intensive staining of AF488-CTB in *Cln3*^{ki} cerebellar cells implicated an elevated uptake of AF488-CTB compared to wild-type cells. Partial co-localisation of AF488-CTB with Gm130-positive structures indicated transport of AF488-CTB to the Golgi compartment within 30 min (Figure 17, right panel).

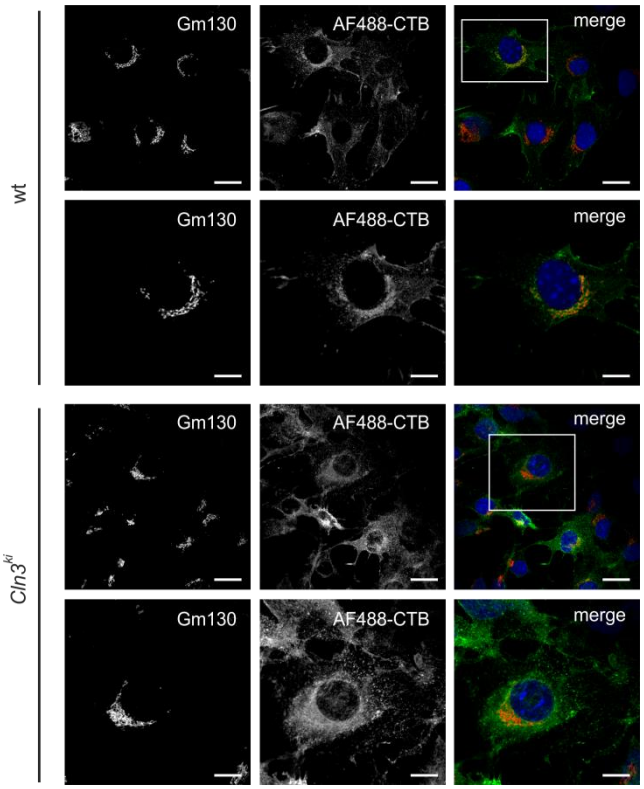

Figure 17: Internalisation of AF488-CTB in wild-type and Cln3^{ki} cerebellar cells
Wild-type and Cln3^{ki} cerebellar cells were incubated in serum-free medium containing 1 µg/ml AF488-CTB at 33 °C for 30 min. Cells were fixed, permeabilised and subsequently co-stained with an antibody against Gm130. Localisation of AF488-CTB (green) and Gm130 (red) was analysed by confocal immunofluorescence microscopy. Images were captured with identical exposure settings. The regions marked by the white rectangles are presented in 2-fold higher magnification in the lower image row. Nuclei were visualised with DAPI (blue). Yellow in merged images indicates co-localisation. Left panel and middle panel: stainings of Gm130 and AF488-CTB are depicted as grayscale images. Scale bars = 20 µm.

In addition, binding of AF488-CTB to the cell surface was investigated. Wild-type and *Cln3*^{ki} cerebellar cells were cooled to 4 °C for 15 min and then incubated with 1 µg/ml

AF488-CTB at 4 °C for 30 min. Subsequently, cells were fixed and analysed by confocal fluorescence microscopy. In both genotypes, AF488-CTB was mainly detectable at the cell surface but less in vesicular structures (Figure 18). In *Cln3*^{ki} cerebellar cells AF488-CTB binding to the cell surface was increased relative to wild-type cells.

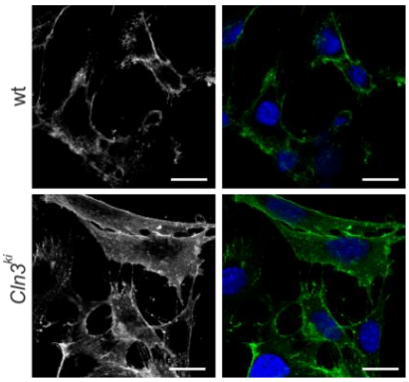

Figure 18: Cell surface labelling of AF488-CTB
Wild-type and *Cln3*^{ki} cerebellar cells were incubated with 1 µg/ml AF488-CTB in serum-free medium for 30 min at 4 °C and subsequently fixed. Confocal immuno-fluorescence images were captured with identical exposure settings. Nuclei were visualised with DAPI (blue). Left panel: stainings of AF488-CTB are depicted as grayscale images. Scale bars = 20 µm.

4.3.2 Fluid-phase endocytosis of dextran

Fluid-phase endocytosis or pinocytosis includes several endocytic mechanisms, such as micropinocytosis using uncoated vesicles, or caveolae-mediated endocytosis. Dextrans are inert glucose polymers and widely used as marker for fluid-phase endocytosis. Due to their α-1,6 glycosidic linkages, dextrans are not digested by cellular glycosidases.

To observe the uptake of dextran through the process of fluid-phase endocytosis, wild-type and *Cln3*^{ki} cerebellar cells were incubated in serum-free medium containing 100 µg/ml AlexaFluor546-dextran (AF546-dextran) at 33 °C for 24 h, and were subsequently fixed and analysed by confocal fluorescence microscopy. The images were captured with identical exposure settings. AF546-dextran was localised in vesicular structures and distributed throughout the cells in both genotypes. However, *Cln3*^{ki} cerebellar cells displayed a strong enrichment of dextran, which was less distinct in wild-type cells (Figure 19).

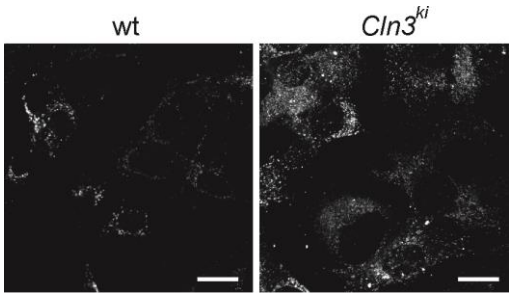

Figure 19: Fluid-phase endocytosis of AF546-dextran in wild-type and *Cln3*^{ki} cerebellar cells
Wild-type and *Cln3*^{ki} cerebellar cells were incubated in medium containing 100 µg/ml AF546-dextran at 33 °C for 24 h and subsequently fixed. Confocal immunofluorescence images were captured with identical exposure settings. Scale bars = 20 µm.

4.4 Analysis of the immune phenotype of *Cln3*^{ki} mice

Lysosomes and lysosome-related organelles are essential for normal function of the immune system, including antigen processing and presentation, phagocytosis, toll-like receptor signalling, and secretion of molecules (Colbert *et al.* 2009). Alterations in systemic responses might influence or accompany CLN3 pathology. So far, the relationship between lymphocytic storage or dysregulation in the lysosomal compartment and possible immune abnormalities has not been elucidated. To investigate the immune phenotype of the *Cln3*^{ki} mouse model, biochemical and *in vivo* functional assays were performed, covering different ages at 2.5 and 7.5 months of life.

4.4.1 Analysis of the immune cell composition in *Cln3*^{ki} mice

In order to define the immune cell composition, cells from spleen and bone marrow of wild-type and *Cln3*^{ki} mice were isolated and analysed by flow cytometry. Flow cytometry allowed the characterisation of the different cell types based on the expression of their specific surface receptors. Figure 20 shows a representative dot plot of the gating strategy that was used to exclude cell doublets and non-viable cells. Living cells were gated according to the expression of their surface markers. B and T cells were characterised by the B cell lineage-specific CD19 surface marker and the CD3 T cell co-receptor, respectively. The latter were further divided into T helper and cytotoxic T cells depending on the presence of the co-receptors CD4 and CD8, respectively. Granulocytes were defined by expression of the granulocyte receptor antigen 1 (Gr1) and the glycosylphophatidylinositol (GPI)-anchored protein lymphocyte antigen complex 6 locus C (Ly6C), whereas monocytes were identified by the expression of Ly6C and the integrin CD11b. Dendritic cells were gated according to their surface

expression of integrin CD11c and the major histocompatibility complex class II (MHCII).

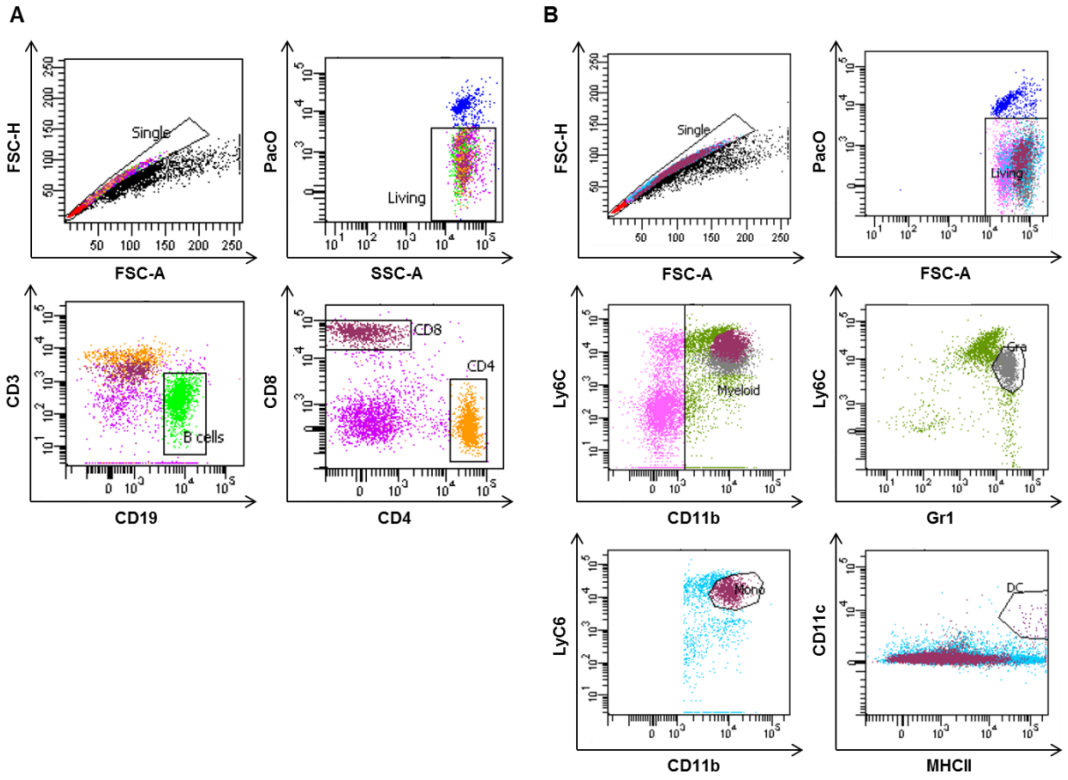

Figure 20: Gating scheme for the analysis of the immune cell composition in wild-type and *Cln3*^{ki} mice

Representative dot plots of immune cells isolated from **(A)** spleen and **(B)** bone marrow of a 7.5 months old wild-type mouse. In FSC-H/FSC-A dot plots single cells were gated, thereby excluding cell doublets. Dead cells were identified as Pacific Orange (PacO)-positive and excluded from the analysis. Living cells were then gated upon the expression of their specific surface markers as described in the text.

The relative frequency of the respective cell type is represented as percentage of living cells (Figure 21). Under steady-state conditions, no differences between wild-type and *Cln3*^{ki} mice were observed in the relative frequency of B cells, CD4^{+} and CD8^{+} T cells, granulocytes, monocytes and dendritic cells isolated from spleen and bone marrow.

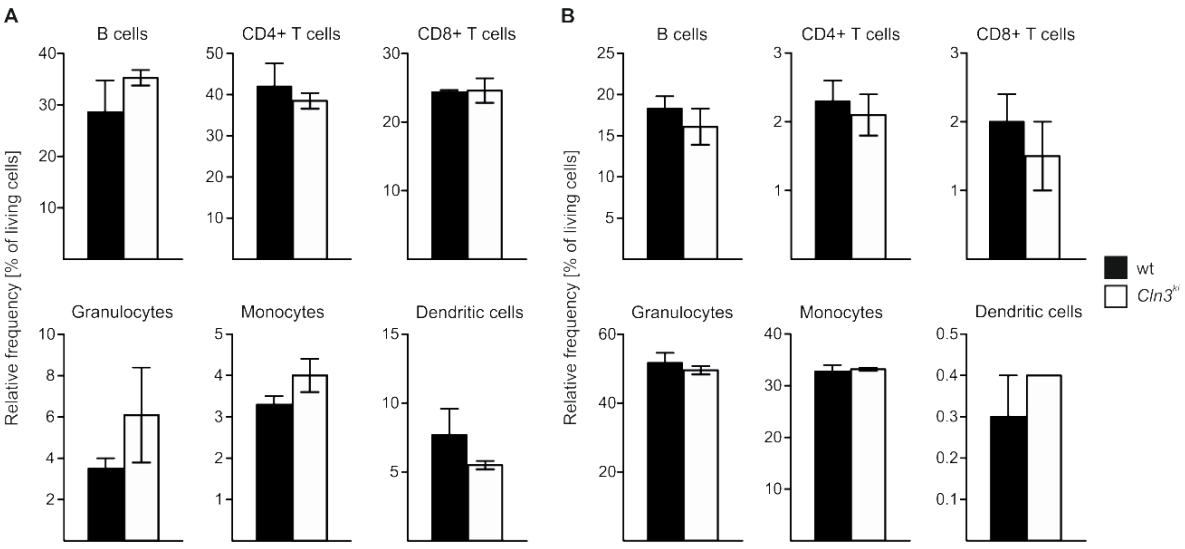

Figure 21: Analysis of the relative frequency of immune cells in spleen and bone marrow of wild-type and *Cln3*^{ki} mice

Immune cells isolated from **(A)** spleen and **(B)** bone marrow of 2.5 months old wild-type (black column) and *Cln3*^{ki} (white column) mice were analysed by flow cytometry and represented as relative frequency of living cells (mean ±SD; n = 3). The experiment was repeated twice with animals of 2.5 months and once with animals of 7.5 months with consistent results.

4.4.2 Storage material in immune cells of *Cln3*^{ki} mice

One pathologic hallmark of CLN3 disease is lysosomal accumulation of the subunit c of the mitochondrial ATP synthase in various tissues (Cotman and Staropoli 2012; Staropoli *et al.* 2012). The presence of storage material in T cells, B cells and macrophages was analysed by electron microscopy, confocal immunofluorescence microscopy and western blotting.

4.4.2.1 Storage in T and B cells

Splenocytes were isolated from 2.5 months old wild-type and *Cln3*^{ki} mice and cultured in medium containing anti-CD3 and IL-2, and LPS to obtain enriched cultures of T and B cell blasts, respectively. To investigate these cells morphologically, electron microscopic analyses were carried out. Lysosomes of splenic T cells from *Cln3*^{ki} mice contained abnormally increased amounts of electron-dense material seen by electron microscopy (Figure 22 A). A higher magnification of the images revealed homogenously appearing lysosomes filled with electron-dense structures (arrow head), as well as lysosomes that appeared heterogeneous being filled with both electron-dense and electron-lucent material (*). Additionally, autophagosomes were observed (Au). In line with these findings, western blot analysis of enriched cultures of T cell blasts from

Cln3^{ki} splenocytes presented increased protein levels of Lamp1 (Figure 22 B). In contrast, B cell blasts did not present morphological abnormalities or storage material-like structures (not shown). However, western blot analysis of B cell blasts also revealed elevated Lamp1 levels (Figure 22 B), indicating an increase in size and number of lysosomes. These findings were underlined by the identification of accumulating subunit c levels in insoluble fractions of B cell blasts (Figure 22 C).

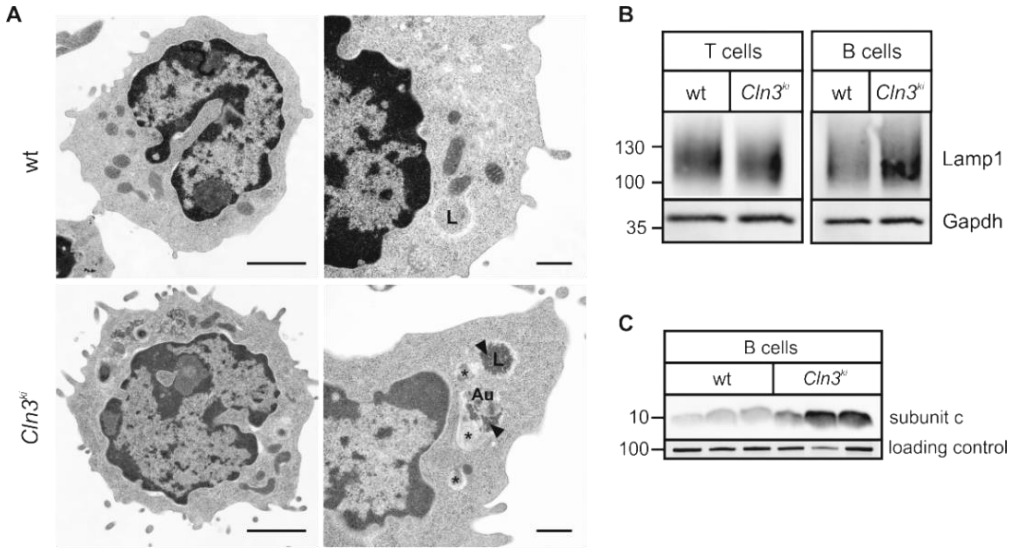

Figure 22: Storage material in *Cln3*^{ki} T and B cell blasts

(A) Ultra-structural analysis of storage material in splenic T cells of 2.5 months old *Cln3*^{ki} mice. Lysosomes (L) contain electron-dense (arrow head) and electron-lucent (*) material. Autophagosomes (Au). Scale bar = 1 µm **(B)** Total cell extracts of splenic T and B cell blasts (10 µg protein) of wild-type and *Cln3*^{ki} mice, respectively, were separated by SDS-PAGE under reducing conditions and analysed by Lamp1 western blotting. The positions of molecular mass marker proteins are indicated in kDa. Gapdh was used as loading control. **(C)** Insoluble fractions of three individual samples of wild-type and *Cln3*^{ki} B cell blasts were analysed by subunit c western blotting. An unspecific band at 100 kDa was used as loading control.

4.4.2.2 Storage in peritoneal macrophages

Peritoneal macrophages were isolated 6 days post-injection with thioglycolate. After 5 days in culture, macrophages were ultra-structurally analysed by electron microscopy (Figure 23 A). Lysosomal vacuoles (Lv) were visible in both genotypes, whereas *Cln3*^{ki} macrophages contained more and smaller vacuoles compared to wild-type cells. However, storage material-like structures were not observed. The same cell preparation was also analysed for subunit c accumulation by confocal immunofluorescence microscopy. Interestingly, subunit c levels were elevated in respect to normal wild-type levels in *Cln3*^{ki} macrophages and subunit c was detectable in lysosomal structures as

revealed by co-staining with Lamp1 (Figure 23 B, right panel). Similarly, western blot analysis showed a strong increase in subunit c levels in *Cln3*^{ki} macrophages compared to wild-type cells (Figure 23 C).

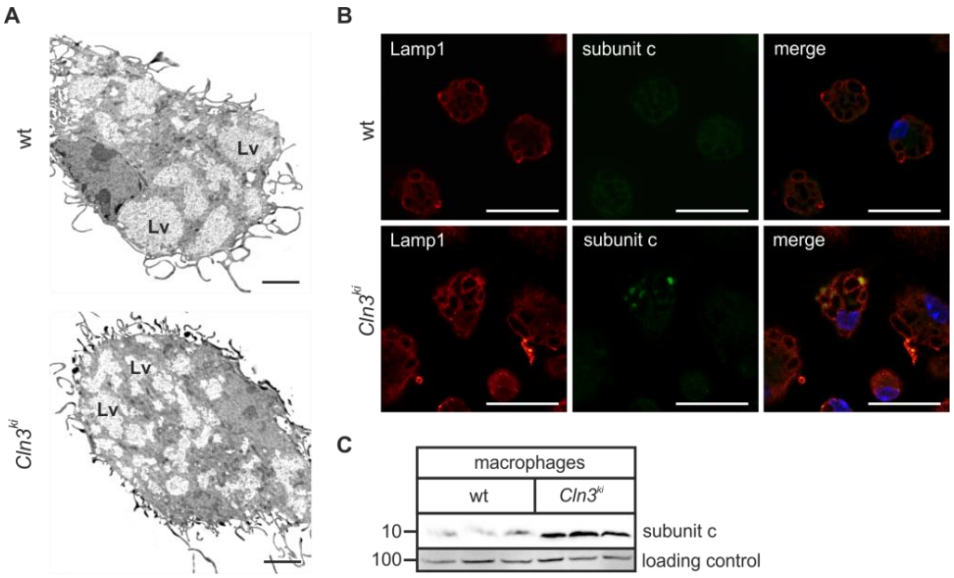

Figure 23: Storage material in *Cln3*^{ki} macrophages
(A) Ultra-structural analysis of *Cln3*^{ki} peritoneal macrophages. Lysosomal vacuoles (Lv) are indicated. Scale bars = 3 µm **(B)** Wild-type and *Cln3*^{ki} peritoneal macrophages were stained with antibodies against Lamp1 (red) and subunit c (green). Confocal immunofluorescence images were captured with identical exposure settings. Nuclei were visualised with DAPI (blue). Yellow in merged images indicates co-localisation. Scale bars = 20 µm. **(C)** Total cell extracts (10 µg protein) of three individual samples of wild-type and *Cln3*^{ki} peritoneal macrophages were separated by SDS-PAGE under reducing conditions and analysed by subunit c western blotting. The positions of molecular mass marker proteins are indicated in kDa. An unspecific band at 100 kDa was used as loading control.

4.4.3 Cathepsin expression and proteolytic processing in *Cln3*^{ki} macrophages

Lysosomes contain a considerable number of proteases, of which cathepsins constitute a major proportion. In addition to their main function in lysosomal protein degradation and recycling, cathepsins play a significant role in immunological processes such as antigen processing and presentation, which is essential for effective adaptive immunity. Antigen presenting cells, such as B cells, dendritic cells and macrophages, internalise extracellular antigens that are subsequently cleaved in the MHCII compartment, a lysosome-related organelle. The formation of appropriate peptides, followed by their binding to and presentation by MHCII complexes, is crucial for a specific adaptive immune response (Bird *et al.* 2009).

Cathepsin S is involved in the elimination of the invariant chain chaperone (CD74), which associates with the MHCII complex in the ER to prevent pre-mature antigen binding (Honey and Rudensky 2003). The expression of cathepsin S in macrophages of *Cln3*^{ki} mice was investigated by western blotting and subsequent densitometric analysis. Peritoneal macrophages of *Cln3*^{ki} mice revealed 1.4-fold higher protein amount compared to wild-type cells (Figure 24). Strikingly, protein levels of the substrate of cathepsin S, the invariant chain, were also elevated by 2.3-fold in *Cln3*^{ki} cells.

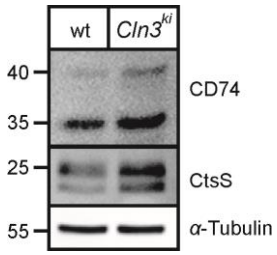

Figure 24: Expression of cathepsin S and invariant chain in peritoneal macrophages of wild-type and *Cln3*^{ki} mice
Total cell extracts (15 µg protein) of wild-type and *Cln3*^{ki} peritoneal macrophages were separated by SDS-PAGE under reducing conditions and analysed by western blotting using antibodies against invariant chain (CD74) and cathepsin S (CtsS). The positions of molecular mass marker proteins are indicated in kDa. α-Tubulin was used as loading control.

In contrast, western blotting of cathepsin B and densitometric analysis revealed that the amount of the precursor (38 kDa) and mature (35 kDa) form was significantly reduced by 20 % in *Cln3*^{ki} macrophages compared to wild-type cells (Figure 23 A). Cathepsin D is synthesised as a 53 kDa precursor form and then proteolytically cleaved to an intermediate form of 43 kDa and two mature forms of 31 and 14 kDa. The precursor and the 14 kDa mature forms were not detectable in both genotypes. However, the intermediate and the 35 kDa mature form of cathepsin D were decreased by 45 % in *Cln3*^{ki} macrophages compared to wild-type cells. Cathepsin Z is expressed as a 40 kDa precursor protein and then proteolytically processed to a mature 37 kDa form, which was only slightly decreased by 15 % in *Cln3*^{ki} macrophages.

In order to evaluate whether small disturbances in the lysosomal protease composition may have an impact on the proteolytic processing in the lysosome, DQ-BSA endocytosis and processing assays were performed. Wild-type and *Cln3*^{ki} macrophages were incubated with DQ-BSA for 10 min and subsequently chased for 15, 30, 45 and 60 min. DQ-BSA emits fluorescence only upon degradation in the endo-lysosomal compartment (Figure 25 B). During 60 min chase time, a linear increase in DQ-BSA-specific fluorescence was observed in wild-type macrophages. In contrast, it appears that in *Cln3*^{ki} macrophages a plateau is reached between 45 and 60 min of chase. Quantification of DQ-BSA-specific fluorescence by flow cytometry revealed that

during the chase time of 60 min, the proteolytic processing of DQ-BSA was significantly reduced in average by 45 % in *Cln3*^{ki} macrophages compared to the wild-type (Figure 25 C).

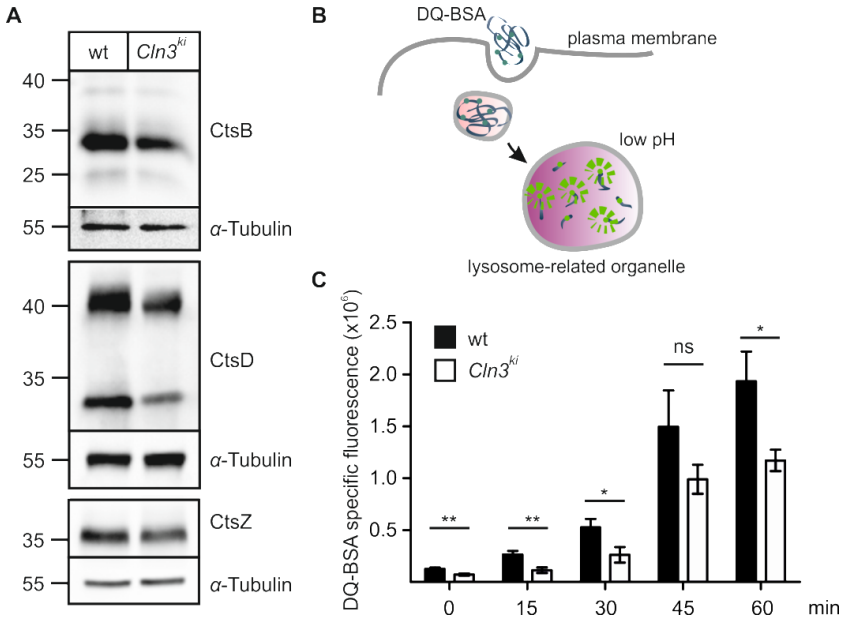

Figure 25: Proteolytic processing of endocytosed DQ-BSA in peritoneal macrophages of wild-type and *Cln3*^{ki} mice

(A) Total cell extracts (15 µg protein) of peritoneal macrophages isolated from wild-type and *Cln3*^{ki} mice were separated by SDS-PAGE under reducing conditions and analysed by western blotting using antibodies against cathepsin B (CtsB), cathepsin D (CtsD) and cathepsin Z (CtsZ). The positions of molecular mass marker proteins are indicated in kDa. *α*-Tubulin was used as loading control. **(B)** Schematic view of DQ-BSA endocytosis and degradation: The self-quenched DQ-BSA is internalised via fluid phase endocytosis and emits fluorescence upon degradation of BSA in lysosome-related organelles. **(C)** Wild-type and *Cln3*^{ki} peritoneal macrophages were incubated with DQ-BSA (10 µg/ml) at 37 °C for 10 min and chased for the indicated time points. Cells were harvested and fixed and DQ-BSA-specific fluorescence was quantified by flow cytometry.

4.4.4 Control of *L. monocytogenes* infection in *Cln3*^{ki} mice

Cathepsins residing within the lysosomal compartment of macrophages are responsible for the degradation and processing of antigens derived from phagocytosed material. A disturbed composition of lysosomal proteases may impair proteolytic processing in lysosomes. *Cln3*^{ki} macrophages displayed reduced protein levels of cathepsin B, D and Z. In order to evaluate whether a decrease of these proteases had an impact on the ability of macrophages to clear bacteria during an infection, wild-type and *Cln3*^{ki} mice were infected intravenously with 5 x 10^6 *L. monocytogenes* strain EGD. Three days post infection, bacterial burdens were determined in spleen and liver, being the main sites of

listeria replication. In the liver, both genotypes harboured similar bacterial titers (Figure 26). In contrast, bacterial titers in the spleen of *Cln3*^{ki} mice were slightly elevated compared to wild-type mice, although differences did not reach a level of significance.

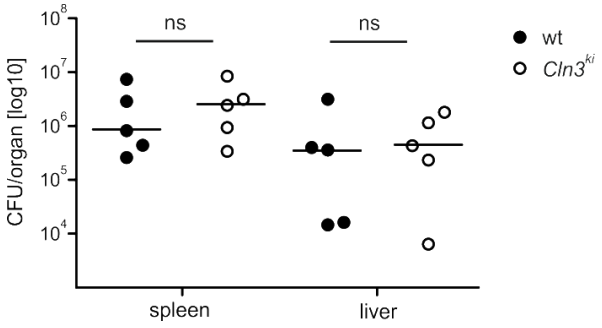

Figure 26: Control of *L. monocytogenes* infection in wild-type and *Cln3*^{ki} mice
Wild-type and *Cln3*^{ki} mice were infected with 1 x 10^6 *L. monocytogenes* intravenously and *L. monocytogenes* titers were determined in spleen and liver. Colony forming units (CFU) for individual mice and median values are shown (n = 5, detection limit was 20 CFU).

In conclusion, *Cln3*^{ki} macrophages contain reduced levels of cathepsin B, D and Z. Additionally, DQ-BSA degradation assays *in-vitro* revealed a reduced proteolytic processing capacity in the lysosomal compartment of these cells. However, this had no impact on the control of listeria infection, as no differences in the ability to efficiently clear listeria were observed between genotypes.

4.4.5 T cell response in *Cln3*^{ki} mice

T cell function is controlled by the interaction of the T cell receptor (TCR) with ligand-loaded MHC molecules. T cells expressing the αβ TCR are divided into groups, depending on their expression of the co-receptor molecules CD4 and CD8. CD8$^+$ T cells recognise peptides that are derived from cytosolic proteins and are presented on MHCI molecules. CD4$^+$ T cells, in contrast, interact with peptides in the context of MHCII molecules. These peptides derived from proteins cleaved in the MHCII compartment (Bird *et al.* 2009).

Ultra-structural and biochemical analysis revealed the presence of storage material in T cells of *Cln3*^{ki} mice (Figure 22). To evaluate whether dysfunction of lysosome-related organelles including the accumulation of lysosomal storage material had an impact on T cell function, T cells of *Cln3*^{ki} mice were phenotypically characterised and their response to specific T cell receptor stimulation was investigated.

4.4.5.1 Phenotypic analysis of T cell in *Cln3*^{ki} mice

In order to phenotypically analyse $CD4^+$ and $CD8^+$ T cells, the surface expression of the adhesion molecules CD62L and CD44 was determined by flow cytometry. Activated T cells are defined as $CD44^+CD62L^-$. CD44 is an adhesion molecule and is expressed on effector and on memory T cells in order to mediate cell-cell interactions and migration processes (Goodison *et al.* 1999). Naïve T cells express the adhesion molecule CD62L or L-selectin, which facilitates the entry into secondary lymphoid tissues. Effector and memory T cells do not express CD62L, as they are circulating in the periphery and directly exerting their effector function upon antigen encounter (Veerman *et al.* 2007).

Flow cytometry revealed that 2.1 ± 0.3 % and 1.9 ± 0.4 % of $CD8^+$ T cells of wild-type and *Cln3*^{ki} spleen cells, respectively, were mature effector T cells. In the population of splenic $CD4^+$ T cells, frequencies of effector T cells were comparable in both genotypes (19.8 ± 1 % and 22.0 ± 0.4 %, respectively). In contrast, in $CD8^+$ T cells isolated from the bone marrow, *Cln3*^{ki} mice displayed a slight increase in the frequency of mature effector T cells (33.5 ± 4.1 %) compared to wild-type mice (40.8 ± 7.1 %). Similarly, the frequency of bone marrow $CD4^+$ effector T cells was slightly higher in *Cln3*^{ki} mice (84.4 ± 2.1 %) than in wild-type mice (77.2 ± 7.3 %). However, these differences were not statistically significant.

In conclusion, in spleen and bone marrow, the proportional distribution of naïve, memory and effector T cells was comparable in both genotypes (Figure 27 A), not presenting any dysregulations in T cell maintenance and development under steady-state conditions.

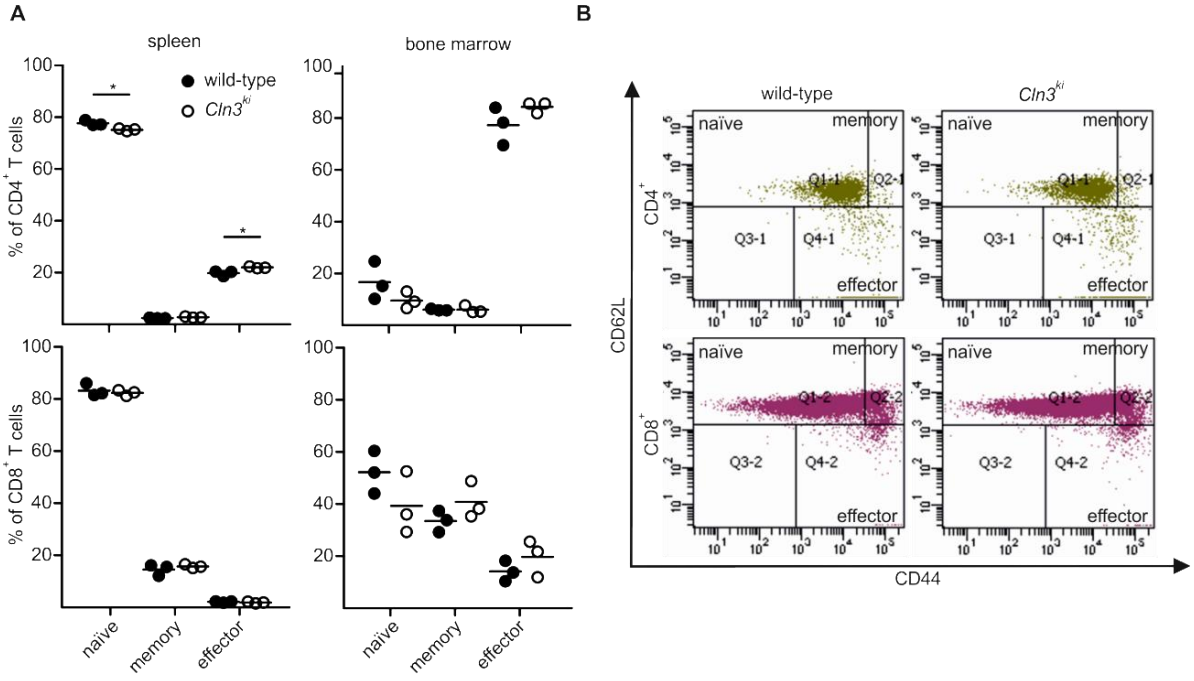

Figure 27: Phenotypical analysis of CD4$^+$ and CD8$^+$ T cells in wild-type and *Cln3*^{ki} mice
(A) Lymphocytes isolated from spleen and bone marrow of wild-type (filled circle) and *Cln3*^{ki} mice (empty circle) were analysed for CD62L and CD44 expression. Naïve, memory and effector T cells are represented as percentage of CD4$^+$ and CD8$^+$ T cells, respectively. Values for individual mice and the mean are shown (n = 3, *$P \leq 0.05$). **(B)** Representative dot plots of CD62L and CD44 expression on CD4$^+$ (upper panel) and CD8$^+$ T cells (lower panel). Regions of naïve (CD62L$^+$/CD44$^-$), memory (CD62L$^+$/CD44$^+$) and effector (CD62L$^-$/CD44$^+$) T cells are indicated.

4.4.5.2 Functional characterisation of T cells in *Cln3*^{ki} mice

T cell activation and production of the pro-inflammatory cytokines IFNγ and TNFα was analysed in wild-type and *Cln3*^{ki} mice. Lymphocytes were isolated from spleen and bone marrow and incubated with phorbol-12-myristate-acetate (PMA) and the calcium ionophore ionomycin in the presence of brefeldin A. Treatment with PMA/ionomycin leads to a polyclonal stimulation of T cells resulting in the production of cytokines. Brefeldin A blocks intracellular protein transport by inducing the fusion of the Golgi stacks with the endoplasmic reticulum (Donaldson *et al.* 1992), thereby preventing the secretion of newly synthesised cytokines. Therefore, cytokines can be stained intracellularly and measured by flow cytometry.

Without stimulation, no production of IFNγ and TNFα by T cells was observed. Upon stimulation with PMA/ionomycin, IFNγ and TNFα production of splenic T cells was comparable in both genotypes (Figure 28 B, left panel). Contrarily, in bone marrow of *Cln3*^{ki} mice the frequencies of IFNγ$^+$ CD4 and CD8 T cells were significantly increased

from 28.2 ± 1.6 to 37.6 ± 2.0 % and from 33.0 ± 1.5 to 47.5 ± 4.3 %, respectively, compared to cells from wild-type mice. Also the frequencies of TNFα^{+} CD4 and CD8 T cells were elevated in *Cln3*^{ki} mice from 32.9 ± 0.2 to 41.7 ± 1.0 % and from 18.8 ± 0.5 to 28.0 ± 2.5 %, respectively (Figure 28 B, right panel).

In conclusion, T cell activation and subsequent IFNγ and TNFα production in splenic T cells was not changed between wild-type and *Cln3*^{ki} mice. In contrast, an enhanced T cell response was observed in the bone marrow of *Cln3*^{ki} mice. *Cln3*^{ki} T cells residing in the bone marrow presented a phenotype, which was hyper-responsive in terms of IFNγ and TNFα production upon PMA/ionomycin stimulation.

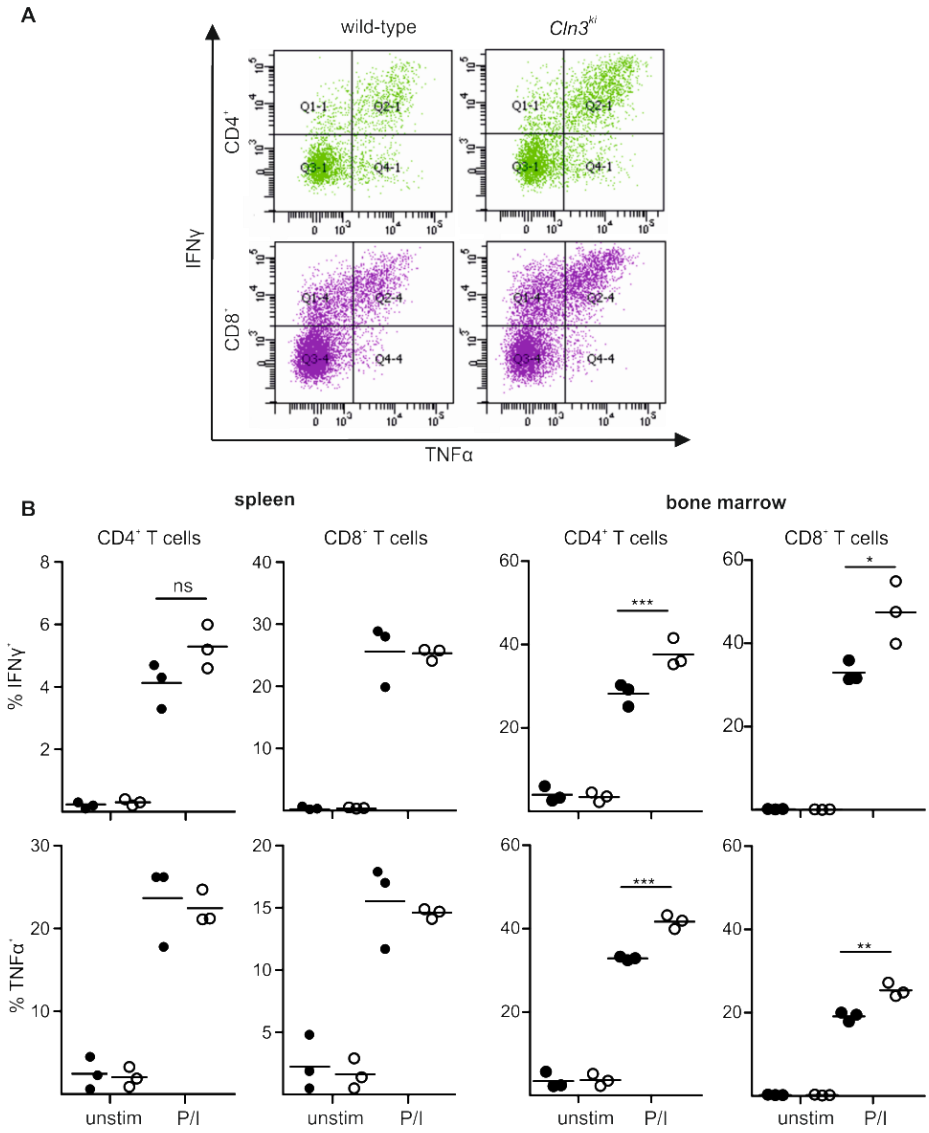

Figure 28: Cytokine production in T cells of wild-type and *Cln3*^{ki} mice

(A) Representative dot plots of IFNγ^{+} and TNFα^{+} CD4 (upper panel) and CD8 T cells (lower panel). **(B)** Lymphocytes isolated from spleen and bone marrow of wild-type(filled circle) and *Cln3*^{ki} mice (empty

circle) were either stimulated for 4 h with PMA/ionomycin (P/I) in the presence of brefeldin A or were not stimulated (unstim). $CD4^+$ and $CD8^+$ T cells were gated and analysed for IFNγ and TNFα production. Percentage of IFNγ- and TNFα-expressing T cells for individual mice and the mean of one representative experiment of three experiments are shown (n = 3, $*P \leq 0.05$, $**P \leq 0.01$, $***P \leq 0.001$).

As a next step, T cell activation and production of cytokines were investigated after infection of mice with *L. monocytogenes*. To evaluate the response of T cells that have already encountered an antigen during the infection, lymphocytes were isolated eight days post infection and re-stimulated *in-vitro* with listeria-specific antigens.

In mice, infection with *L. monocytogenes* leads to a rapid activation of the innate immune system, which is essential for the restriction of bacterial replication and host defence. Nevertheless, the adaptive immune system is responsible for the final elimination of listeria, with T cells playing the main role in controlling the inflammatory response (Pamer 2004). *L. monocytogenes* induce a classical T cell response that leads to increased synthesis of the inflammatory cytokines IFNγ and TNFα by $CD4^+$ and $CD8^+$ T cells, reaching a maximum in response between day 8 and 10.

So far, no listeria-specific antigen has been identified for $CD8^+$ T cells in C57BL/6 mice. Therefore, wild-type and $Cln3^{ki}$ mice were infected intravenously with 1 x 10^4 *Lm*OVA, a listeria strain expressing ovalbumin. Secreted ovalbumin is processed into the peptide $OVA_{257-264}$ and presented via the MHCI complex, which is recognised by *Lm*OVA specific $CD8^+$ T cells, leading to T cell receptor-specific activation of these cells. The listeria-specific toxin listeriolysin O (LLO) is immuno-dominant for $CD4^+$ T cells (Pamer 2004). The combination of infection with *Lm*OVA and subsequent *in-vitro* stimulation of isolated splenocytes with $OVA_{257-264}$ and $LLO_{189-201}$ peptides allowed the identification of IFNγ and TNFα producing $CD8^+$ and $CD4^+$ T cells, representing a listeria-specific T cell response.

On day 8 after infection splenocytes from wild-type and $Cln3^{ki}$ mice were isolated and either stimulated non-specifically with PMA/ionomycin or listeria-specifically with the peptides $LLO_{189-201}$ and $OVA_{257-264}$, or were not stimulated. Subsequently, listeria-specific $CD4^+$ and $CD8^+$ T cells were analysed for IFNγ and TNFα production by flow cytometry (Figure 28).

Without stimulation, no production of IFNγ and TNFα was observed, independent of the genotype. Upon non-specific stimulation of the T cell receptor by PMA/ionomycin

treatment, IFNγ production by $CD4^+$ T cells was significantly increased from 8.8 ± 1.0 to 14.7 ± 1.5 % in *Cln3*^{ki} compared to wild-type mice, whereas $CD8^+$ T cells produced similar levels of IFNγ in both genotypes. Moreover, no differences in TNFα production by T cells were observed between genotypes.

Upon listeria-specific stimulation with the peptides $LLO_{189-201}$ and $OVA_{257-264}$, IFNγ production by $CD4^+$ T cells increased from 2.5 ± 0.6 to 5.2 ± 0.9 %, while $CD8^+$ T cells presented an increase from 7.8 ± 1.3 to 12.7 ± 1.7 % in IFNγ levels. Strikingly, upon stimulation with $LLO_{189-201}$ and $OVA_{257-264}$ peptides, TNFα production was neither induced in $CD4^+$ nor in $CD8^+$ T cells.

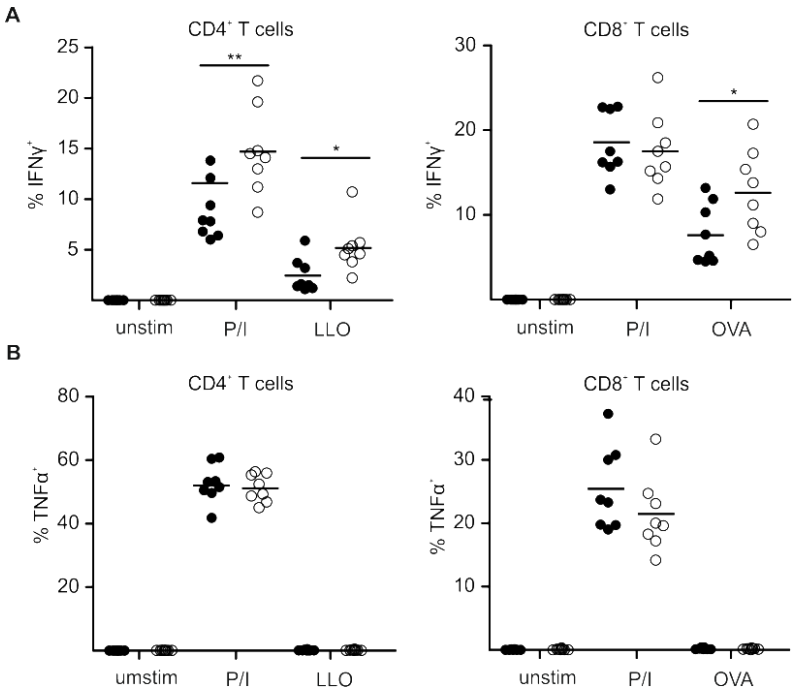

Figure 29: T cell response upon *L. monocytogenes* infection in wild-type and *Cln3*^{ki} mice
Wild-type (filled circle) and *Cln3*^{ki} mice (empty circle) were intravenously infected with 1 x 10^4 *Lm*OVA. Eight days post infection, splenocytes were isolated and either stimulated for 4 h with PMA/ionomycin (P/I), $LLO_{189-201}$ or $OVA_{257-264}$ in the presence of brefeldin A, respectively, or not stimulated (unstim). $CD4^+$ and $CD8^+$ T cells were gated and analysed for **(A)** IFNγ and **(B)** TNFα production. Percentage of IFNγ- and TNFα-expressing T cells for individual mice and the mean of one representative experiment out of two are shown (n = 8, **P*≤0.05, ***P*≤0.01).

Taken together, in naïve mice the T cell response in spleen did not differ between the genotypes in terms of cytokine production. In bone marrow of naïve mice, however, *Cln3*^{ki} mice showed a slightly elevated T cell response, as presented by an increase in IFNγ and TNFα production. After infection with *L. monocytogenes*, a significant increase in IFNγ production by *Cln3*^{ki} $CD4^+$ T cells was observed, when cells were

stimulated non-specifically with PMA/ionomycin or listeria-specifically with the peptide $LLO_{189-201}$. In contrast, *Cln3*^{ki} $CD8^+$ T cells presented only elevated IFNγ levels upon listeria-specific stimulation with $OVA_{257-264}$.

5 Discussion

CLN3 disease is a neurodegenerative lysosomal storage disorder caused by mutations in the *CLN3* gene, coding for a lysosomal transmembrane protein. CLN3 protein function is still poorly understood but its localisation implies a direct role in lysosomal function. A dysfunctional CLN3 protein results in accumulation of storage material, which predominantly consists of the highly hydrophobic proteolipid subunit c of the mitochondrial ATP synthase (Palmer *et al.* 1992). However, the pathomechanisms that are leading to accumulation of lysosomal storage material and neurodegeneration remain unclear. Various mechanisms of lysosomal dysfunction resulting in accumulation of lysosomal storage material are conceivable, such as impaired degradation in the lysosome (Ezaki *et al.* 1996) missing or defective selected lysosomal enzymes, changes in lysosomal ion homeostasis, which may affect pH, Ca^{2+} or Cl^- concentration, or disrupted trafficking pathways to and from the lysosome (Seehafer and Pearce 2006; Cotman and Staropoli 2012).

So far, it has not been investigated whether the absence of functional CLN3 protein and lysosomal dysfunction is manifested in an altered lysosomal protein composition. Lysosomes contain more than 60 soluble hydrolases and accessory proteins, playing a key role in lysosomal degradation of macromolecules, and 140 - 300 lysosomal membrane proteins are involved in processes such as membrane fusion, maintaining lysosomal integrity and transport of molecules (Schröder *et al.* 2007; Chapel *et al.* 2013).

In the present study, the approach of SILAC-based quantitative proteomic analysis of purified lysosomes was used in order to gain insights into possible dysregulation of lysosomal protein composition in CLN3 disease. The entire experimental procedure was performed on the previously established immortalised cerebellar neuronal precursor cell line from *Cln3*^{ki} mice, carrying the most common patient mutation, the 1 kb deletion leading to loss of exons 7 and 8 (Fossale *et al.* 2004). Biochemical and molecular biological methods were subsequently applied to verify the proteomic data. Based on these findings, different mechanisms of clathrin-dependent and clathrin-independent endocytosis were analysed in wild-type and *Cln3*^{ki} cerebellar cells.

5.1 Lysosomal protein composition in *Cln3*^{ki} cerebellar cells

SILAC-based quantitative proteomic analysis of isolated lysosomes revealed a total number of 70 lysosomal proteins in wild-type and *Cln3*^{ki} cerebellar cells. Among them, 29 soluble and eight membrane proteins were identified to be differentially expressed *Cln3*^{ki} in respect to wild-type cerebellar cells.

The amounts of cathepsin D and Z in lysosomal fractions of *Cln3*^{ki} cerebellar cells were significantly reduced by 27 and 46 %, respectively, whereas protein levels of cathepsin B and L remained rather unchanged (Figure 3). These data were confirmed by western blotting of total cell extracts (Figure 4 A and B).

Cathepsin D represents the most abundant acid aspartic protease, whereas cathepsin B, L and Z belong to the cysteine protease family. Cathepsins are synthesised as precursor polypeptides that undergo proteolytic processing steps within the endo-lysosomal compartment, required for enzymatic activity. The correct proteolytically processed forms indicate normal transport to the endo-lysosomal compartment and the presence of the required processing proteases. Decreased amounts of cathepsin D have been previously described for *Cln3*^{ki} cerebellar cells and *Cln3*^{ki} mouse brain (Fossale *et al.* 2004) and reduced cathepsin B activity was observed in CLN3 siRNA treated HeLa cells (Metcalf *et al.* 2008). In these reports, proteolytic maturation of cathepsin B and D has been described as defective, reflecting impairments in vesicular trafficking or lysosomal pH. In CLN3 siRNA treated cells, however, reduced cathepsin B activity (Metcalf *et al.* 2008) and normally processed forms of cathepsin D (Pohl *et al.* 2007) suggest that the transient down-regulation of CLN3 protein to 4 to 20 % of normal levels cannot be directly compared with *Cln3*^{ki} cerebellar cells or *Cln3*^{ki} mouse brain. In contrast, the presence of the mature forms in both wild-type and *Cln3*^{ki} cerebellar cells indicates correct transport to the endo-lysosomal compartment. In addition, western blot analysis of conditioned media revealed also a reduction of cathepsin B, D and Z protein levels, excluding missorting of these proteases. Decreased protein levels of cathepsin B, D and also of cathepsin Z can be rather explained by the reduction of their mRNA expression levels (Figure 4 C). Furthermore, decreased protein levels of cathepsin B, D and Z were also found in *Cln3*^{ki} primary mouse embryonic fibroblast cells, indicating that the absence of functional Cln3 protein has also an effect on non-neuronal cell types.

In contrast, cathepsin L remained unchanged on protein and mRNA levels (Figure 3, Figure 4 B and C). Similar to observations in NIH 3T3 cells (Sahagian and Gottesman 1982), in both genotypes, the majority of newly synthesised cathepsin L is secreted, while only small amounts of the precursor and mature forms were detectable intracellularly. The sorting efficiency of lysosomal enzymes is dependent on the nature of the oligosaccharides they carry. Two M6P groups on different oligosaccharides bind to Mpr300 with higher affinity than two M6P groups on one bi-antennary oligosaccharide (Dong *et al.* 1989; Dong and Sahagian 1990). In cerebellar cells, cathepsin L most probably carries one bi-antennary phosphorylated oligosaccharide, as it was described for NIH 3T3 cells, and escapes sorting by the Mpr300 in the TGN, subsequently leading to the secretion of the majority of newly synthesised cathepsin L. In contrast, cathepsin L synthesised by CHO cells carries two different oligosaccharides and is correctly sorted intracellularly (Dong and Sahagian 1990).

SILAC-based proteomic analysis further revealed that the concentration of enzymes and accessory proteins involved in sphingolipid degradation, such *β*-hexosaminidase, *α-N*-acetylgalactosaminidase, galactocerebrosidase, arysulfatase A, acid ceramidase and saposins, were decreased by 28 to 61 % in lysosomes of *Cln3*^{ki} cerebellar cells. In line with these results, *β*-hexosaminidase and arylsulfatase A enzyme activities, as well as *β-hexosaminidase* transcript levels were also significantly decreased (Figure 6). The transcript levels of the other enzymes involved in sphingolipid degradation remain to be determined. Generally it is assumed that 5 – 10 % of normal activity of a single lysosomal enzyme is sufficient to maintain its specific function in the lysosome (Sawkar *et al.* 2006). Nevertheless, minor changes in protein levels and enzyme activities of multiple lysosomal proteins involved in a common degradative pathway may cause lysosomal dysfunction, accumulation of storage material, and abnormal cellular homeostasis in an additive manner.

Several of the enzymes involved in sphingolipid degradation require accessory proteins, i.e. sphingolipid-binding proteins, GM2-activator proteins or saponins, for proper enzymatic activity and degradation of their endogenous substrates (Fürst and Sandhoff 1992; Kishimoto *et al.* 1992). Saposins are synthesised as a common 70 kDa prosaposin precursor protein that is proteolytically cleaved to four mature saposin forms A, B, C and D. Saposin A activates galactocerebrosidase, an enzyme being involved in the

removal of galactose from ceramide derivates. Saposin B stimulates the activity of arylsulfatase A, responsible for hydrolysis of cerebroside-sulfatides, a constituent of the myelin sheath. Acid ceramidase requires saposin D as a cofactor for the catalysis of ceramides into sphingosines and fatty acids. Reduced levels of acid ceramidase and also of other enzymes involved in sphingolipid degradation, such as *α-N*-acetylgalactosaminidase, galactocerebrosidase and arysulfatase A, may lead to accumulation of ceramide and ceramide derivates in lysosomes of *Cln3*^{ki} cerebellar cells. Elevated ceramide levels have been described to be present in brains of JNCL patients and Cln3$^{-/-}$ mice (Puranam *et al.* 1997; Mencarelli and Martinez-Martinez 2013). In Alzheimer's disease (AD) and non-AD dementia elevated ceramide levels have been associated with neuronal apoptosis and neuro-inflammation (Filippov *et al.* 2012).

Ceramide accumulation is a characteristic feature of Farber's disease, a lysosomal storage disorder caused by mutations in the *acid ceramidase* gene. It has been shown that ceramide does not only accumulate in the endo-lysosomal system but is translocated to lipid-rich domains in the plasma membrane. Being a part of the endomembrane system, ceramide may overflow to interconnected compartments, once the lysosome becomes saturated with ceramide derivates (Ferreira *et al.* 2014). Ceramide-enriched membrane microdomains on the cell surface serve as a platform that clusters proteins of the death receptor signalling pathway to trigger an apoptotic cascade (Gulbins 2003). It has been shown that ceramide levels in lipid rafts are decreased upon overexpression of palmitoyl-protein thioesterase 1 (Ppt1) in CHO cells. Ppt1 is a de-palmitolyting enzyme and is present in lysosomes. Interestingly, in *Cln3*^{ki} lysosomes Ppt1 protein levels were most strongly increased by 2.4-fold, accompanied by a 25 % up-regulation on mRNA expression levels (Figure 3, Figure 6 B). The increase in Ppt1 protein and mRNA levels in *Cln3*^{ki} cerebellar cells may indicate towards compensatory effects to control apoptotic signalling pathways.

Since several lysosomal hydrolases, such as cathepsins and enzymes involved in glycan and sphingolipid degradation were decreased in *Cln3*^{ki} lysosomes (Figure 3), the subsequent lysosomal dysfunction is thought to be sensed by the lysosomal nutrient sensing (LYNUS) machinery (Settembre *et al.* 2013). This machinery responds to the lysosomal amino acid content and transfers the signal both to cytoplasm and nucleus.

Recently it was found that most lysosomal genes present a coordinated transcriptional behaviour, which is regulated by the transcription factor EB (TFEB). By binding to the 'Coordinated Lysosomal Expression And Regulation' (CLEAR) target site in the promoter region of various lysosomal genes, TFEB induces their expression. Under normal physiological conditions, TFEB is retained in an inactivated and phosphorylated state in the cytosol, whereas under stress conditions, such as nutrient deprivation or aberrant lysosomal storage conditions, TFEB is dephosphorylated and activated and translocates to the nucleus, inducing its own transcription. Up-regulation of TFEB induces an increase in size and number of lysosomes and up-regulation of lysosomal genes, resulting in increased activities of these enzymes (Sardiello *et al.* 2009). Several genes, including *cathepsin D, B* and *Z, palmitoyl-protein thioesterase 1, prosaposin, α-hexosaminidase, acid ceramidase, galactocerebrosidase, Lamp1, Lamp2, Lyaat1* and *Mpr300* contain the CLEAR target site in their promotor region. Whether the transcriptional regulation of lysosomal and non-lysosomal genes in cells lacking functional Cln3 proteins is mediated by TFEB or by an alternative pathway is unknown and requires further evaluation.

Lysosomal membrane proteins play an essential role in various cellular processes, such as lysosomal acidification, transport of lysosomal hydrolases, metabolites and ions, autophagy, cell death, membrane fusion and maintaining membrane integrity (Schwake *et al.* 2013). SILAC-based proteomic analysis revealed that protein levels of the subunits d and subunit s of the V-type ATPase were 1.6-fold increased in $Cln3^{ki}$ lysosomes (Figure 7). The V-type ATPase consists of multiple subunits, which are distributed in two sectors called V_0 and V_1 complex, and is responsible for lysosomal acidification by using the energy of ATP hydrolysis to pump protons across the lysosomal membrane (Figure 30).

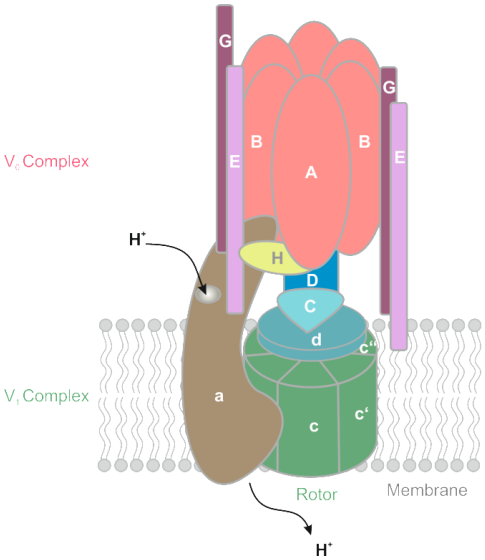

Figure 30: Structure of the V-type proton ATPase
The soluble V_1 complex consists of the ATP-hydrolysing subunits A and B (red). The integral membrane V_0 complex consists of subunits a, c, and d. Subunit c and its isoforms c' and c'' form the proton binding rotor (green) that is embedded in the membrane and carries protons from the cytosolic to the luminal side of the membrane. Subunit a (brown) presents the proton channel across the membrane. Subunit D of the V_1 complex and subunit d of the V_0 complex compose the central stalk (blue), connecting the rotor to the ATPase domain. The G (purple) and E (light purple) subunits compose the peripheral stalks (adapted from Marshansky et al. 2014).

Subunit d (in blue, Figure 30) mediates the coupling between cytosolic and membrane domains (Marshansky *et al.* 2014), while subunit s represents an ATPase accessory protein that may facilitate the assembly of the complex or regulate ATPase activity (Supek *et al.* 1994). The amounts of ATPase subunit a (brown), subunit D (blue), subunit C (blue), subunit E (light purple), subunit H (yellow), subunit A (red), subunit B (red) and subunit G (purple) were only slightly decreased by 8 to 25 %.

The catalytic activity of the ATPase drives intraluminal accumulation of protons, generating a transmembrane voltage difference. If left uncompensated, the activity of the ATPase is restricted and limits the pH gradient. Therefore, counter-ions must move to dissipate voltage and to facilitate proton transport. This is achieved by either the influx of cytosolic anions into lysosomes, or the efflux of luminal cations (Mindell 2012). The chloride channel 7 (Clc7) is expressed in endosomes and lysosomes (Kornak *et al.* 2001) and functions as a Cl^-/H^+ exchanger, which is involved in the process of net pumping. Electrogenic Cl^-/H^+ exchange together with transporter-mediated efflux of cations, efficiently support proton pumping and vesicular acidification (Novarino *et al.* 2010; Weinert *et al.* 2010). Clc7 is highly voltage-dependent and mediates ion transport only at positive cytoplasmic potentials (Stauber and Jentsch 2013). Interestingly, the protein amount of Clc7 was increased by 1.4-fold in *Cln3*^{ki} lysosomes. The increase in both, subunit s and d of the ATPase and Clc7, may suggest alterations in lysosomal pH homeostasis. In fact, the *Δbtn*-yeast CLN3 model and patient fibroblasts have been described to display defects in lysosomal acidification, estimated by spectrofluorometric

assays (Pearce and Sherman 1998; Holopainen *et al.* 2001; Gachet *et al.* 2005). Ratiometric lysosomal pH measurements, however, revealed that at steady-state the lysosomal pH in *Cln3*^{ki} cerebellar cells (4.49 ± 0.10) was comparable to wild-type (4.54 ± 0.09) cells (Figure 8). Thus, dysregulated expression of V-type ATPase subunits, as well as Clc7 has no impact on pH homeostasis in *Cln3*^{ki} cerebellar cells. In addition to the role in ion homeostasis, recent studies reported a pH-independent function of the ATPase V_0 subunit in membrane fusion during synaptic vesicle exocytosis and phagocytosis (Hiesinger *et al.* 2005; Peri and Nusslein-Volhard 2008; Strasser *et al.* 2011), whose impact in Cln3-deficient cells remains to be determined.

Lysosomal proteolysis of polypeptides contributes to normal protein turnover and the elimination of damaged or misfolded proteins. The resulting hydrolysis products, amino acids and dipeptides, are eventually exported into the cytosol by specific transporters. Lyaat1 is a lysosomal amino acid transporter and mediates the symport of protons and small neutral amino acids, such as glycine, alanine, and proline (Sagne *et al.* 2001). The transport activity is pH-dependent and protons are supplied by the lysosomal V-type ATPase. As revealed by proteomic analysis, Lyaat1 protein concentration was 1.9-fold increased in *Cln3*^{ki} lysosomal fractions (Figure 7), which was additionally confirmed by western blot analysis of whole cell extracts (Figure 9). Preliminary data of our group suggests an involvement of CLN3 protein in lysosomal export of neutral amino acids, which may explain a compensatory increase of Lyaat1 levels in *Cln3*^{ki} lysosomes.

Lysosomal membrane proteins are usually highly glycosylated, forming a glycosylated layer at the luminal side of lysosomes. This layer may be important for the stability and integrity of the lysosomal membrane. Here, proteomic analysis revealed that Lamp1 and Lamp2 protein levels were decreased in *Cln3*^{ki} lysosomes by 32 and 40 %, respectively, while Limp2 concentration remained unchanged (Figure 7). Although reduced levels of *Lamp1* mRNA were measured in *Cln3*^{ki} cells, elevated protein levels were observed both by western blotting and immunofluorescence microscopy (Figure 10 A and B). Lysosomes of *Cln3*^{ki} cerebellar cells displayed stronger fluorescence intensity and were increased in size and number. This discrepancy can only be explained by a prolonged half-life of the protein due to reduced lysosomal degradation. Moreover, it cannot be excluded that transcriptional down-regulation of

Lamp1, *Lamp2* and *Limp2* transcripts may present a regulatory feedback mechanism triggered by increased size and number of lysosomes and prolonged half-life of the proteins.

However, the identification of membrane proteins by peptide mass fingerprinting (PMF) might be misleading. The PMF method is used to identify proteins based on the specificity of a mass spectrum of the peptide mixture. The method is dependent on the number of peptides that have been generated and detected for a given protein. Identification of some membrane proteins by PMF can be limited by the lack of hydrophilic domains that are accessible to trypsin cleavage. In addition, the presence of detergents may decrease the efficiency of peptide recovery from the analytic column (Bensalem *et al.* 2007). These limitations may only affect certain membrane proteins, depending on their structure and topology. For the proteins Lamp1, Lamp2 and Limp2 the database protein sequence was covered by 3 to 4 matching peptides, yielding to a sequence coverage of only 13, 9 and 10 %, respectively. These cases show the difficulty that can arise in the detection of membrane proteins by mass spectrometry and may contribute to the contradictory results that have been obtained by SILAC-based proteomic analysis of isolated lysosomes, western blotting of total cerebellar cell extracts or immunofluorescence microscopy.

5.2 Disturbed endocytic pathways in *Cln3*^{ki} cerebellar cells

Besides lysosomal soluble and membrane proteins, SILAC-based quantitative proteomics also revealed dysregulation of three cargo receptors, Mpr300, Lrp1 and Lrp2, in *Cln3*^{ki} lysosomal fractions (Figure 11 A). Receptors of the endocytic pathway are usually not found in the lysosome, unless they are targeted there for degradation. However, endocytic receptors localise to endosomal compartments, which may be co-purified during the procedure of lysosome isolation.

Internalisation assays of Mpr300 and Lrp1-specific ligands revealed impaired endocytic mechanisms that can be correlated either to alterations in their expression levels, altered recycling kinetics, or both. For comparison, transferrin receptor (TfR)-mediated internalisation experiments, lipid-mediated uptake of cholera toxin, and fluid-phase endocytosis of dextran were included in these studies.

The main function of the Mpr300 is the delivery of newly synthesised lysosomal enzymes from the TGN to endosomes, from which the enzymes will reach their final destination, the lysosome. Mpr300-ligand complexes exit the TGN in clathrin-coated vesicles, subsequently fusing with endosomes. The low endosomal pH leads to dissociation of the complexes, allowing the Mpr300 to re-cycle back to the TGN (Braulke and Bonifacino 2009). In addition, 5 – 10 % of the total Mpr300 are localised at the plasma membrane (Braulke *et al.* 1987), being constitutively exchanged within the endosomal system. M6P-containing lysosomal enzymes that have been secreted, as well as non-glycosylated insulin-like growth factor II, can be re-internalised by the Mpr300 from the extracellular space (Hickman and Neufeld 1972).

The proteomic analysis revealed a 1.8-fold increase in Mpr300 protein levels, which was verified by western blot analysis (Figure 11 A and B). Interestingly, elevated Mpr300 protein levels could be correlated to increased mRNA expression (Figure 11 C). In cerebellar cells, the uptake of human recombinant M6P-containing arylsulfatase B (ASB) by the Mpr300 is specific and can be completely inhibited by excess of M6P. Corresponding to increased Mpr300 levels, endocytosis was 1.5-fold elevated in *Cln3*^{ki} compared to wild-type cerebellar cells (Figure 13 A and B). Due to a low basal expression of Mpr300, an increase of Mpr300 on the cell surface could not be evaluated by the available tools (Figure 13 C). On the other hand, elevated endocytosis of ASB in *Cln3*^{ki} cerebellar cells could be explained by alterations in the recycling routes of Mpr300 between early endosomes, recycling endosomes and the plasma membrane. This might affect the intracellular distribution of steady-state and transport kinetics of Mpr300. After endocytosis the initial delivery site of the ligand-loaded Mpr300 are early endosomes, followed by targeting to late endosomes and pH-dependent ligand dissociation. The prevailing opinion has been that internalised Mpr300 join the pool of receptors in the late endosomes that cycle between endosomes and the TGN (Braulke and Bonifacino 2009). Recycling of the Mpr300 to the plasma membrane can either occur directly and fast (‘fast recycling’) via early endosomes, or indirectly and slowly via the endosome recycling compartment (‘slow recycling’) (Maxfield and McGraw 2004). To evaluate whether recycling pathways of the Mpr300 in *Cln3*^{ki} cerebellar cells are altered, a detailed evaluation of the distribution of the Mpr300 by immunofluorescence microscopy and immunogold electron microscopy is needed. Metcalf *et al*. proposed that the reduction of CLN3 protein upon CLN3 siRNA

treatment prevents Mpr300 exit from the TGN, resulting in reduced levels of Mpr300 both at the plasma membrane and the endocytic compartment, as well as in defective processing of cathepsin D and targeting of cathepsin B (Metcalf *et al.* 2008). However, in the present study that was performed on cerebellar cells, carrying the most common patient mutation (1 kb deletion), total Mpr300 and most likely receptor levels at the plasma membrane were increased, which resulted in an elevated uptake of the lysosomal enzyme ASB in an M6P-dependent manner. Interestingly, protein levels of cathepsin B, D and Z, α-hexosaminidase and α-*L*-1-fucosidase, which were quantified both by SILAC-based proteomics and western blotting, approximately correlated to the reduction in their mRNA expression levels (Figure 4 and 6). These observations imply that even reduced amounts of distinct newly synthesised lysosomal enzymes are correctly transported to lysosomes and processed. On the other hand, transcriptional regulation of lysosomal enzymes and their cargo receptor Mpr300 appears to be altered in *Cln3*^{ki} cerebellar cells. Nevertheless, a reduction in lysosomal enzyme concentration may suggest impairment in the proteolytic processing of internalised exogenous ligands. Quantification of the 68 kDa precursor, the 47 kDa intermediate and the 15 kDa mature ASB forms during different chase periods revealed similar kinetics of processing and degradation of ASB in both genotypes (Figure 14 B). Thus, the reduced levels of lysosomal enzymes in *Cln3*^{ki} cerebellar cells are sufficient for proper proteolytic activation processes of lysosomal enzymes such as ASB or cathepsins, and presumably for degradation of proteins in general.

In addition to Mpr300, the low density lipoprotein related receptors 1 and 2 (Lrp1 and Lrp2) are dysregulated in *Cln3*^{ki} cerebellar cells. Lrp1 and Lrp2 belong to the LDL receptor family, which are involved in the regulation of cholesterol homeostasis, receptor-mediated endocytosis of various ligands and cellular signaling (Herz and Bock 2002). Furthermore, Lrp1 mediates the cellular uptake of pro-cathepsin D and pro-saposin (Hiesberger *et al.* 1998; Derocq *et al.* 2012), but recent studies showed that Lrp1 represents an alternative receptor for M6P-independent targeting of lysosomal enzymes via secretion-recapture mechanisms (Markmann *et al*. 2015). Lrp1 is abundantly expressed in neurons, mainly of the entorhinas cortex, hippocampus, cerebellum, and also in astrocytes and microglia (Marzolo *et al.* 2000; Andersen and Willnow 2006). The biological importance of Lrp1 is highlighted by the lethal

embryonic phenotype of Lrp1 knockout mice. Mice lacking Lrp1 only in neurons display a phenotype including severe mobility disorder, hyperactivity and premature death (May *et al.* 2004). The fundamental role of Lrp1 is the uptake and transport of cholesterol, which is an essential component of the neuronal membrane, and its active transport to neurons is needed to support synaptogenesis and maintenance of synaptic function (Mauch *et al.* 2001; Pfrieger 2003). In comparison to cholesterol, the targeting of lysosomal enzymes by Lrp1 does not contribute to the Lrp1 knockout phenotype, since Mpr300 and LDL receptor can compensate the loss of Lrp1 in lysosomal enzyme transport, at least in fibroblasts (Markmann *et al*. 2015).

Cln3^{ki} cerebellar cells present approximately 70 % reduction in Lrp1 levels as revealed by SILAC-based proteomic analysis, western blotting and qRT PCR (Figure 11 A, B and D). In line with these findings, the capability of these cells to internalise the Lrp1-specific ligand α_2-MG was reduced by 43 % (Figure 15). Within 3 h of chase time 50 % of the endocytosed material was degraded, and similar to ASB endocytosis assays, the kinetics of lysosomal degradation was comparable in both genotypes.

The importance of Lrp2 (also called megalin) in the central nervous system was discovered through developmental studies. Lrp2 deficiency leads to abnormal development of the forebrain, absence of the olfactory apparatus and cranio-facial malformations (Assemat *et al.* 2005). In a healthy brain, Lrp2 is expressed in retinal ganglion cells and neurons of the cerebral cortex, hippocampus, striatum, thalamus, olfactory bulb and cerebellum (Alvira-Botero *et al.* 2010), and also in astrocytes (Bento-Abreu *et al.* 2008). In *Cln3*^{ki} cerebellar cells Lrp2 protein concentration were 10-fold increased, accompanied by a 31-fold up-regulation of *Lrp2* mRNA expression (Figure 11 A, C and D). The strong up-regulation of Lrp2 may be due to its neuro-protective role upon neuronal damage or degenerative processes. In Alzheimer's disease patients Lrp2 was observed to be enriched in TUNEL-positive apoptotic neurons (LaFerla *et al.* 1997). Moreover, in cerebellar granular cells, Lrp2 acts as a receptor for the neuroprotective factor metallothioein (Ambjorn *et al.* 2008). The authors suggest that increased levels of metallothioein following brain injury triggers up-regulation of Lrp2, possibly in combination with other yet unidentified stress factors, to initiate signal transduction pathways that promote neurite outgrowth and survival.

The transferrin receptor (TfR) was chosen as a control cargo receptor, as it internalises its ligands similarly to Mpr300 via clathrin-mediated endocytosis. However, TfR concentration was not altered in *Cln3*^{ki} cerebellar cells (Figure 16 B and C). Transferrin mediates the iron uptake into the cell via the TfR. Transferrin can bind two iron ions (Fe^{3+}) and is therefore termed di-ferric transferrin. The transferrin-TfR complex is initially delivered to early endosomes, where the two Fe^{3+} ions are liberated from transferrin (apo-transferrin) and transported into the cytoplasm by the divalent metal transporter 1 (Montalbetti *et al.* 2013). From early endosomes the apo-transferrin-TfR complexes return back to the plasma membrane, followed by release of apo-transferrin from the receptor at neutral extracellular pH. The transport to the plasma membrane occurs either directly via the fast recycling route or indirectly via the slow recycling route that includes transport to the endocytic recycling compartment (Maxfield and McGraw 2004; Mayle *et al.* 2012). In *Cln3*^{ki} cerebellar cells the amount of endocytosed transferrin was increased compared to wild-type cells, as revealed by confocal microscopy (Figure 16 A), which was also observed in fibroblasts of CLN3 patients (Luiro *et al.* 2004). These findings suggest that the sorting and recycling kinetics of various endocytic cargo receptors in the endosomal compartment, and the subsequent delivery of their ligands is dysregulated in cells lacking functional CLN3 protein. The molecular mechanisms and players of the vesicular transport machinery that cause changes in distribution and transport kinetics of various cargo receptors in *Cln3*^{ki} cerebellar cells are still unknown. However, it is most likely that more TfR recycle to the plasma membrane via the fast recycling pathway, which is believed to be regulated by the GTPases Rab35 and Arf6 (Klein *et al.* 2006; Kouranti *et al.* 2006; Montagnac *et al.* 2011). Furthermore, loss of the Rab11 effector protein Rab11FIP5 has been shown to lead to increased recycling of the TfR via the fast recycling route from early endosomes directly to the plasma membrane (Schonteich *et al.* 2008). This shift towards the fast re-cycling pathway that involves direct transport of TfR from early endosomes to the plasma membrane may explain increased recycling kinetics and therefore elevated uptake of transferrin in cells lacking functional Cln3 protein. However, the underlying mechanisms of increased recycling kinetics need to be assessed.

Alternatively, defective lysosomal degradation of lipids may affect the composition of endosomal membranes, impairing fluidity and consequently fusion and fission events

required for transport of integral cargo receptors. In addition, alterations in plasma membrane composition, and consequently membrane fluidity, have also an impact on the process of fluid-phase endocytosis, indicated by an increased uptake of dextran in *Cln3*^{ki} in respect to wild-type cerebellar cells (Figure 19). Moreover, GM1 ganglioside-dependent binding and internalisation of cholera toxin was increased in *Cln3*^{ki} cerebellar cells compared to wild-type cells (Figure 17 and 18), suggesting elevated levels of GM1 gangliosides in these cells. In fact, it has been previously described that lymphoblasts from CLN3 patients display an abnormal expression pattern of the gangliosides GM1, GM2 and GM3 (Kang *et al.* 2014).

5.3 Immune phenotype of *Cln3*^{ki} mice

The function of lysosomes and lysosome-related organelles is associated with a variety of essential cellular pathways, including clearance of substrates, autophagy, exocytosis, membrane repair, cell signalling and apoptosis. In particular, as the primary degradative compartment of the cell, these organelles are crucial for the proper function of the immune system. Their catabolic role in immunological processes, such as removal of pathogens by phagocytosis, cytokine secretion and antigen processing and presentation has been widely studied (Colbert *et al.* 2009). CLN3 disease, which predominantly displays profound neurological impairment, has also been associated with alterations in the immune system. Several studies mainly focused on neuroimmune responses, such as microglia activation and infiltration of T-lymphocytes into the brain, preceding or in response to neurodegeneration (Castaneda *et al.* 2008). However, no reports have been published whether alterations in systemic responses affect or accompany CLN3 pathology.

The last part of the present study focused on the role of the immune system in CLN3 disease. The relationship between lymphocytic storage or dysregulation in the lysosomal compartment and the modulation of the immune system has been investigated in the *Cln3*^{ki} mouse model, using both biochemical *in vitro* and functional *in vivo* assays.

5.3.1 Immune cell composition in *Cln3*^{ki} mice

Several lysosomal storage disorders have been shown to display alterations in the immune system, contributing to disease pathology. For instance, Niemann-Pick type C1 (NPC1) patients were observed to suffer from recurrent and severe respiratory infections that resulted in premature death (Morisot *et al.* 2005). NPC1 disease is typically a neurodegenerative disorder and characterised by intracellular accumulation of cholesterol and glycosphingolipids (Cruz *et al.* 2000). Whether the patients were immunocompromised due to mutations in the *NPC1* gene or due to secondary pathological effects such as lipid storage is not clear. NPC1-deficient mice lack a certain subtype of natural killer T cells, specialised in recognising glycosphingolipids of gram-negative bacteria (Kinjo *et al.* 2005), and exhibited a reduced capability to clear bacterial infections *in vivo* (Sagiv *et al.* 2006). It remains to be elucidated whether NPC1 patients also present natural killer T cell dysfunction, possibly explaining their predisposition towards immune suppression.

An additional example of a lysosomal storage disorder presenting an immunosuppressive phenotype is mucolipidosis type II (MLII). The loss of phosphotransferase activity in MLII disease prevents the formation of M6P-recognition marker, consequently leading to missorting and hyper-secretion of various lysosomal enzymes (Braulke *et al.* 2013). In MLII patients low levels of memory B cells and a poor antibody response to vaccination were observed, which was recently confirmed in an MLII mouse model. Strongly decreased levels of lysosomal proteases in MLII B cells resulted in impaired antigen processing and presentation, accompanied by reduced B cell maturation in response to antigen exposure, and consequently decreased immunoglobulin production and defective immunoglobulin class switch (Otomo *et al*. 2015, in press).

Clinically it has not been observed that CLN3 patients are predisposed towards immune suppression. This is primarily in agreement with data from the present study. Under steady-state conditions, no differences between wild-type and *Cln3*^{ki} mice of 2.5 and 7.5 months of age were observed in the relative frequency of B cells, $CD4^+$ and $CD8^+$ T cells, granulocytes, monocytes and dendritic cells (Figure 21). In addition, no alterations in the maturation and activation status of B cells and dendritic cells were observed (data not shown).

5.3.2 Accumulation of storage material in immune cells of *Cln3*^{ki} mice

CLN3 pathology is characterised by the widespread lysosomal accumulation of storage material in neuronal and extra-neuronal tissues (Anderson *et al.* 2013). In addition, vacuolated lymphocytes have been observed in peripheral blood of CLN3 patients, a feature that is unique for CLN3 disease and is still routinely used to diagnose the disease (Schulz *et al.* 2013). Moreover, by electron microscopic characterisation, disease-specific lysosomal inclusions were identified in T lymphocytes and monocytes of peripheral blood from CLN3 patients (Anderson *et al.* 2013). In the *Cln3*^{ki} mouse model, harbouring the most common genetic defect of CLN3 patients (1 kb deletion), abnormal vacuolation in 5 – 15 % of the peripheral lymphocytes were also observed (Staropoli *et al.* 2012). So far, ultrastructural and biochemical analyses of the storage material in immune cells from the *Cln3*^{ki} mouse model have not been performed.

In the present study, storage material-containing immune cells were ultra-structurally characterised for the first time. Heterogeneous electron-dense and electron-lucent material was detected in lysosomes of splenic T cells from 2.5 months old *Cln3*^{ki} mice (Figure 22 A). These findings may suggest the presence of heterogeneous storage material. Subunit c of the mitochondrial ATP synthase has been described to predominantly accumulate in CLN3 disease and to constitute approximately 50 % of the storage material (Palmer *et al.* 1989). Surprisingly, neither in *Cln3*^{ki} B cells nor in peritoneal macrophages accumulating storage material was observed. However, increase in the amount of lysosomal membrane protein Lamp1 (Figure 22 B), the size of lysosomes and the predominant accumulating material subunit c of the mitochondrial ATP synthase (Figure 22 C, Figure 23 B and C) are indicators of lysosomal dysfunction and first biochemical signs of lysosomal storage. It cannot be excluded that B cells and/or macrophages, displaying an advanced stage of lysosomal dysfunction and accumulating storage material, will be eliminated immediately without significantly affecting the total number of these cells.

5.3.3 Proteolytic capacity of *Cln3*^{ki} macrophages

The immune system is composed of a variety of cells and molecules that together generate a coordinated immune response upon exposure to a foreign antigen. Within the immune response endo-lysosomal cathepsins play a key role, including processes such

as antigen processing and presentation, cytokine regulation, induction of apoptosis and TLR signalling (Colbert *et al.* 2009). Antigen presenting cells, such as B cells, dendritic cells and macrophages, internalise extracellular antigens that are subsequently cleaved by cathepsins in the MHCII compartment. Correct peptide binding by MHCII complexes involves the proteolytic activities of cathepsin L and S to remove the invariant chain chaperone (CD74), which is inserted into the peptide binding site of the MHCII complex to prevent antigen binding outside the endo-lysosomal system (Bird *et al.* 2009).

Expression of cathepsin S in cultured *Cln3*^{ki} peritoneal macrophages was increased in respect to wild-type cells, and strikingly also levels of the invariant chain, the substrate of cathepsin S, were elevated (Figure 24). Possibly, increased levels of the invariant chain may correspond to elevated MHCII levels. It has been previously shown that certain cytokines are able to regulate cathepsin expression and activity (Fiebiger *et al.* 2001). For instance, IFNγ stimulation of keratinocytes and monocytes resulted in a selective up-regulation of mRNA and protein levels of cathepsin S, leading to increased cathepsin S activity in those cells. In parallel, elevated expression of MHCII molecules were observed in response to IFNγ stimulation (Schwarz *et al.* 2002). Whether IFNγ production is increased *Cln3*^{ki} macrophages requires further characterisation.

While cathepsin S levels were increased, cathepsin B, D and Z levels were significantly decreased in *Cln3*^{ki} macrophages compared to wild-type cells (Figure 25 A). Whether this decrease in cathepsin B, D and Z protein levels is caused by transcriptional down-regulation, as it was shown for *Cln3*^{ki} cerebellar cells, requires further evaluation.

A specific adaptive immune response is dependent on the appropriate formation of peptides derived from foreign antigens. At present it is not known to which extent the reduction of a single or multiple proteases may significantly impair the antigen or invariant chain processing within the MHCII compartment of antigen-presenting cells. Pulse-chase experiments of DQ-BSA revealed that the proteolytic capacity of *Cln3*^{ki} macrophages was significantly reduced by 45 % in respect to wild-type cells (Figure 25 C). This may have an impact on their capacity to clear bacteria over time during an infection. When wild-type and *Cln3*^{ki} mice were infected with *L. monocytogenes*, they rapidly disseminate to the liver and spleen, where they are internalised by hepatic and splenic macrophages (Pamer 2004; Shi and Pamer 2011). Three days post infection

similar bacterial burdens in spleen and liver of both genotypes were observed (Figure 26). Thus, reduced proteolytic capacity of *Cln3*^{ki} macrophages does not impair control and clearance of listeria three days after infection. This might be explained by the distinct phagocytic pathway of listeria, which quickly escape from the phagocytic vacuole and translocate to the cytoplasm. For comparison, wild-type and *Cln3*^{ki} mice have to be infected with bacteria, such as *M. tuberculosis* or *Salmonella*, which reside in the phagosome during the infection (Rosenberger and Finlay 2003). Reduced proteolytic capacity of *Cln3*^{ki} macrophages may support those bacteria in exerting their survival mechanisms in the phagosome to establish and maintain infection.

5.3.4 T cell response in *Cln3*^{ki} mice

Ultra-structural and biochemical analysis revealed the presence of storage material in T cells of *Cln3*^{ki} mice (Figure 22). So far, it has not been examined whether the accumulation of storage material impairs T cell function or their proliferation and maturation process. As shown here, neither the number nor the proportional tissue distribution of naïve, memory and effector T cells are affected by storage material in *Cln3*^{ki} mice (Figure 27 A).

When bone marrow T cells were stimulated with PMA/ionomycin, the frequencies of IFNγ^+ and TNFα^+ CD4 and CD8 T cells were increased in *Cln3*^{ki} in respect to wild-type mice. However, the cytokine response in splenic T cells was comparable in both genotypes (Figure 28 A and B). In conclusion, *Cln3*^{ki} T cells residing in the bone marrow presented a phenotype, which was hyper-responsive upon stimulation. Presumably, *Cln3*^{ki} mice contain a higher proportion of antigen-specific CD4$^+$ and CD8$^+$ T cells that relocated to the bone marrow after having encountered their antigen in the periphery (Price and Cerny 1999; Di Rosa and Santoni 2002). However, it remains to be investigated whether these T cells display a memory phenotype. When mice were infected with *L. monocytogenes* (*Lm*OVA) and splenic T cells were re-stimulated *in-vitro* with listeria-specific peptides, an elevated cytokine response was observed in *Cln3*^{ki} compared to wild-type mice, further suggesting that a minor pool of pre-primed T cells exist in a hyper-reactive state. At present it is not known to which extent a hyper-responsive T cell phenotype may contribute to disease pathology.

6 Summary

The neurodegenerative lysosomal storage disorder CLN3 is caused by mutations in the *CLN3* gene, encoding a lysosomal transmembrane protein of unknown function. The absence of non-functional CLN3 protein results in lysosomal dysfunction and accumulation of lysosomal storage material in neuronal and non-neuronal tissues. However, the underlying pathomechanisms remain poorly understood.

In the present study it was analysed whether absence of functional Cln3 protein and lysosomal dysfunction is manifested in an altered lysosomal protein composition in *Cln3*^{ki} cerebellar cells. Furthermore, the relationship between dysregulation of the lysosomal compartment, including accumulation of storage material, and the modulation of the immune system was investigated in the *Cln3*^{ki} mouse model.

- SILAC-based proteomic analysis of isolated lysosomes revealed that 29 soluble and eight lysosomal membrane proteins, as well as three cargo receptors of the endocytic pathway were differentially expressed in *Cln3*^{ki} compared to wild-type cerebellar cells.
- Protein concentrations of several enzymes involved in glycan and sphingolipid degradation, as well as in proteolytic processing of proteases, were predominantly decreased *Cln3*^{ki} lysosomes. In addition, reduced transcript levels of the respective genes indicated towards an altered transcriptional regulation in the absence of functional Cln3 protein.
- Internalisation assays of Mpr300 and Lrp1-specific ligands revealed that the sorting and recycling kinetics of various endocytic cargo receptors in the endosomal compartment, and the subsequent delivery of their ligands is dysregulated in cells lacking functional Cln3 protein.

- Storage material-containing immune cells were ultra-structurally and biochemically characterised. Although the presence of storage material in T lymphocytes could not be directly correlated to impaired function, *Cln3*^{ki} macrophages displayed a reduced proteolytic capacity that is, however, sufficient to control and clear listeria *in vivo*. Furthermore, only a minor pool of *Cln3*^{ki} T cells presented a phenotype that was hyper-responsive for cytokine production upon stimulation.

In conclusion, the data show that the deficiency of the lysosomal membrane protein Cln3 impairs the biogenesis and composition of lysosomes in a cell type-dependent manner and, moreover, affects processes of internalisation and recycling of cargo receptors and their ligands, as well as T cell and macrophage-dependent immune functions.

7 Zusammenfassung

Die lysosomale Speichererkrankung CLN3 ist eine der häufigsten neurodegenerativen Erkrankungen im Kindesalter und wird durch Mutationen im *CLN3* Gen ausgelöst, das ein lysosomales Transmembranprotein mit unbekannter Funktion kodiert. Defektes CLN3 Protein führt zur Störung der lysosomalen Homöostase und zu Anreicherung von Speichermaterial in Lysosomen neuronaler als auch nicht-neuronaler Gewebe. Die der Erkrankung zu Grunde liegenden Pathomechanismen werden nur unzureichend verstanden.

In der vorliegenden Studie wurde untersucht, ob der Verlust von funktionalem Cln3 Protein in $Cln3^{ki}$ cerebellaren Zellen Auswirkungen auf die lysosomale Proteinzusammensetzung hat. Des Weiteren wurde mit Hilfe des $Cln3^{ki}$ Mausmodell analysiert, ob sich Einschränkungen der lysosomalen Funktion, sowie die Anreicherung von Speichermaterial, auf zelluläre Prozesse in Immunzellen auswirken und somit möglicherweise Funktionen des Immunsystems beeinträchtigen.

- Mit Hilfe von SILAC-basierten Proteomanalysen isolierter Lysosomen wurde die Dysregulation von 29 löslichen und acht lysosomalen Membranproteinen, sowie von drei endozytotischen Cargo-Rezeptoren in $Cln3^{ki}$ cerebellaren Zellen festgestellt.
- Die Proteinkonzentrationen mehrerer Enzyme, die am Glykan- und Sphingolipidabbau, als auch an proteolytischer Prozessierung von Proteasen beteiligt sind, waren in Lysosomen von $Cln3^{ki}$ cerebellaren Zellen überwiegend erniedrigt. Da auch die Transkriptionsrate der jeweiligen Gene reduziert war, ließ dies auf eine Cln3-abhängige veränderte Regulation der Transkription lysosomaler Gene schließen.
- Internalisierungsexperimente von Mpr300- und Lrp1-spezifischen Liganden weisen auf Veränderungen in der Sortierung und Recycling Kinetik verschiedener endozytotischer Rezeptoren und des anschließenden Ligandentransport im endosomalen Kompartiment Cln3-defizienter Zellen hin.

- Speichermaterial anreichernde Immunzellen wurden ultrastrukturell und biochemisch untersucht. Das in *Cln3*^{ki} T-Lymphozyten enthaltene Speichermaterial hatte keine direkten Auswirkungen auf deren Funktion, während *Cln3*^{ki} Makrophagen eine verminderte Fähigkeit in proteolytischer Prozessierung zeigten. Dies hatte jedoch keine Auswirkungen auf die Kontrolle und Klärung einer Listerieninfektion *in vivo*. Des Weiteren konnte festgestellt werden, dass bei Stimulation von Lymphozyten nur ein kleiner Anteil der *Cln3*^{ki} T-Zellen mit einer stärkeren Zytokinproduktion reagierte.

Zusammenfassend zeigen die Daten, dass eine Defizienz des lysosomalen Membranproteins Cln3 Auswirkungen auf die Biogenese und Zusammensetzung des Lysosoms hat und Internalisierung und Recycling von Cargo-Rezeptoren und deren Liganden, sowie T-Zellen- und Makrophagen-spezifische Funktionen beeinträchtigt.

8 Literature

(1995). "Isolation of a novel gene underlying Batten disease, CLN3. The International Batten Disease Consortium." Cell 82(6): 949-957.

Alvira-Botero, X., R. Perez-Gonzalez, C. Spuch, T. Vargas, D. Antequera, M. Garzon, F. Bermejo-Pareja and E. Carro (2010). "Megalin interacts with APP and the intracellular adapter protein FE65 in neurons." Mol Cell Neurosci 45(3): 306-315.

Ambjorn, M., J. W. Asmussen, M. Lindstam, K. Gotfryd, C. Jacobsen, V. V. Kiselyov, S. K. Moestrup, M. Penkowa, E. Bock and V. Berezin (2008). "Metallothionein and a peptide modeled after metallothionein, EmtinB, induce neuronal differentiation and survival through binding to receptors of the low-density lipoprotein receptor family." J Neurochem 104(1): 21-37.

Andersen, O. M. and T. E. Willnow (2006). "Lipoprotein receptors in Alzheimer's disease." Trends Neurosci 29(12): 687-694.

Anderson, G. W., H. H. Goebel and A. Simonati (2013). "Human pathology in NCL." Biochim Biophys Acta 1832(11): 1807-1826.

Ashcom, J. D., S. E. Tiller, K. Dickerson, J. L. Cravens, W. S. Argraves and D. K. Strickland (1990). "The human alpha 2-macroglobulin receptor: identification of a 420-kD cell surface glycoprotein specific for the activated conformation of alpha 2-macroglobulin." J Cell Biol 110(4): 1041-1048.

Assemat, E., F. Chatelet, J. Chandellier, F. Commo, O. Cases, P. Verroust and R. Kozyraki (2005). "Overlapping expression patterns of the multiligand endocytic receptors cubilin and megalin in the CNS, sensory organs and developing epithelia of the rodent embryo." Gene Expr Patterns 6(1): 69-78.

Ballabio, A. and V. Gieselmann (2009). "Lysosomal disorders: from storage to cellular damage." Biochim Biophys Acta 1793(4): 684-696.

Bensalem, N., S. Masscheleyn, J. Mozo, B. Vallee, F. Brouillard, S. Trudel, D. Ricquier, A. Edelman, I. C. Guerrera and B. Miroux (2007). "High sensitivity identification of membrane proteins by MALDI TOF-MASS spectrometry using polystyrene beads." Journal of Proteome Research 6(4): 1595-1602.

Bento-Abreu, A., A. Velasco, E. Polo-Hernandez, P. L. Perez-Reyes, A. Tabernero and J. M. Medina (2008). "Megalin is a receptor for albumin in astrocytes and is required for the synthesis of the neurotrophic factor oleic acid." J Neurochem 106(3): 1149-1159.

Bird, P. I., J. A. Trapani and J. A. Villadangos (2009). "Endolysosomal proteases and their inhibitors in immunity." Nat Rev Immunol 9(12): 871-882.

Braulke, T. and J. S. Bonifacino (2009). "Sorting of lysosomal proteins." Biochim Biophys Acta 1793(4): 605-614.

Braulke, T., C. Gartung, A. Hasilik and K. von Figura (1987). "Is movement of mannose 6-phosphate-specific receptor triggered by binding of lysosomal enzymes?" J Cell Biol 104(6): 1735-1742.

Braulke, T., A. Raas-Rothschild and R. Kornfeld (2013). I-Cell Disease and Pseudo-Hurler Polydystrophy: Disorders of Lysosomal Enzyme Phosphorylation and Localization. The Online Metabolic and Molecular Bases of Inherited Disease. B. M. Valle, A., Vogelstein, B., Kinzler, K., Antonarakis, S.,, A. Ballabio, Sciver, C., Sly, W. S., Childs, B., Bunz, F., Gibson, K. M. and and G. Mitchell.

Braun, M., A. Waheed and K. von Figura (1989). "Lysosomal acid phosphatase is transported to lysosomes via the cell surface." EMBO J 8(12): 3633-3640.

Cao, Y., J. A. Espinola, E. Fossale, A. C. Massey, A. M. Cuervo, M. E. MacDonald and S. L. Cotman (2006). "Autophagy is disrupted in a knock-in mouse model of juvenile neuronal ceroid lipofuscinosis." J Biol Chem 281(29): 20483-20493.

Castaneda, J. A., M. J. Lim, J. D. Cooper and D. A. Pearce (2008). "Immune system irregularities in lysosomal storage disorders." Acta Neuropathol 115(2): 159-174.

Chang, J. W., H. Choi, H. J. Kim, D. G. Jo, Y. J. Jeon, J. Y. Noh, W. J. Park and Y. K. Jung (2007). "Neuronal vulnerability of CLN3 deletion to calcium-induced cytotoxicity is mediated by calsenilin." Hum Mol Genet 16(3): 317-326.

Chang, M., J. D. Cooper, D. E. Sleat, S. H. Cheng, J. C. Dodge, M. A. Passini, P. Lobel and B. L. Davidson (2008). "Intraventricular enzyme replacement improves disease phenotypes in a mouse model of late infantile neuronal ceroid lipofuscinosis." Mol Ther 16(4): 649-656.

Chapel, A., S. Kieffer-Jaquinod, C. Sagne, Q. Verdon, C. Ivaldi, M. Mellal, J. Thirion, M. Jadot, C. Bruley, J. Garin, B. Gasnier and A. Journet (2013). "An extended proteome map of the lysosomal membrane reveals novel potential transporters." Mol Cell Proteomics 12(6): 1572-1588.

Codlin, S., R. L. Haines, J. J. Burden and S. E. Mole (2008). "Btn1 affects cytokinesis and cell-wall deposition by independent mechanisms, one of which is linked to dysregulation of vacuole pH." J Cell Sci 121(Pt 17): 2860-2870.

Colbert, J. D., S. P. Matthews, G. Miller and C. Watts (2009). "Diverse regulatory roles for lysosomal proteases in the immune response." Eur J Immunol 39(11): 2955-2965.

Cotman, S. L. and J. F. Staropoli (2012). "The juvenile Batten disease protein, CLN3, and its role in regulating anterograde and retrograde post-Golgi trafficking." Clin Lipidol 7(1): 79-91.

Cotman, S. L., V. Vrbanac, L. A. Lebel, R. L. Lee, K. A. Johnson, L. R. Donahue, A. M. Teed, K. Antonellis, R. T. Bronson, T. J. Lerner and M. E. MacDonald (2002). "Cln3(Deltaex7/8) knock-in mice with the common JNCL mutation exhibit progressive neurologic disease that begins before birth." Hum Mol Genet 11(22): 2709-2721.

Cruz, J. C., S. Sugii, C. Yu and T. Y. Chang (2000). "Role of Niemann-Pick type C1 protein in intracellular trafficking of low density lipoprotein-derived cholesterol." J Biol Chem 275(6): 4013-4021.

Dahms, N. M., P. Lobel and S. Kornfeld (1989). "Mannose 6-phosphate receptors and lysosomal enzyme targeting." J Biol Chem 264(21): 12115-12118.

De Duve, C., B. C. Pressman, R. Gianetto, R. Wattiaux and F. Appelmans (1955). "Tissue fractionation studies. 6. Intracellular distribution patterns of enzymes in rat-liver tissue." Biochem J 60(4): 604-617.

Derocq, D., C. Prebois, M. Beaujouin, V. Laurent-Matha, S. Pattingre, G. K. Smith and E. Liaudet-Coopman (2012). "Cathepsin D is partly endocytosed by the LRP1 receptor and inhibits LRP1-regulated intramembrane proteolysis." Oncogene 31(26): 3202-3212.

Di Rosa, F. and A. Santoni (2002). "Bone marrow CD8 T cells are in a different activation state than those in lymphoid periphery." Eur J Immunol 32(7): 1873-1880.

Donaldson, J. G., D. Finazzi and R. D. Klausner (1992). "Brefeldin A inhibits Golgi membrane-catalysed exchange of guanine nucleotide onto ARF protein." Nature 360(6402): 350-352.

Dong, J. M., E. M. Prence and G. G. Sahagian (1989). "Mechanism for selective secretion of a lysosomal protease by transformed mouse fibroblasts." J Biol Chem 264(13): 7377-7383.

Dong, J. M. and G. G. Sahagian (1990). "Basis for low affinity binding of a lysosomal cysteine protease to the cation-independent mannose 6-phosphate receptor." J Biol Chem 265(8): 4210-4217.

Eliason, S. L., C. S. Stein, Q. Mao, L. Tecedor, S. L. Ding, D. M. Gaines and B. L. Davidson (2007). "A knock-in reporter model of Batten disease." J Neurosci 27(37): 9826-9834.

Ezaki, J., L. S. Wolfe and E. Kominami (1996). "Specific delay in the degradation of mitochondrial ATP synthase subunit c in late infantile neuronal ceroid lipofuscinosis is derived from cellular proteolytic dysfunction rather than structural alteration of subunit c." J Neurochem 67(4): 1677-1687.

Ferreira, N. S., M. Goldschmidt-Arzi, H. Sabanay, J. Storch, T. Levade, M. G. Ribeiro, L. Addadi and A. H. Futerman (2014). "Accumulation of ordered ceramide-cholesterol domains in farber disease fibroblasts." JIMD Rep 12: 71-77.

Fiebiger, E., P. Meraner, E. Weber, I. F. Fang, G. Stingl, H. Ploegh and D. Maurer (2001). "Cytokines regulate proteolysis in major histocompatibility complex class II-dependent antigen presentation by dendritic cells." J Exp Med 193(8): 881-892.

Filippov, V., M. A. Song, K. Zhang, H. V. Vinters, S. Tung, W. M. Kirsch, J. Yang and P. J. Duerksen-Hughes (2012). "Increased ceramide in brains with Alzheimer's and other neurodegenerative diseases." J Alzheimers Dis 29(3): 537-547.

Finn, R., A. D. Kovacs and D. A. Pearce (2011). "Altered sensitivity of cerebellar granule cells to glutamate receptor overactivation in the Cln3(Deltaex7/8)-knock-in mouse model of juvenile neuronal ceroid lipofuscinosis." Neurochem Int 58(6): 648-655.

Forgac, M. (2007). "Vacuolar ATPases: rotary proton pumps in physiology and pathophysiology." Nat Rev Mol Cell Biol 8(11): 917-929.

Fossale, E., P. Wolf, J. A. Espinola, T. Lubicz-Nawrocka, A. M. Teed, H. Gao, D. Rigamonti, E. Cattaneo, M. E. MacDonald and S. L. Cotman (2004). "Membrane trafficking and mitochondrial abnormalities precede subunit c deposition in a cerebellar cell model of juvenile neuronal ceroid lipofuscinosis." BMC Neurosci 5: 57.

Foulds, K. E., L. A. Zenewicz, D. J. Shedlock, J. Jiang, A. E. Troy and H. Shen (2002). "Cutting Edge: CD4 and CD8 T Cells Are Intrinsically Different in Their Proliferative Responses." The Journal of Immunology 168(4): 1528-1532.

Fuller, M., P. J. Meikle and J. J. Hopwood (2006). "Epidemiology of lysosomal storage diseases: an overview."

Fürst, W. and K. Sandhoff (1992). "Activator proteins and topology of lysosomal sphingolipid catabolism." Biochim Biophys Acta 1126(1): 1-16.

Gachet, Y., S. Codlin, J. S. Hyams and S. E. Mole (2005). "btn1, the Schizosaccharomyces pombe homologue of the human Batten disease gene CLN3, regulates vacuole homeostasis." J Cell Sci 118(Pt 23): 5525-5536.

Getty, A. L., J. W. Benedict and D. A. Pearce (2011). "A novel interaction of CLN3 with nonmuscle myosin-IIB and defects in cell motility of Cln3(-/-) cells." Exp Cell Res 317(1): 51-69.

Ghosh, P., N. M. Dahms and S. Kornfeld (2003). "Mannose 6-phosphate receptors: new twists in the tale." Nat Rev Mol Cell Biol 4(3): 202-212.

Gieselmann, V., A. Hasilik and K. von Figura (1985). "Processing of human cathepsin D in lysosomes in vitro." J Biol Chem 260(5): 3215-3220.

Goodison, S., V. Urquidi and D. Tarin (1999). "CD44 cell adhesion molecules." Mol Pathol 52(4): 189-196.

Griffey, M. A., D. Wozniak, M. Wong, E. Bible, K. Johnson, S. M. Rothman, A. E. Wentz, J. D. Cooper and M. S. Sands (2006). "CNS-directed AAV2-mediated gene therapy ameliorates functional deficits in a murine model of infantile neuronal ceroid lipofuscinosis." Mol Ther 13(3): 538-547.

Gulbins, E. (2003). "Regulation of death receptor signaling and apoptosis by ceramide." Pharmacol Res 47(5): 393-399.

Herrmann, P., C. Druckrey-Fiskaaen, E. Kouznetsova, K. Heinitz, M. Bigl, S. L. Cotman and R. Schliebs (2008). "Developmental impairments of select neurotransmitter systems in brains of Cln3(Deltaex7/8) knock-in mice, an animal model of juvenile neuronal ceroid lipofuscinosis." J Neurosci Res 86(8): 1857-1870.

Herz, J. and H. H. Bock (2002). "Lipoprotein receptors in the nervous system." Annu Rev Biochem 71: 405-434.

Hickman, S. and E. F. Neufeld (1972). "A hypothesis for I-cell disease: defective hydrolases that do not enter lysosomes." Biochem Biophys Res Commun 49(4): 992-999.

Hiesberger, T., S. Huttler, A. Rohlmann, W. Schneider, K. Sandhoff and J. Herz (1998). "Cellular uptake of saposin (SAP) precursor and lysosomal delivery by the low density lipoprotein receptor-related protein (LRP)." EMBO J 17(16): 4617-4625.

Hiesinger, P. R., A. Fayyazuddin, S. Q. Mehta, T. Rosenmund, K. L. Schulze, R. G. Zhai, P. Verstreken, Y. Cao, Y. Zhou, J. Kunz and H. J. Bellen (2005). "The v-ATPase V0 subunit a1 is required for a late step in synaptic vesicle exocytosis in Drosophila." Cell 121(4): 607-620.

Holopainen, J. M., J. Saarikoski, P. K. Kinnunen and I. Jarvela (2001). "Elevated lysosomal pH in neuronal ceroid lipofuscinoses (NCLs)." Eur J Biochem 268(22): 5851-5856.

Honey, K. and A. Y. Rudensky (2003). "Lysosomal cysteine proteases regulate antigen presentation." Nat Rev Immunol 3(6): 472-482.

Kang, S., T. H. Heo and S. J. Kim (2014). "Altered levels of alpha-synuclein and sphingolipids in Batten disease lymphoblast cells." Gene 539(2): 181-185.

Katz, M. L., J. R. Coates, C. M. Sibigtroth, J. D. Taylor, M. Carpentier, W. M. Young, F. A. Wininger, D. Kennedy, B. R. Vuillemenot and C. A. O'Neill (2014). "Enzyme replacement therapy attenuates disease progression in a canine model of late-infantile neuronal ceroid lipofuscinosis (CLN2 disease)." J Neurosci Res 92(11): 1591-1598.

Katz, M. L., H. Shibuya, P. C. Liu, S. Kaur, C. L. Gao and G. S. Johnson (1999). "A mouse gene knockout model for juvenile ceroid-lipofuscinosis (Batten disease)." J Neurosci Res 57(4): 551-556.

Kim, Y., D. Ramirez-Montealegre and D. A. Pearce (2003). "A role in vacuolar arginine transport for yeast Btn1p and for human CLN3, the protein defective in Batten disease." Proc Natl Acad Sci U S A 100(26): 15458-15462.

Kinjo, Y., D. Wu, G. Kim, G. W. Xing, M. A. Poles, D. D. Ho, M. Tsuji, K. Kawahara, C. H. Wong and M. Kronenberg (2005). "Recognition of bacterial glycosphingolipids by natural killer T cells." Nature 434(7032): 520-525.

Kishimoto, Y., M. Hiraiwa and J. S. O'Brien (1992). "Saposins: structure, function, distribution, and molecular genetics." J Lipid Res 33(9): 1255-1267.

Kitzmüller, C., R. L. Haines, S. Codlin, D. F. Cutler and S. E. Mole (2008). "A function retained by the common mutant CLN3 protein is responsible for the late onset of juvenile neuronal ceroid lipofuscinosis." Hum Mol Genet 17(2): 303-312.

Klein, S., M. Franco, P. Chardin and F. Luton (2006). "Role of the Arf6 GDP/GTP cycle and Arf6 GTPase-activating proteins in actin remodeling and intracellular transport." J Biol Chem 281(18): 12352-12361.

Kollmann, K., K. Uusi-Rauva, E. Scifo, J. Tyynela, A. Jalanko and T. Braulke (2013). "Cell biology and function of neuronal ceroid lipofuscinosis-related proteins." Biochim Biophys Acta 1832(11): 1866-1881.

Kornak, U., D. Kasper, M. R. Bosl, E. Kaiser, M. Schweizer, A. Schulz, W. Friedrich, G. Delling and T. J. Jentsch (2001). "Loss of the ClC-7 chloride channel leads to osteopetrosis in mice and man." Cell 104(2): 205-215.

Kornfeld, R., M. Bao, K. Brewer, C. Noll and W. Canfield (1999). "Molecular cloning and functional expression of two splice forms of human N-acetylglucosamine-1-phosphodiester alpha-N-acetylglucosaminidase." J Biol Chem 274(46): 32778-32785.

Kornfeld, R. and S. Kornfeld (1985). "Assembly of asparagine-linked oligosaccharides." Annu Rev Biochem 54: 631-664.

Kouranti, I., M. Sachse, N. Arouche, B. Goud and A. Echard (2006). "Rab35 regulates an endocytic recycling pathway essential for the terminal steps of cytokinesis." Curr Biol 16(17): 1719-1725.

Kovacs, A. D., J. M. Weimer and D. A. Pearce (2006). "Selectively increased sensitivity of cerebellar granule cells to AMPA receptor-mediated excitotoxicity in a mouse model of Batten disease." Neurobiol Dis 22(3): 575-585.

Kursar, M., K. Bonhagen, A. Köhler, T. Kamradt, S. H. E. Kaufmann and H.-W. Mittrücker (2002). "Organ-Specific CD4+ T Cell Response During Listeria monocytogenes Infection." The Journal of Immunology 168(12): 6382-6387.

Kyttälä, A., G. Ihrke, J. Vesa, M. J. Schell and J. P. Luzio (2004). "Two motifs target Batten disease protein CLN3 to lysosomes in transfected nonneuronal and neuronal cells." Mol Biol Cell 15(3): 1313-1323.

Kyttälä, A., K. Yliannala, P. Schu, A. Jalanko and J. P. Luzio (2005). "AP-1 and AP-3 facilitate lysosomal targeting of Batten disease protein CLN3 via its dileucine motif." J Biol Chem 280(11): 10277-10283.

Laatsch, A., M. Merkel, P. J. Talmud, T. Grewal, U. Beisiegel and J. Heeren (2009). "Insulin stimulates hepatic low density lipoprotein receptor-related protein 1 (LRP1) to increase postprandial lipoprotein clearance." Atherosclerosis 204(1): 105-111.

LaFerla, F. M., J. C. Troncoso, D. K. Strickland, C. H. Kawas and G. Jay (1997). "Neuronal cell death in Alzheimer's disease correlates with apoE uptake and intracellular Abeta stabilization." J Clin Invest 100(2): 310-320.

Lefrancois, S., T. May, C. Knight, D. Bourbeau and C. R. Morales (2002). "The lysosomal transport of prosaposin requires the conditional interaction of its highly conserved d domain with sphingomyelin." J Biol Chem 277(19): 17188-17199.

Lübke, T., P. Lobel and D. E. Sleat (2009). "Proteomics of the lysosome." Biochim Biophys Acta 1793(4): 625-635.

Luiro, K., O. Kopra, M. Lehtovirta and A. Jalanko (2001). "CLN3 protein is targeted to neuronal synapses but excluded from synaptic vesicles: new clues to Batten disease." Hum Mol Genet 10(19): 2123-2131.

Luiro, K., K. Yliannala, L. Ahtiainen, H. Maunu, I. Jarvela, A. Kyttala and A. Jalanko (2004). "Interconnections of CLN3, Hook1 and Rab proteins link Batten disease to defects in the endocytic pathway." Hum Mol Genet 13(23): 3017-3027.

Luzio, J. P., Y. Hackmann, N. M. Dieckmann and G. M. Griffiths (2014). "The biogenesis of lysosomes and lysosome-related organelles." Cold Spring Harb Perspect Biol 6(9): a016840.

Makrypidi, G., M. Damme, S. Muller-Loennies, M. Trusch, B. Schmidt, H. Schluter, J. Heeren, T. Lubke, P. Saftig and T. Braulke (2012). "Mannose 6 dephosphorylation of lysosomal proteins mediated by acid phosphatases Acp2 and Acp5." Mol Cell Biol 32(4): 774-782.

Marshansky, V., J. L. Rubinstein and G. Gruber (2014). "Eukaryotic V-ATPase: novel structural findings and functional insights." Biochim Biophys Acta 1837(6): 857-879.

Marzolo, M. P., R. von Bernhardi, G. Bu and N. C. Inestrosa (2000). "Expression of alpha(2)-macroglobulin receptor/low density lipoprotein receptor-related protein (LRP) in rat microglial cells." J Neurosci Res 60(3): 401-411.

Mauch, D. H., K. Nagler, S. Schumacher, C. Goritz, E. C. Muller, A. Otto and F. W. Pfrieger (2001). "CNS synaptogenesis promoted by glia-derived cholesterol." Science 294(5545): 1354-1357.

Maxfield, F. R. and T. E. McGraw (2004). "Endocytic recycling." Nat Rev Mol Cell Biol 5(2): 121-132.

May, P., A. Rohlmann, H. H. Bock, K. Zurhove, J. D. Marth, E. D. Schomburg, J. L. Noebels, U. Beffert, J. D. Sweatt, E. J. Weeber and J. Herz (2004). "Neuronal LRP1 functionally associates with postsynaptic proteins and is required for normal motor function in mice." Mol Cell Biol 24(20): 8872-8883.

May, P., E. Woldt, R. L. Matz and P. Boucher (2007). "The LDL receptor-related protein (LRP) family: an old family of proteins with new physiological functions." Ann Med 39(3): 219-228.

Mayle, K. M., A. M. Le and D. T. Kamei (2012). "The intracellular trafficking pathway of transferrin." Biochim Biophys Acta 1820(3): 264-281.

Mehta, A. B. and B. Winchester (2013). Lysosomal storage disorders : a practical guide. Chichester, West Sussex, Wiley-Blackwell.

Mencarelli, C. and P. Martinez-Martinez (2013). "Ceramide function in the brain: when a slight tilt is enough." Cell Mol Life Sci 70(2): 181-203.

Metcalf, D. J., A. A. Calvi, M. Seaman, H. M. Mitchison and D. F. Cutler (2008). "Loss of the Batten disease gene CLN3 prevents exit from the TGN of the mannose 6-phosphate receptor." Traffic 9(11): 1905-1914.

Miedel, M. T., K. M. Weixel, J. R. Bruns, L. M. Traub and O. A. Weisz (2006). "Posttranslational cleavage and adaptor protein complex-dependent trafficking of mucolipin-1." J Biol Chem 281(18): 12751-12759.

Mindell, J. A. (2012). "Lysosomal acidification mechanisms." Annu Rev Physiol 74: 69-86.

Mitchison, H. M., D. J. Bernard, N. D. Greene, J. D. Cooper, M. A. Junaid, R. K. Pullarkat, N. de Vos, M. H. Breuning, J. W. Owens, W. C. Mobley, R. M. Gardiner, B. D. Lake, P. E. Taschner and R. L. Nussbaum (1999). "Targeted disruption of the Cln3 gene provides a mouse model for Batten disease. The Batten Mouse Model Consortium [corrected]." Neurobiol Dis 6(5): 321-334.

Mokuno, H., S. Brady, L. Kotite, J. Herz and R. J. Havel (1994). "Effect of the 39-kDa receptor-associated protein on the hepatic uptake and endocytosis of chylomicron remnants and low density lipoproteins in the rat." J Biol Chem 269(18): 13238-13243.

Mole, S. E., R. E. Williams and H. H. Goebel (2011). The neuronal ceroid lipofuscinoses (Batten disease). Oxford, Oxford University Press.

Montagnac, G., H. de Forges, E. Smythe, C. Gueudry, M. Romao, J. Salamero and P. Chavrier (2011). "Decoupling of activation and effector binding underlies ARF6 priming of fast endocytic recycling." Curr Biol 21(7): 574-579.

Montalbetti, N., A. Simonin, G. Kovacs and M. A. Hediger (2013). "Mammalian iron transporters: families SLC11 and SLC40." Mol Aspects Med 34(2-3): 270-287.

Montesano, R., J. Roth, A. Robert and L. Orci (1982). "Non-coated membrane invaginations are involved in binding and internalization of cholera and tetanus toxins." Nature 296(5858): 651-653.

Morisot, C., G. Millat, A. Coeslier, B. Bourgois, E. Fontenoy, D. Dobbelaere, L. Verot, N. Haouari, C. Vaillant, F. Gottrand, E. Bogaert, P. Thelliez, S. Klosowski, A. Djebara, A. Bachiri, S. Manouvrier and M. T. Vanier (2005). "[Fatal neonatal respiratory distress

in Niemann-Pick C2 and prenatal diagnosis with mutations in gene HE1/NPC2]." Arch Pediatr 12(4): 434-437.

Munroe, P. B., H. M. Mitchison, A. M. O'Rawe, J. W. Anderson, R. M. Boustany, T. J. Lerner, P. E. Taschner, N. de Vos, M. H. Breuning, R. M. Gardiner and S. E. Mole (1997). "Spectrum of mutations in the Batten disease gene, CLN3." Am J Hum Genet 61(2): 310-316.

Ni, X. and C. R. Morales (2006). "The lysosomal trafficking of acid sphingomyelinase is mediated by sortilin and mannose 6-phosphate receptor." Traffic 7(7): 889-902.

Nielsen, R., P. J. Courtoy, C. Jacobsen, G. Dom, W. R. Lima, M. Jadot, T. E. Willnow, O. Devuyst and E. I. Christensen (2007). "Endocytosis provides a major alternative pathway for lysosomal biogenesis in kidney proximal tubular cells." Proc Natl Acad Sci U S A 104(13): 5407-5412.

Nijssen, P. C., E. Brusse, A. C. Leyten, J. J. Martin, J. L. Teepen and R. A. Roos (2002). "Autosomal dominant adult neuronal ceroid lipofuscinosis: parkinsonism due to both striatal and nigral dysfunction." Mov Disord 17(3): 482-487.

Novarino, G., S. Weinert, G. Rickheit and T. J. Jentsch (2010). "Endosomal chloride-proton exchange rather than chloride conductance is crucial for renal endocytosis." Science 328(5984): 1398-1401.

Osorio, N. S., B. Sampaio-Marques, C. H. Chan, P. Oliveira, D. A. Pearce, N. Sousa and F. Rodrigues (2009). "Neurodevelopmental delay in the Cln3Deltaex7/8 mouse model for Batten disease." Genes Brain Behav 8(3): 337-345.

Ostergaard, J. R., T. B. Rasmussen and H. Molgaard (2011). "Cardiac involvement in juvenile neuronal ceroid lipofuscinosis (Batten disease)." Neurology 76(14): 1245-1251.

Otomo, T., M. Schweizer, K. Kollmann, V. Schumacher, N. Muschol, E. Tolosa, H.W. Mittrücker, T . Braulke (2014) "Mannose 6-phosphorylation of lysosomal enzymes controls B-cellfunctions" JCB, in press

Palmer, D. N., I. M. Fearnley, S. M. Medd, J. E. Walker, R. D. Martinus, S. L. Bayliss, N. A. Hall, B. D. Lake, L. S. Wolfe and R. D. Jolly (1989). "Lysosomal storage of the DCCD reactive proteolipid subunit of mitochondrial ATP synthase in human and ovine ceroid lipofuscinoses." Adv Exp Med Biol 266: 211-222; discussion 223.

Palmer, D. N., I. M. Fearnley, J. E. Walker, N. A. Hall, B. D. Lake, L. S. Wolfe, M. Haltia, R. D. Martinus and R. D. Jolly (1992). "Mitochondrial ATP synthase subunit c storage in the ceroid-lipofuscinoses (Batten disease)." Am J Med Genet 42(4): 561-567.

Pamer, E. G. (2004). "Immune responses to Listeria monocytogenes." Nat Rev Immunol 4(10): 812-823.

Pearce, D. A. and F. Sherman (1998). "A yeast model for the study of Batten disease." Proc Natl Acad Sci U S A 95(12): 6915-6918.

Peri, F. and C. Nusslein-Volhard (2008). "Live imaging of neuronal degradation by microglia reveals a role for v0-ATPase a1 in phagosomal fusion in vivo." Cell 133(5): 916-927.

Persaud-Sawin, D. A., J. O. McNamara, 2nd, S. Rylova, A. Vandongen and R. M. Boustany (2004). "A galactosylceramide binding domain is involved in trafficking of CLN3 from Golgi to rafts via recycling endosomes." Pediatr Res 56(3): 449-463.

Peters, C., W. Rommerskirch, S. Modaressi and K. von Figura (1991). "Restoration of arylsulphatase B activity in human mucopolysaccharidosis-type-VI fibroblasts by retroviral-vector-mediated gene transfer." Biochem J 276 (Pt 2): 499-504.

Pfrieger, F. W. (2003). "Cholesterol homeostasis and function in neurons of the central nervous system." Cell Mol Life Sci 60(6): 1158-1171.

Pohl, S., H. M. Mitchison, A. Kohlschutter, O. van Diggelen, T. Braulke and S. Storch (2007). "Increased expression of lysosomal acid phosphatase in CLN3-defective cells and mouse brain tissue." J Neurochem 103(6): 2177-2188.

Pontikis, C. C., C. V. Cella, N. Parihar, M. J. Lim, S. Chakrabarti, H. M. Mitchison, W. C. Mobley, P. Rezaie, D. A. Pearce and J. D. Cooper (2004). "Late onset neurodegeneration in the Cln3-/- mouse model of juvenile neuronal ceroid lipofuscinosis is preceded by low level glial activation." Brain Res 1023(2): 231-242.

Pontikis, C. C., S. L. Cotman, M. E. MacDonald and J. D. Cooper (2005). "Thalamocortical neuron loss and localized astrocytosis in the Cln3Deltaex7/8 knock-in mouse model of Batten disease." Neurobiol Dis 20(3): 823-836.

Price, P. W. and J. Cerny (1999). "Characterization of CD4+ T cells in mouse bone marrow. I. Increased activated/memory phenotype and altered TCR Vbeta repertoire." Eur J Immunol 29(3): 1051-1056.

Puranam, K., W. H. Qian, K. Nikbakht, M. Venable, L. Obeid, Y. Hannun and R. M. Boustany (1997). "Upregulation of Bcl-2 and elevation of ceramide in Batten disease." Neuropediatrics 28(1): 37-41.

Rakheja, D., S. B. Narayan, J. V. Pastor and M. J. Bennett (2004). "CLN3P, the Batten disease protein, localizes to membrane lipid rafts (detergent-resistant membranes)." Biochem Biophys Res Commun 317(4): 988-991.

Rappsilber, J., M. Mann and Y. Ishihama (2007). "Protocol for micro-purification, enrichment, pre-fractionation and storage of peptides for proteomics using StageTips." Nat Protoc 2(8): 1896-1906.

Reczek, D., M. Schwake, J. Schroder, H. Hughes, J. Blanz, X. Jin, W. Brondyk, S. Van Patten, T. Edmunds and P. Saftig (2007). "LIMP-2 is a receptor for lysosomal mannose-6-phosphate-independent targeting of beta-glucocerebrosidase." Cell 131(4): 770-783.

Reitman, M. L. and S. Kornfeld (1981). "Lysosomal enzyme targeting. N-Acetylglucosaminylphosphotransferase selectively phosphorylates native lysosomal enzymes." J Biol Chem 256(23): 11977-11980.

Rosenberger, C. M. and B. B. Finlay (2003). "Phagocyte sabotage: disruption of macrophage signalling by bacterial pathogens." Nat Rev Mol Cell Biol 4(5): 385-396.

Saftig, P. and J. Klumperman (2009). "Lysosome biogenesis and lysosomal membrane proteins: trafficking meets function." Nat Rev Mol Cell Biol 10(9): 623-635.

Saftig, P., B. Schroder and J. Blanz (2010). "Lysosomal membrane proteins: life between acid and neutral conditions." Biochem Soc Trans 38(6): 1420-1423.

Sagiv, Y., K. Hudspeth, J. Mattner, N. Schrantz, R. K. Stern, D. Zhou, P. B. Savage, L. Teyton and A. Bendelac (2006). "Cutting edge: impaired glycosphingolipid trafficking and NKT cell development in mice lacking Niemann-Pick type C1 protein." J Immunol 177(1): 26-30.

Sagne, C., C. Agulhon, P. Ravassard, M. Darmon, M. Hamon, S. El Mestikawy, B. Gasnier and B. Giros (2001). "Identification and characterization of a lysosomal transporter for small neutral amino acids." Proc Natl Acad Sci U S A 98(13): 7206-7211.

Sahagian, G. G. and M. M. Gottesman (1982). "The predominant secreted protein of transformed murine fibroblasts carries the lysosomal mannose 6-phosphate recognition marker." J Biol Chem 257(18): 11145-11150.

Santavuori, P. (1988). "Neuronal ceroid-lipofuscinoses in childhood." Brain Dev 10(2): 80-83.

Sardiello, M., M. Palmieri, A. di Ronza, D. L. Medina, M. Valenza, V. A. Gennarino, C. Di Malta, F. Donaudy, V. Embrione, R. S. Polishchuk, S. Banfi, G. Parenti, E. Cattaneo and A. Ballabio (2009). "A gene network regulating lysosomal biogenesis and function." Science 325(5939): 473-477.

Sawkar, A. R., W. D'Haeze and J. W. Kelly (2006). "Therapeutic strategies to ameliorate lysosomal storage disorders--a focus on Gaucher disease." Cell Mol Life Sci 63(10): 1179-1192.

Schonteich, E., G. M. Wilson, J. Burden, C. R. Hopkins, K. Anderson, J. R. Goldenring and R. Prekeris (2008). "The Rip11/Rab11-FIP5 and kinesin II complex regulates endocytic protein recycling." J Cell Sci 121(Pt 22): 3824-3833.

Schröder, B., C. Wrocklage, C. Pan, R. Jager, B. Kosters, H. Schafer, H. P. Elsasser, M. Mann and A. Hasilik (2007). "Integral and associated lysosomal membrane proteins." Traffic 8(12): 1676-1686.

Schulz, A., A. Kohlschutter, J. Mink, A. Simonati and R. Williams (2013). "NCL diseases - clinical perspectives." Biochim Biophys Acta 1832(11): 1801-1806.

Schwake, M., B. Schroder and P. Saftig (2013). "Lysosomal membrane proteins and their central role in physiology." Traffic 14(7): 739-748.

Schwarz, G., W. H. Boehncke, M. Braun, C. J. Schroter, T. Burster, T. Flad, D. Dressel, E. Weber, H. Schmid and H. Kalbacher (2002). "Cathepsin S activity is detectable in human keratinocytes and is selectively upregulated upon stimulation with interferon-gamma." J Invest Dermatol 119(1): 44-49.

Seehafer, S. S. and D. A. Pearce (2006). "You say lipofuscin, we say ceroid: defining autofluorescent storage material." Neurobiol Aging 27(4): 576-588.

Seehafer, S. S., D. Ramirez-Montealegre, A. M. Wong, C. H. Chan, J. Castaneda, M. Horak, S. M. Ahmadi, M. J. Lim, J. D. Cooper and D. A. Pearce (2011). "Immunosuppression alters disease severity in juvenile Batten disease mice." J Neuroimmunol 230(1-2): 169-172.

Seigel, G. M., A. Lotery, A. Kummer, D. J. Bernard, N. D. Greene, M. Turmaine, T. Derksen, R. L. Nussbaum, B. Davidson, J. Wagner and H. M. Mitchison (2002). "Retinal pathology and function in a Cln3 knockout mouse model of juvenile Neuronal Ceroid Lipofuscinosis (batten disease)." Mol Cell Neurosci 19(4): 515-527.

Settembre, C., A. Fraldi, D. L. Medina and A. Ballabio (2013). "Signals from the lysosome: a control centre for cellular clearance and energy metabolism." Nat Rev Mol Cell Biol 14(5): 283-296.

Shevchenko, A., H. Tomas, J. Havlis, J. V. Olsen and M. Mann (2006). "In-gel digestion for mass spectrometric characterization of proteins and proteomes." Nat Protoc 1(6): 2856-2860.

Shevtsova, Z., M. Garrido, J. Weishaupt, P. Saftig, M. Bahr, F. Luhder and S. Kugler (2010). "CNS-expressed cathepsin D prevents lymphopenia in a murine model of congenital neuronal ceroid lipofuscinosis." Am J Pathol 177(1): 271-279.

Shi, C. and E. G. Pamer (2011). "Monocyte recruitment during infection and inflammation." Nat Rev Immunol 11(11): 762-774.

Shogomori, H. and A. H. Futerman (2001). "Cholera toxin is found in detergent-insoluble rafts/domains at the cell surface of hippocampal neurons but is internalized via a raft-independent mechanism." J Biol Chem 276(12): 9182-9188.

Song, J. W., T. Misgeld, H. Kang, S. Knecht, J. Lu, Y. Cao, S. L. Cotman, D. L. Bishop and J. W. Lichtman (2008). "Lysosomal activity associated with developmental axon pruning." J Neurosci 28(36): 8993-9001.

Staropoli, J. F., L. Haliw, S. Biswas, L. Garrett, S. M. Holter, L. Becker, S. Skosyrski, P. Da Silva-Buttkus, J. Calzada-Wack, F. Neff, B. Rathkolb, J. Rozman, A. Schrewe, T. Adler, O. Puk, M. Sun, J. Favor, I. Racz, R. Bekeredjian, D. H. Busch, J. Graw, M. Klingenspor, T. Klopstock, E. Wolf, W. Wurst, A. Zimmer, E. Lopez, H. Harati, E. Hill, D. S. Krause, J. Guide, E. Dragileva, E. Gale, V. C. Wheeler, R. M. Boustany, D. E. Brown, S. Breton, K. Ruether, V. Gailus-Durner, H. Fuchs, M. H. de Angelis and S. L. Cotman (2012). "Large-scale phenotyping of an accurate genetic mouse model of JNCL identifies novel early pathology outside the central nervous system." PLoS One 7(6): e38310.

Stauber, T. and T. J. Jentsch (2013). "Chloride in vesicular trafficking and function." Annu Rev Physiol 75: 453-477.

Stein, C. S., P. H. Yancey, I. Martins, R. D. Sigmund, J. B. Stokes and B. L. Davidson (2010). "Osmoregulation of ceroid neuronal lipofuscinosis type 3 in the renal medulla." Am J Physiol Cell Physiol 298(6): C1388-1400.

Stein, M., J. E. Zijderhand-Bleekemolen, H. Geuze, A. Hasilik and K. von Figura (1987). "Mr 46,000 mannose 6-phosphate specific receptor: its role in targeting of lysosomal enzymes." EMBO J 6(9): 2677-2681.

Steinberg, B. E., K. K. Huynh, A. Brodovitch, S. Jabs, T. Stauber, T. J. Jentsch and S. Grinstein (2010). "A cation counterflux supports lysosomal acidification." J Cell Biol 189(7): 1171-1186.

Storch, S., S. Pohl and T. Braulke (2004). "A dileucine motif and a cluster of acidic amino acids in the second cytoplasmic domain of the batten disease-related CLN3 protein are required for efficient lysosomal targeting." J Biol Chem 279(51): 53625-53634.

Storch, S., S. Pohl, A. Quitsch, K. Falley and T. Braulke (2007). "C-terminal prenylation of the CLN3 membrane glycoprotein is required for efficient endosomal sorting to lysosomes." Traffic 8(4): 431-444.

Strasser, B., J. Iwaszkiewicz, O. Michielin and A. Mayer (2011). "The V-ATPase proteolipid cylinder promotes the lipid-mixing stage of SNARE-dependent fusion of yeast vacuoles." EMBO J 30(20): 4126-4141.

Supek, F., L. Supekova, S. Mandiyan, Y. C. Pan, H. Nelson and N. Nelson (1994). "A novel accessory subunit for vacuolar H(+)-ATPase from chromaffin granules." J Biol Chem 269(39): 24102-24106.

Tamaki, S. J., Y. Jacobs, M. Dohse, A. Capela, J. D. Cooper, M. Reitsma, D. He, R. Tushinski, P. V. Belichenko, A. Salehi, W. Mobley, F. H. Gage, S. Huhn, A. S. Tsukamoto, I. L. Weissman and N. Uchida (2009). "Neuroprotection of host cells by human central nervous system stem cells in a mouse model of infantile neuronal ceroid lipofuscinosis." Cell Stem Cell 5(3): 310-319.

Truneh, A., F. Albert, P. Golstein and A. M. Schmitt-Verhulst (1985). "Early steps of lymphocyte activation bypassed by synergy between calcium ionophores and phorbol ester." Nature 313(6000): 318-320.

Tyynelä, J., D. N. Palmer, M. Baumann and M. Haltia (1993). "Storage of saposins A and D in infantile neuronal ceroid-lipofuscinosis." FEBS Lett 330(1): 8-12.

Tyynelä, J. and J. Suopanki (2000). "Biochemical aspects of neuronal ceroid lipofuscinoses." Neurol Sci 21(3 Suppl): S21-25.

Uusi-Rauva, K., K. Luiro, K. Tanhuanpaa, O. Kopra, P. Martin-Vasallo, A. Kyttala and A. Jalanko (2008). "Novel interactions of CLN3 protein link Batten disease to dysregulation of fodrin-Na+, K+ ATPase complex." Exp Cell Res 314(15): 2895-2905.

Veerman, K. M., M. J. Williams, K. Uchimura, M. S. Singer, J. S. Merzaban, S. Naus, D. A. Carlow, P. Owen, J. Rivera-Nieves, S. D. Rosen and H. J. Ziltener (2007). "Interaction of the selectin ligand PSGL-1 with chemokines CCL21 and CCL19 facilitates efficient homing of T cells to secondary lymphoid organs." Nat Immunol 8(5): 532-539.

Waheed, A., R. Pohlmann, A. Hasilik, K. von Figura, A. van Elsen and J. G. Leroy (1982). "Deficiency of UDP-N-acetylglucosamine:lysosomal enzyme N-acetylglucosamine-1-phosphotransferase in organs of I-cell patients." Biochem Biophys Res Commun 105(3): 1052-1058.

Weinert, S., S. Jabs, C. Supanchart, M. Schweizer, N. Gimber, M. Richter, J. Rademann, T. Stauber, U. Kornak and T. J. Jentsch (2010). "Lysosomal pathology and osteopetrosis upon loss of H+-driven lysosomal Cl- accumulation." Science 328(5984): 1401-1403.

Willnow, T. E., S. A. Armstrong, R. E. Hammer and J. Herz (1995). "Functional expression of low density lipoprotein receptor-related protein is controlled by receptor-associated protein in vivo." Proc Natl Acad Sci U S A 92(10): 4537-4541.

Xiong, J. and T. Kielian (2013). "Microglia in juvenile neuronal ceroid lipofuscinosis are primed toward a pro-inflammatory phenotype." J Neurochem 127(2): 245-258.

9 Supplement

9.1 Primer for genotyping

Table 23: Primer for genotyping

Name	***Sequence 5'-3'***
WtF	CAGCATCTCCTCAGGGCTA
WtR	CCAACATAGAAAGTAGGGTGTGC
552F	GAGCTTTGTTCTGGTTGCCTTC
Ex9RA	GCAGTCTCTGCCTCGTTTTCT

9.2 TaqMan Assays for qRT PCR

Table 24: TaqMan Assays for qRT PCR

Name	***Sequence 5'-3'***
Arsa	Mm00802173_g1
Cln3	Mm00487021_m1
Ctsb	Mm01310506_m1
Ctsd	Mm00515587_m1
Ctsl	Mm00515597_m1
Ctsz	Mm00517687_m1
Fuca1	Mm00502778_m1
Hexb	Mm00599880_m1
Igf2r (Mpr300)	Mm00439576_m1
Lamp1	Mm00495262_m1
Lamp2	Mm00495267_m1
Lrp1	Mm00464608_m1
Lrp2	Mm01328171_m1
Mpr46	Mn04208409_gH
Ppt1	Mm00477078_m1
slc36a1	Mm00462410_m1
Tpp1	Mm00487016_m1
Trfc	Mm00441941_m1

9.3 Lysosomal proteins identified in endosomal-lysosomal fractions by SILAC-based proteomic analysis

Table 25: Lysosomal soluble proteins identified in endosomal-lysosomal fractions of wild-type and *Cln3^{ki}* cerebellar cells

Uniprot ID	*Protein Name*	*Gene Name*	*Replicate 1*	*Replicate 2*	*Replicate 3*	*Mean*	*SD*
O88531	Palmitoyl-protein thioesterase 1	Ppt1	1,969	2,892	2,519	**2,460**	**0,464**
P51569	Alpha-galactosidase A	Gla	1,491	2,229	1,763	**1,828**	**0,373**
P70699	Lysosomal alpha-glucosidase	Gaa	1,379	1,872	1,605	**1,619**	**0,246**
Q9CQ01	Ribonuclease T2	Rnaset2	1,269	1,502	1,987	**1,586**	**0,366**
O89023	Tripeptidyl-peptidase 1	Tpp1	1,260	1,441	1,422	**1,375**	**0,100**
O35657	Sialidase-1	Neu1	0,969	1,216	1,444	**1,210**	**0,238**
P06797	Cathepsin L1	Ctsl	1,120	1,222	1,262	**1,202**	**0,073**
Q920A5	Retinoid-inducible serine carboxypeptidase	Scpep1	1,015	1,289	1,161	**1,155**	**0,137**
Q60648	Ganglioside GM2 activator	Gm2a	1,019	1,234	1,125	**1,126**	**0,108**
Q9ET22	Dipeptidyl peptidase 2	Dpp7	0,961	1,142	1,225	**1,109**	**0,135**
P17439	Glucosylceramidase	Gba	0,913	1,235	1,078	**1,075**	**0,161**
P24638	Lysosomal acid phosphatase	Acp2	0,905	1,192	0,999	**1,032**	**0,147**
Q8BFR4	N-acetylglucosamine-6-sulfatase	Gns	1,109	0,926	0,895	**0,977**	**0,116**
Q64191	N(4)-(beta-N-acetylglucosaminyl)-L-asparaginase	Aga	0,855	1,000	0,981	**0,946**	**0,079**
P10605	Cathepsin B	Ctsb	0,761	1,026	0,956	**0,914**	**0,138**
Q8R242	Di-N-acetylchitobiase	Ctbs	0,855	0,794	0,945	**0,865**	**0,076**
P16675	Lysosomal protective protein	Ctsa	0,744	0,855	0,899	**0,833**	**0,080**
O09159	Lysosomal alpha-mannosidase	Man2b1	0,779	0,679	0,912	**0,790**	**0,117**
Q3UMW8	Ceroid-lipofuscinosis neuronal protein 5 homolog	Cln5	0,716	0,843	0,790	**0,783**	**0,064**
P23780	Beta-galactosidase	Glb1	0,624	0,872	0,844	**0,780**	**0,136**

Q9Z0J0	Epididymal secretory protein E1	Npc2	0,733	0,748	0,813	**0,765**	**0,043**
P50429	Arylsulfatase B	Arsb	0,805	0,712	0,750	**0,756**	**0,047**
Q9D7V9	N-acylethanolamine-hydrolyzing acid amidase	Naaa	0,699	0,716	0,845	**0,753**	**0,080**
P18242	Cathepsin D	Ctsd	0,685	0,714	0,802	**0,733**	**0,061**
Q9QWR8	Alpha-N-acetyl-galactosaminidase	Naga	0,594	0,766	0,800	**0,720**	**0,110**
O54782	Epididymis-specific alpha-mannosidase	Man2b2	0,740	0,634	0,706	**0,693**	**0,054**
P20060	Beta-hexosaminidase subunit beta	Hexb	0,625	0,678	0,688	**0,664**	**0,034**
P56542	Deoxyribonuclease-2-alpha	Dnase2	0,490	0,819	0,679	**0,663**	**0,165**
Q61207	Sulfated glycoprotein 1	Psap	0,799	-	0,503	**0,651**	**0,210**
Q3TCN2	Putative phospholipase B-like 2	Plbd2	0,583	0,622	0,619	**0,608**	**0,022**
P29416	Beta-hexosaminidase subunit alpha	Hexa	0,536	0,593	0,682	**0,604**	**0,074**
Q9WUU7	Cathepsin Z	Ctsz	0,516	0,503	0,599	**0,539**	**0,052**
P54818	Galactocerebrosidase	Galc	0,507	0,542	0,410	**0,486**	**0,068**
Q7TMR0	Lysosomal Pro-X carboxypeptidase	Prcp	0,476	0,346	0,585	**0,469**	**0,120**
Q571E4	N-acetyl-galactosamine-6-sulfatase	Galns	0,446	0,472	0,450	**0,456**	**0,014**
Q8K2I4	Beta-mannosidase	Manba	0,509	0,365	-	**0,437**	**0,102**
P12265	Beta-glucuronidase	Gusb	0,397	0,489	0,417	**0,434**	**0,048**
Q99LJ1	Tissue alpha-L-fucosidase	Fuca1	0,379	0,466	0,421	**0,422**	**0,044**
P50428	Arylsulfatase A	Arsa	0,396	0,434	0,369	**0,400**	**0,033**
Q9WV54	Acid ceramidase	Asah1	0,411	0,359	0,389	**0,387**	**0,026**
Q8VEB4	Group XV phospholipase A2	Pla2g15	0,397	0,369	0,370	**0,378**	**0,016**
O88668	Protein CREG1	Creg1	0,341	0,394	0,382	**0,372**	**0,028**
O89017	Legumain	Lgmn	0,304	0,277	0,353	**0,312**	**0,039**
Q9Z0M5	Lysosomal acid lipase	Lipa	0,306	0,249	0,355	**0,303**	**0,053**
Q9WVJ3	Carboxypeptidase Q	Cpq	0,246	0,350	-	**0,298**	**0,074**
P70665	Sialate O-acetylesterase	Siae	-	0,272	0,205	**0,239**	**0,048**

Q99M71	Mammalian ependymin-related protein 1	Epdr1	0,228	0,172	0,182	**0,194**	**0,030**

Table 26: Lysosomal membrane proteins identified in endosomal-lysosomal fractions of wild-type and *Cln3^{ki}* cerebellar cells

Uniprot ID	***Protein Name***	***Gene Name***	***Replicate 1***	***Replicate 2***	***Replicate 3***	***Mean***	***SD***
Q8K4D3	Proton-coupled amino acid transporter 1	S36A1	1,433	2,523	1,697	**1,884**	**0,568**
P51863	V-type proton ATPase subunit d 1	VA0D1	1,429	1,781	1,683	**1,631**	**0,182**
Q9R1Q9	V-type proton ATPase subunit S1	VAS1	1,690	1,654	1,422	**1,589**	**0,145**
O70496	H+/Cl− exchange transporter 7	CLCN7	1,153	1,563	1,378	**1,364**	**0,205**
P15920	V-type proton ATPase 116 kDa subunit a isoform 2	VPP2	0,935	1,295	1,040	**1,090**	**0,185**
Q8VE96	Transmembrane protein C2orf18 (p40)/Solute carrier family 35 member F6	S35F6	1,000	1,081	0,873	**0,985**	**0,105**
P17047	Lysosome-associated membrane protein 2	LAMP2	0,827	1,172	0,924	**0,974**	**0,178**
P49769	Presenilin-1	PSN1	0,851	1,027	0,979	**0,952**	**0,091**
Q9Z1G4	V-type proton ATPase 116 kDa subunit a isoform 1	VPP1	0,724	1,080	0,965	**0,923**	**0,181**
P41731	CD63	CD63	0,656	1,065	0,953	**0,891**	**0,211**
O35604	Niemann–Pick C1 protein	NPC1	0,757	0,929	0,948	**0,878**	**0,105**
P57746	V-type proton ATPase subunit D	VATD	0,693	1,053	0,849	**0,865**	**0,181**
Q9Z1G3	V-type proton ATPase subunit C 1	VATC1	0,700	1,029	0,860	**0,863**	**0,164**
P50518	V-type proton ATPase subunit E 1	VATE1	0,723	0,998	0,832	**0,851**	**0,138**
Q8BVE3	V-type proton ATPase subunit H	VATH	0,715	1,012	0,806	**0,844**	**0,152**
P50516	V-type proton ATPase catalytic subunit A	VATA	0,703	0,997	0,816	**0,839**	**0,148**
P62814	V-type proton	VATB2	0,706	0,981	0,789	**0,825**	**0,141**

	ATPase subunit B, brain isoform						
Q9CZX7	Transmembrane protein 55A	TM55A	0,708	0,799	0,886	**0,798**	**0,089**
Q9CR51	V-type proton ATPase subunit G 1	VATG1	0,697	0,807	0,743	**0,749**	**0,055**
P70280	Vesicle-associated membrane protein 7	VAMP 7	0,703	0,763	0,776	**0,747**	**0,039**
O35114	LIMP-2	SCRB2	0,660	0,715	0,655	**0,677**	**0,034**
P57716	Nicastrin	NICA	0,533	0,670	0,678	**0,627**	**0,082**
P11438	Lysosome-associated membrane protein 1	LAMP1	0,583	0,432	0,775	**0,597**	**0,171**
Q60961	Lysosomal-associated transmembrane protein 4A	LAP4A	0,475	0,350	0,508	**0,445**	**0,083**

Table 27: Cargo receptors identified in endosomal-lysosomal fractions of wild-type and *Cln3*^{ki} cerebellar cells

Uniprot ID	***Protein Name***	***Gene Name***	***Replicate 1***	***Replicate 2***	***Replicate 3***	***Mean***	***SD***
A2ARV4	Low-density lipoprotein receptor-related protein 2	Lrp2	13,654	6,511	10,222	10,129	3,572
Q07113	Cation-independent mannose-6-phosphate receptor	Igf2r	1,542	1,964	1,852	1,786	0,219
Q91ZX7	Prolow-density lipoprotein receptor-related protein 1	Lrp1	0,337	0,322	0,376	0,345	0,027

10 Publications and Conference Contributions

Publications

Schmidtke C, Makrypidi G, Pohl S, Thelen M, Schweizer M, Jabs S, Storch S, Cotman SL, Gieselmann G, Braulke T, Schulz A
Cln3$^{\Delta ex7/8}$ impairs endocytic receptor trafficking and efflux of lysosomal amino acids
In preparation

Conference Contributions

Oral presentations

- **Schmidtke C:** Analysis of the immune phenotype in *Cln3*$^{\Delta ex7/8}$ mice
  14th International Conference On Neuronal Ceroid Lipofuscinoses
  22.-26.10.2014, Córdoba, Argentina
- **Schmidtke C:** Analysis of the immune phenotype in *Cln3*$^{\Delta ex7/8}$ mice
  ESGLD Workshop (European Study Group on Lysosomal Diseases)
  25.-29.9.2013, Leibnitz, Austria
- **Schmidtke C:** Work package 4: Biomarkers and Modifiers of CLN3
  DEM-CHILD, 7th Framework Programme
  18.-20.10.2012, 1st General Assembly Meeting, Verona, Italy
- **Schmidtke C:** Work package 4: Biomarkers and Modifiers of CLN3
  DEM-CHILD, 7th Framework Programme
  2.-4.9.2013, 2nd General Assembly Meeting, Helsinki, Finland

Poster presentations

- **Schmidtke C:** Analysis of the immune phenotype in *Cln3*$^{\Delta ex7/8}$ mice
  6th Autumn School – Current Concepts of Immunology
  5.-10.10.2014, Merseburg

Acknowledgements

At this point I would like to thank my supervisors Prof. Dr. Thomas Braulke and Dr. Angela Schulz for giving me the opportunity to be part of their working group. I received enormous personal and scientific support. Thank you for numerous inspiring discussions and being critical and encouraging!

I thank PD Dr. Kramer for evaluating and grading this dissertation.

Thanks to Dr. Michaela Schweizer who performed the electron microscopic analyses, Dr. Sabrina Jabs who made the ratiometric pH measurements and Dr. Melanie Thelen who analysed the proteomic data.

I thank the members of the Mittrücker and Tolosa lab for introducing me into the immunological methods and the nice working atmosphere in their lab.

Georgia, thank you for being always helpful, caring and patient. I very much appreciated your very special (pitiless) honesty.

I thank all my colleagues for the great working atmosphere, funny times in and outside the lab, especially Sarah and Laura, Jessica, Raffa and Mine.

Finally, I thank my family and Jon for their constant trust and support. You encouraged me in all my decisions.

Declaration of the Authorship

I hereby declare that I have written this thesis without any help from others and without the use of documents and aids other than those stated above, and that I have mentioned all used sources, which I have cited correctly according to established academic citation rules.

Date	Signature